PUNCHING SHEAR OF CONCRETE FLAT SLABS REINFORCED WITH FIBRE REINFORCED POLYMER BARS

Abdulhamid AL AJAMI

Submitted for the Degree of
Doctor of Philosophy

Faculty of Engineering and Informatics

University of Bradford

2018

ABSTRACT

PUNCHING SHEAR OF CONCRETE FLAT SLABS REINFORCED WITH FIBRE REINFORCED POLYMER BARS

ABDULHAMID Al AJAMI

UNIVERSITY OF BRADFORD, UK, 2018

Keywords: Punching shear, glass fibre reinforced polymer bars, flat slab, finite element, artificial neural networks.

Fibre reinforcement polymers (FRP) are non-corrodible materials used instead of conventional steel and have been approved to be an effective way to overcome corrosion problems. FRP, in most cases, can have a higher tensile strength, but a lower tensile modulus of elasticity compared to that of conventional steel bars. This study aimed to examine flat slab specimens reinforced with glass fibre reinforced polymer (GFRP) and steel bar materials for punching shear behaviour. Six full-scale two-way slab specimens were constructed and tested under concentric load up to failure. One of the main objectives is to study the effect of reinforcement spacing with the same reinforcement ratio on the punching shear strength. In addition, two other parameters were considered, namely, slab depth, and compressive strength of concrete.

The punching shear provisions of two code of practises CSA S806 (Canadian Standards 2012) and JSCE (JSCE et al. 1997) reasonably predicted the load capacity of GFRP reinforced concrete flat slab, whereas, ACI 440 (ACI Committee 440 2015) showed very conservative load capacity prediction.

On the other hand, a dynamic explicit solver in nonlinear finite element (FE) modelling is used to analyse a connection of column to concrete flat slabs reinforced with GFRP bars in terms of ultimate punching load. All FE modelling

was performed in 3D with the appropriate adoption of element size and mesh. The numerical and experimental results were compared in order to evaluate the developed FE, aiming to predict the behaviour of punching shear in the concrete flat slab. In addition, a parametric study was created to explore the behaviour of GFRP reinforced concrete flat slab with three parameters, namely, concrete strength, shear load perimeter to effective depth ratio, and, flexural reinforcement ratio. It was concluded that the developed models could accurately capture the behaviour of GFRP reinforced concrete flat slabs subjected to a concentrated load

Artificial Neural Networks (ANN) is used in this research to predict punching shear strength, and the results were shown to match more closely with the experimental results. A parametric study was performed to investigate the effects of five parameters on punching shear capacity of GFRP reinforced concrete flat slab. The parametric investigation revealed that the effective depth has the most substantial impact on the load carrying capacity of the punching shear followed by reinforcement ratio, column perimeter, the compressive strength of the concrete, and, the elastic modulus of the reinforcement.

ACKNOWLEDGEMENTS

It is a pleasure to thank those who made this thesis possible. First and foremost, I would like to thank **Allah**; our Lord, the All-Knowing, the Almighty, the most Merciful and the most Compassionate.

First and foremost, I would like to express my heartfelt gratitude to my supervisors **Prof. Ashraf Ashour, Prof. Dennis Lam and Dr. Therese Sheehan** for their excellent supervision, constant encouragement and approachability throughout this work. I sincerely appreciate **Prof. Ashour** for his great support and help especially through difficult times. I am genuinely grateful to have such a great supervisor as well as other supervisors.

A very concerned thanks to the **Laboratory staff** who were always ready to help technically whenever needed. I would like to particularly thank **Steve Robinson**, **Owen Baines** and **Michael Procter** for their expert advice and support during the experimental investigation.

I am always grateful to my dear family, **my parents, my wife and my three daughters and a son, my sisters and a brother** for their ethical, financial and compassionate support during my studies.

I do appreciate Pultrall company for their providing GFRP bars which were used in experimental work.

Finally, I would like to thank everybody who was involved in this work as well as expressing my apology to those I did not mention in this acknowledgement.

Table of Contents

LIST OF FIGURES

LIST OF TABLES

LIST OF ABBREVIATIONS

The following abbreviations are used in this report:

ANN	Artificial neural network
BR	Bayesian regularization
CFRP	Carbon Fibre Reinforcement Polymer
COV	Coefficient of variation
FRP	Fibre Reinforced Polymers
GFRP	Glass Fibre Reinforcement Polymer
MAE	Mean absolute percentage error
R	Regression
RC	Reinforced concrete
SCG	Scaled Conjugate Gradient
SRC	Steel Reinforced Concrete
SRCS	Steel reinforced concrete structures
SSE	Sum squared error
STD	Standard deviation

LIST OF MATHEMATICAL SYMBOLS

The following mathematical symbols are used in this report:

A	Cross-sectional area of specimen
A_c	Column area
A_s	Steel reinforcement area.
A_{FRP}, A_f	Fiber Reinforcement Area
B	Bias vector
b	Column perimeter
b_{cr}	Edge length of the failure perimeter
b_{cr}	edge length of the failure perimeter.
b_o	critical punching shear parameter.
c	Cracked transformed section neutral axis depth.
c_1	Dimension of the square column cross-section
d	Slab depth
d/a	Depth to length Ratio
E_0	standard Young's modulus $(200\,kN/mm^2)$
E_{co}	Initial elastic modulus of concrete.
E_f or E_{FRP}	Young-Modulus of Fiber reinforcement
E_{fu}	Young's modulus of FRP tensile reinforcement
E_s	Young-Modulus of Steel reinforcement
F_u	Tensile capacity
K_c	Ratio of the second stress invariant in tension to that in compression
k	ratio of depth of neutral axis to reinforcement depth
L_1	Orthogonal of span beam one
L_2	Orthogonal of span beam two
V_0	Volume of water or ethanol in the cylinder before immersing the specimen.

V_1	Volume of water or ethanol when the specimen is immersed in the water or ethanol.
V_c	Concrete contribution (V_c) for shear design
V_{cr}	Cracking shear force
$V_{exp.}$	Experimental punching shear
V_f	FRP stirrup contribution for shear design
$V_{pred.}$	Punching shear capacity prediction
$V_{u,1}$	Shear resistance of orthogonal beam one
$V_{u,2}$	Shear resistance of orthogonal beam two
V_u	Punching shear resistance
v	Poisson's ratio
v_c	Design concrete shear stress
f_c	Compressive strength of concrete
f_c'	Mean cylinder compressive strength of concrete
f_{cd}'	design compressive strength of concrete N/mm^2
f_t	Tensile strength of concrete
f_t'	Tensile strength of concrete at the peak value of concrete stress.
f_u	Tensile strength
L	Specimen length
N	continuity effect of the slab on the punching capacity
n	Neuron
n_f	ratio of modulus of elasticity of FRP to the modulus of elasticity of concrete.
W	Weight matrix
u	peripheral length of loaded area
u_p	peripheral length of the design cross-section at *d*/2 from the loaded area

α	angle of the failure surface
α_p	Dilatancy
α_s	4 for interior columns, 3 for edge columns, and 2 for corner columns.
β_c	Ratio of the long side to short side of the column, concentrated load, or reaction area
Δ_{cr}	Cracking deflection
ΔV	Change in the cylinder volume reading when specimen is immersed in the water or ethanol.
Δ_u	Ultimate deflection
ε	Hyperbolic flow potential eccentricity
ε_c	Cmpressive strain of concrete at any stress σ_c
ε_{c1}	Strain at peak stress
ε_{cr}	Strain of concrete at peak stress (at cracking).
ε_{FRP}	Fiber Reinforcement Strain
ε_s	Steel Reinforcement Strain
γ_b	member standard safety factor generally equal 1.3
λ	Factor to account for concrete density
$\emptyset_c$	Material resistance factor
ψ	Dilation angle
ρ	Reinforcement Ratio
ρ_f	Fiber Reinforcement Ratio
μ	Viscosity
σ_{bo}/σ_{co}	Ratio of initial equibiaxial compressive yield stress to initial uniaxial compressive yield stress,
σ_t	Tensile stress of concrete.

CHAPTER ONE

INTRODUCTION

1.1 Background

Traditionally, the most prolific materials used in the construction industry are concrete, steel, timber, and stone. In the last twenty years, steel and reinforced concrete (RC) have become the most dominant elements in the building structure, since these are the most suitable materials to meet the increasing demand for infrastructure (Shi et al. 2012). However, they both (steel and concrete) suffer from different forms of deterioration. One of the main forms of degradation of RC is steel corrosion. Steel in any conventional concrete structures is initially protected against corrosion by concrete alkalinity. Usually, alkalinity of concrete results in durable construction, but, continuous exposure of deicing salt in the presence of moisture and chlorides reduces the concentration of the concrete alkalinity which results in the corrosion of steel reinforcement. Subsequently, deterioration of concrete is the ultimate resultant from the corrosion process. Composite materials made of fibres embedded in a polymeric resin, also known as the fibre-reinforcement polymer (FRP), are an alternative to steel reinforcement for concrete structures ACI Committee 440 (2015). FRP has been used in applications in the automotive and aerospace industries for more than 50 years, where their high strength and lightweight can be used to greatest advantage (Bisby 2003). In recent years, civil engineers have raised concerns about the durability of RC structures. As a result, they have been given increasing attention to advanced composite materials for reinforcing, strengthening, and rehabilitating existing and new civil engineering constructions. The key advantages of composites over other traditional materials are their low density

(FRP bars have a density ranging from 1/6 to 1/4 that of steel (ACI Committee 440 2015)), decreasing the cost of handling and transportation and high specific strength (tensile strength of FRP approximately two to three times of that of steel). In addition, FRP has good corrosion resistance, improved thermal insulation and low thermal expansion. However, the behaviour of FRP bars varies from that of steel in some aspects. For example, FRP bars don't show ductile behaviour in RC structures, FRP bars have perfectly linear-elastic behaviour until failure without a yielding point. Moreover, FRP bars have a relatively lower modulus of elasticity compared with that of steel (FRP modulus of elasticity is about 1/4 or 1/3 that of steel). Furthermore, FRP bars have different bond characteristics to steel bars, for example, sand-coated GFRP bars have adhesion and friction bond which homogeneously distribute the bond stresses along the embedded length of the bar, whereas, the deformed steel bars have a mechanical bond through bearing on the deformation parts of the steel bars. Therefore, GFRP bar-reinforced concrete structures exhibit lower average crack spacings than those of steel bar-reinforced concrete structures.

The RC flat slab is one of the most commonly used structural elements because it possesses many advantages in terms of architectural flexibility, use of space, easier formwork to construct, and shorter construction time required compared with the traditional type of construction (column, beam and slab construction). In addition, RC flat slabs usually reduce story heights with the ability to sustain heavy loads, which for example is very useful for car parks. Reinforced concrete structures are mostly subject to severe environmental conditions, such as freezing and thawing, which usually cause corrosion of the steel bar reinforcement. Adding Advantages of the two materials; FRP and the concrete would overcome the corrosion problem associated with the steel bars, and the

structure would become more sustainable compared to a steel reinforced concrete structure (SRCS). In contrast, the scarcity of analytical and experimental studies on the behaviour of concrete flat slabs reinforced with FRP bars limits the knowledge and understanding of the behaviour of such structures and consequently their wide use and applications. FRP current application in structures is in the form of reinforcing bars. Most known FRP reinforcing materials are made of continuous fibre embedded in a resin matrix. A key number of projects have been constructed using FRP for reinforcement, strengthening and rehabilitating concrete or steel structures all over the world, as can be seen in La Chancelière parking garage in Quebec City Canada (Ahmed et al. 2017) and Havenbrug Harbour Bridge in Holland (Murphy 2013).

1.2 Research Significance

Punching shear failure in flat slab-column connections is currently under an intensive study, with the aim of overcoming uncertainty in punching shear strength prediction, where punching develops in the slab around the column in a very brittle way and is followed by a sudden drop in the load-carrying capacity of the slab. This is particularly true for cases when FRP bars are used for reinforcing the concrete structure instead of conventional steel structural bars.

One of the main objectives of the research is to compare the behaviour of GFRP reinforced concrete slabs with other latest experimental results found in the field studies, such as those done by Dulude (2011); Bouguerra (2011), and Hassan (2014). It also presents experimental results regarding the effects of FRP flexure on the punching-shear capacity of flat slabs. In addition, the effects of perimeter to effective depth ratio on punching shear strength became one of the noteworthy parameter investigations for the prediction of the punching shear strength which had been started from 2013 covered 31 specimens measuring the tested critical

perimeter dimensions of the punching shear failures (Dulude et al. 2013; Hassan et al. 2013a; Hassan et al. 2013b). Moreover, effects of different reinforcement diameters with constant reinforcement ratio which was included in this project weren't addressed previously in the past research work. More test specimens are needed to cover a wider range of data, especially in this part of the mentioned parametric study to enable a more precise prediction of the punching shear stress. On the other hand, the accuracy of current equations in the FRP design codes and guidelines CSA S806 (2012), ACI 440(2015), and JSCE (JSCE et al. 1997) and other design approaches from the literature are assessed. This research also develops a new database of results from concentric punching shear tests of GFRP reinforced concrete flat slabs. Hence, this work aims to provide useful information to researchers and practising engineers. While FRP bar properties have been commercially improved, a review study of punching shear behaviour is required.

1.3 Research Aims and Objective

This study examined the behaviour of flat slabs reinforced with GFRP bars subjected to a concentric load for punching shear strength. The behaviour of the tested specimens was investigated experimentally and analytically.

The main objectives of the current research are summarised as follows:

1- To investigate the behaviour and punching shear capacity of interior slab-column connections subjected to concentric loads.

2- To analyse and examine the current equations used to calculate the punching shear capacity of RC flat slabs.

3- To provide recommendations for designers and researchers regarding the punching shear capacity of GFRP-RC flat slabs.

In addition to the three objectives mentioned above, the main objectives of the experimental study detailed in this research were summarised in the following points:

1- To examine the effects of different diameters of FRP bars (GFRP bars = 15.1 and 19.1 mm, steel bars = 10 mm) on punching shear strength.
2- To study the effects of effective depth on the punching shear strength (94 and 192 mm).
3- To examine the effects of concrete compressive strength on punching shear strength (between 35 N/mm^2 to 53N/mm^2).

The analytical study objectives were carried out by developing a three-dimensional nonlinear finite element model to investigate the effect of the following parameters on the behaviour of the flat slab specimens under concentric load:

1- To develop a three-dimensional nonlinear finite element model to analyse the behaviour of GFRP reinforced concrete flat slabs subjected to concentric load and conduct a series of parametric studies. The proposed model will be evaluated against the current and previous experimental study results.
2- To study the effects of reinforcement ratio on the punching shear strength (1.0 and 1.5% for slab depth 150 mm; 0.85%, 1.1%, 1.5%, and 2.1% for slabs depth 250 mm).
3- Variations of the shear perimeter to depth ratio corresponding to square column cross-section sizes of 150, 200, 300, 400 mm with a slab thickness of 150 mm and 250 mm.
4- Investigate the effects of a wider range of concrete compressive strength on punching shear strength (30 N/mm^2, 50 N/mm^2, and 70 N/mm^2).

In addition to the three-dimensional nonlinear finite element method Artificial Neural Networks (ANN) tool is also used to investigate the effect of the following parameters on the behaviour of the flat slab specimens under concentric load:

1- ANN are used in this research to predict punching shear strength, and the trained ANN model will be evaluated against the present and previous experimental study results, moreover, a series of parametric studies will also be conducted.
2- To study the effects of effective depth on the punching shear strength (90 mm, 128 mm, 166 mm, 204 mm, 242 mm, and 280 mm).
3- To investigate the effects of column perimeter on punching shear strength (500 mm, 760 mm, 1020 mm, 1280 mm, 1540 mm, and 1800 mm).
4- To examine the effects of flexural reinforcement Young Modulus on punching shear strength (34000 MPa, 41200 MPa, 48400 MPa, 55600 MPa, 62800 MPa, and 70000 MPa).
5- To investigate the effects of concrete compressive strength on punching shear strength (28 MPa, 38 MPa, 46 MPa, 54 MPa, 62 MPa, and 70 MPa).
6- Examine a wider range of flexural reinforcement ratios corresponding to variable reinforcement diameters and constant spacing (0.15, 0.46, 0.77, 1.08, 1.32, and 1.63).

1.4 Methodology

This research aimed to examine GFRP reinforced concrete flat slab specimens under punching shear when subjected to concentric gravity loading. To achieve the aims and objectives of this research, six concrete flat slabs reinforced with GFRP and steel bars were constructed and tested to study the influence of three

parameters namely; (i) concrete compressive strength (f_c), (ii) slab depth (d), and, FRP bars diameters. Moreover, a database in the open literature collected for analysis and examining the current equations were used to calculate the prediction of punching shear capacity of RC flat slabs. In addition, experimental results of punching shear strength of flat slabs from the collected database were compared with the theoretical results derived from codes of practice, i.e. CSA S806 (2012); ACI 440. 1R-15 (2015), and JSCE (1997). A three-dimensional nonlinear finite element software ABAQUS 6. 14 was used to develop a model to analyse the effect of different parameters considered in this research on the behaviour of GFRP reinforced concrete flat slabs subjected to concentric gravity load. Moreover, an ANN was also used to predict punching shear strength of a GFRP reinforced concrete flat slab. A series of parametric studies were created from the resultant model. Furthermore, the proposed model was also evaluated against the present and previous experimental study results.

1.5 Report Organisation

This thesis is organised into six chapters. This chapter (chapter one) is an introduction to the study in general. The research aims and objectives are clearly set out in this chapter followed by the methodology to achieve these objectives.

Chapter two includes a review of the critical studies conducted on the punching shear of FRP reinforced two-way slabs or slab deck bridges with general physical and mechanical properties of FRP. It also includes a discussion of different parameters that influence the behaviour of FRP reinforced flat slabs according to the available research in the open literature. This enables some conclusions to be drawn on the effect of key parameters on the punching shear behaviour of FRP reinforced concrete flat slabs. Finally, an introduction is given to the analytical study of predicting punching shear strength.

Chapter three presents the experimental investigation conducted on punching shear FRP reinforced concrete flat slabs covering the description of the test specimens, the details of the instrumentation, as well as the test set-up and procedure. It also includes the analysis and discussion of the experimental phase in terms of mode of failure, ultimate strength and deflections in the slabs. In addition, provisions and analysis of codes and guidelines that have been published are presented in the chapter three which deal with prediction of punching shear strength of FRP reinforced concrete flat slab.

An overview of the finite element (FE) software (ABAQUS 6.14) is presented in chapter four for analytical phase. A three-dimensional FE model is proposed to analyse the behaviour of GFRP reinforced concrete flat slabs. The proposed FE model is verified against experimental results of the current study as well as some case studies from the open literature. In addition, the validated FE model is used for analysis and discussion of the parametric study. The parametric study aims to explore the behaviour of GFRP reinforced concrete flat slab with extended parameter variations.

Chapter five describes the development of the nonlinear ANN technique to predict the punching shear capacity of flat slabs reinforced with FRP. It also demonstrates the application and input structure of the program, along with the results. A series of parametric studies are carried out from the ANN modelling result. The main aim of this chapter is to study the effects of main parameters on the punching shear strength of GFRP reinforced concrete flat slab.

Finally, Chapter six presents the current research conclusions as well as recommendation and suggestions for future work.

CHAPTER TWO

LITERATURE REVIEW

2.1 Introduction

Many research projects have been carried out to investigate the flexural behaviour of concrete members reinforced with FRP bars. However, the shear behaviour in general and punching shear of flat slab floors reinforced with FRP bars has not yet been thoroughly examined.

The punching shear strength is significant when considering connecting systems with flat slab floors. Despite the relatively high strength of FRP, sudden failure is a characteristic of these composite materials. Most research into punching shear behaviour has been conducted on conventional steel reinforced concrete (SRC) flat slabs. As a result, when FRP is used as reinforcement in concrete instead of traditional steel, most codes of practice were modified in order to be applied. The codes took into consideration the differences in mechanical properties between FRP and conventional steel reinforcement. Because the properties of commercial FRP bars have been improved over time, a study revising their punching shear behaviour is required. Moreover, compared to SRC, the combination of the matrix phase (the hydration reactions between water and cement, which serves as the matrix phase for mortar and concrete) with the new reinforcing phase (concrete-matrix phase with FRP bars reinforcement concrete flat slabs) produces a new material system, which requires further experimental study for its behaviour to be adequately determined. For this reason, changes have been introduced to compensate for the differences between the properties of reinforcement material by reducing the shear strength of concrete members reinforced with FRP bars; indeed, most commercial FRP bars have a lower modulus of elasticity compared

to steel bars. However, few research studies have addressed the punching shear behaviour of slabs reinforced by FRP bars .

An overview is presented in this chapter of the most vital information on FRP reinforced concrete flat slabs. The literature of this research started with general properties of FRP including mechanical and physical properties. Followed by an explanation of two modes of concrete flat slab failure, and, then brief literature on punching shear of SRC flat slabs. A review of punching shear of FRP reinforced concrete flat slabs with different parameters that affect the behaviour of FRP reinforced concrete flat slab under concentric load. After that, a literature review of computational nonlinear analysis and ANN are given with a brief definition. Some numerical methods for prediction punching shear of FRP reinforced concrete flat slab introduced with an explanation before ending the chapter with a conclusion.

2.2 Properties of FRP bars

Commercially available FRP reinforcement bars were introduced as a solution for the steel bar corrosion problem of reinforced concrete structures in the late 1980s (Nanni et al. 2014). Demand in the market for non-ferrous reinforcing bars increased greatly because the combination of chlorides and CO_2 in the presence of moisture led to the corrosion of the steel reinforcement. The most common material type for FRP reinforcement bar is glass fibre. There is no rival in the market to compete with GFRP, especially E-glass type GFRP, in terms of cost and specific strength properties. For this reason, it is preferable to carbon and aramid in most RC applications (Nanni et al. 2014).

2.2.1 Physical properties of FRP composites

The concept of polymeric resin controlling the physical nature of FRP composites was illustrated by Nanni et al (2014). The most significant factors are the fibre-type and fibre-volume fraction, which is defined as the ratio of the volume of fibre to the overall volume of the bar. The density of the FRP material is one-sixth to one-fourth of that of steel. The coefficients of thermal expansion of FRP bars are different in the longitudinal and transverse directions. The longitudinal coefficient of thermal expansion depends on the properties of the fibres, while the transverse coefficient depends on the properties of the resin (ACI Committee 440 2015). Hollaway (2010) mentioned that the most dominant properties of polymers are physical and in-service characteristics. Conventional thermosetting matrices are considered to be brittle due to increase in cross-linking density observed during polymerisation (Hollaway 2010).

2.2.2 Mechanical properties of FRP bars

The mechanical characteristics of the polymer composite are determined by the fibre and the quality of the fibre matrix interface. The bar manufacturing process, quality control and rate of thermoset resin curing can also affect tensile strength (ACI Committee 440 2015). The tensile behaviour of FRP bars is represented by a linear-elastic stress-strain relationship, up to failure (Abdalla 2002). FRP in most cases can have high tensile strength, but a lower tensile modulus of elasticity compared to that of steel. In addition, FRP bars have different tensile strengths according to diameter (Nanni et al. 2014). The tensile strength of FRP bars (Glass FRP, Carbon FRP and Aramid FRP) is limited between 483 N/mm^2 to 3689 N/mm^2. On the other hand, the compressive strength reduction of the three FRP types mentioned is between 22 % - 80 % compared to the tensile strength. Basalt composite bars are a new entry into the construction industry

and have promising properties and manufacturing costs. They are non-corrosive, and have a tensile strength three times that of standard steel bars used in the construction of buildings (Thorhallsson et al. 2013). On the other hand, testing the compressive strength of FRP bars is very complicated due to the anisotropic and non-homogeneous nature of the FRP material, which in most cases leads to incorrect measurements. Figure 2-1 shows the stress-strain diagram for three materials carbon fibre reinforced polymer (CFRP), GFRP, and Steel.

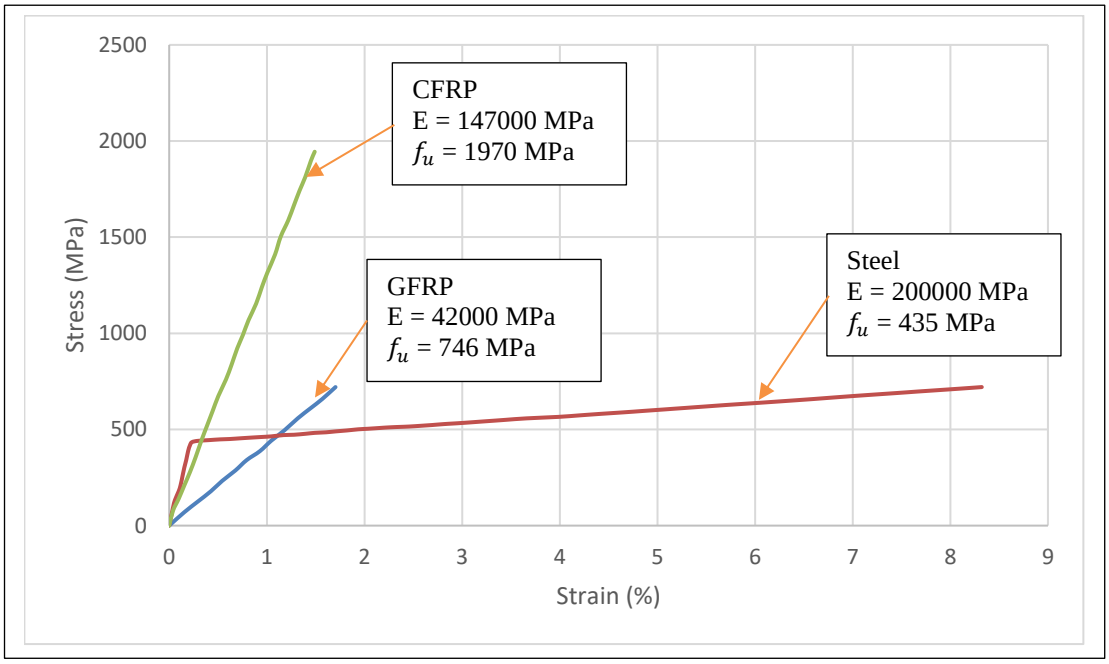

Figure 2-1. Material characteristic of FRP and steel reinforcement (Abdalla 2002)

2.2.3 Transverse shear behaviour of FRP bars

Properties of the matrix are the most dominant factors influencing the behaviour of FRP under transverse shear loading. FRP bars are generally weak in transverse shear. However, shear strength can be increased by braiding or winding additional fibres in the direction transverse to the longitudinal one. In most cases, the shear strength of FRP bars varies between 30 to 50 MPa (Nanni et al. 2014).

2.3 Failure modes of the concrete flat slab

Failure types of flat slab structure had been classified into flexural failure and punching shear failure.

2.3.1 Flexural Failure

Bending moments is the reason behind the flexural failure in which compressive stress is induced in one side of the slab and tensile in the opposite side. In the typical design code of practice, it is assumed that reinforcement bars are usually resisting tensile stress while concrete is resisting compressive stress. It is common to design concrete section reinforced with steel bars under reinforcement to avoid concrete crushing before steel yielding. A ductile behaviour of steel bars in an inelastic region of stress-strain relationship is not available for FRP bars due to the linear elastic behaviour of FRP materials.

2.3.1.1 *Tension failure*

Tension failure is defined by the failure of the reinforcement bars in tension side before the failure of concrete in the compression side. The reinforcement bars will reach its design failure strain before the concrete reaches its ultimate compressive strain. The design failure strain in steel bars is defined by the yield strain which has a negative effect on the punching shear capacity due to the increase of concrete cracks in part. Increasing the width and the depth of cracks in concrete will reduce the compression area in a section, which also partner to resist the shear stress. Although this failure is providing enough warning before it takes place, some codes like Canadian standards (CSA/A23.3-14) permit this type of failure. On the other hand, a rupture strain of FRP bars is a definition of the design failure strain, due to the elastic mechanical behaviour of FRP up to failure. This failure will significantly reduce the cross-sectional area which is

designed to resist punching shear capacity. As a result, sudden failure is more likely to occur in this case with a brittle way of failure.

2.3.1.2 *Balanced failure*

This type of failure rarely happens in the practical field. The failure occurs when the concrete reaches its ultimate compressive strain in compression side while the reinforcement bars reach their design failure strain in the tension side.

2.3.1.3 *Compressive failure*

This failure takes place when the concrete crushes before the reinforcement bars reach their designed failure in quite low strain level. For SRCS, all design codes recommend avoiding this type of failure due to the limited warning before failure. In case of steel, this failure will result in a small degree of cracking before the reinforcement bars reach their yield strain with excessive cross-sectional area resisting the punching shear capacity. In the case of FRP reinforced concrete members, some codes prefer the failure to occur through concrete crushing before the reinforcement bars reach their ultimate strain due to the fact that those members exhibit deformability by the plastic behaviour of the concrete.

2.3.2 Punching Shear Failure

Concrete flat slabs usually encounter two failure mechanisms, which are the one-way shear typical to that of beams and two-way shear. The first type of failure usually is not critical and rarely occurs in concrete flat slabs, whereas, the two-way shear is a failure which surrounds the column creating a cone shape as shown in Figure 2-2. This failure mechanism is called punching shear and usually happens in flat plates and footing.

Figure 2-2. Piper's Row Car Park, Wolverhampton, UK, 1997 (built in 1965) (Zhang 2003)

Since punching shear failure in flat slab-column connections is sudden and brittle, it is a critical part of the design. High transverse stress is produced by the shear force from the slab to the columns causing this type of failure. The design of slab-column connections depends on how precise the calculations are of prediction of shear stress caused by shear forces to prevent the punching shear failure. Moreover, to obtain the optimum performance of flat slab-column connections the design detail is essential.

Resistance to shear in any reinforced concrete slab is usually provided by both concrete and shear reinforcement. In addition, the flexural reinforcement has an influence on the concrete resistance against shear stress. Most FRP reinforced concrete flat slabs are expected to have wider cracks and a higher position of the neutral axis compared to that of SRC flat slabs. Consequently, there is a lower amount of uncracked concrete which supposed to resist the shear stress. Moreover, the anisotropic FRP bars materials with high strength in the longitudinal direction are large compared to the transverse direction which is relatively smaller in strength and stiffness. This will lead to less contribution to

shear resistance due to smaller dowel action of FRP compared to that of steel reinforced concrete structures (SRCS) (ACI Committee 440 2015). Therefore, in general, the resistance of FRP bar-reinforced concrete structures is smaller than that of SRCS; hence, it is not accurate to directly implement the code equations which are used for SRCS for those reinforced with FRP bars.

2.4 Punching shear of steel reinforced concrete flat slabs

Punching shear in flat slabs is one of the most critical failure modes, which is categorised in most cases as a brittle failure. The brittle failure of concrete structures, which are characterised by a sudden decline of load at increasing deflection after the peak stress point, cannot be adequately described by plastic limit analysis, because the failure does not occur simultaneously along the ultimate failure surface (except for very small structures) (Bazant and Cao 1987). In order to overcome this phenomenon, different types of shear reinforcement have been used in flat slabs and bridge deck slabs. Due to this wide variety of shear reinforcement, there are considerable differences in assumptions made in codes of practice and the resulting equations, which consequently lead to uncertainties about their reliability.

Mokhtar (1985) conducted experiments on eight full slab-column connections subjected to concentric loads. Seven specimens were reinforced against punching shear by shear studs, i.e. vertical bars welded at their tops to square anchor heads and at the bottom to a steel strip. The objective was to verify the effectiveness of the stud reinforcement in lightweight slabs, and to determine how the strength is affected by the provision of concrete cover above and below the anchors, as a further verification of the design procedure for this type of reinforcement. Results confirmed that the use of shear stud reinforcement greatly increases the strength and ductility of the slab-column connection. Moreover, the

load-deflection path is approximately the same for the slabs with and without shear reinforcement. The effect of thickness was not considered in this research as all slabs were 150 mm thick, and were categorised as thin slabs. Further investigations were required to examine the influence of slab thickness. Bazant (1987) performed punching shear strength tests on different sizes of RC slabs. In order to determine the effect of slab size, a series of tests of small specimens were carried out. Three reinforced circular slabs with three different thicknesses were cast, cured, and loaded to failure. It was found that the nominal shear stress at failure was not constant, as assumed in previous design formulae, but decreased as the slab size increased. Moreover, it was noted that the punching shear behaviour of thin slabs is closer to plasticity, while in thick slabs, it is closer to linear elastic fracture mechanics. On the other hand, Yamada et al. (1992) conducted thirteen punching shear tests of typical slab-to-column connection specimens. The dimensions of the slab were 2×2×0.2 m, with a centrally located column 0.3×0.3 m in cross section. One of the main objectives in this research was to investigate several types of reinforcement, such as welded-wire fabric, studs, bent bars, and hooked bars. The shear reinforcement ratio was assessed and found to improve both punching shear resistance and ductility. However, additional experimental work was needed to study the effect of reinforcement quantity. Guandalini (2009) presented the results of a series of tests on the punching behaviour of slabs with varying flexural reinforcement ratios and without transverse reinforcement. The aim of the tests was to investigate the behaviour of slabs failing in punching shear with low reinforcement ratios. The results were compared with design codes, and to critical shear crack theory. The ACI 318-08 (2008) formulation can lead to less conservative estimates of the punching strength compared to the test results for thick slabs and for lower reinforcement

ratios. However, further investigation was required into the basis of theoretical and experimental tests to confirm some hypotheses, such as the critical shear crack and yield line theories. Another set of studies were recently commenced with the aim of confirming the applicability of hypotheses with greater attention to the combination of depth, reinforcement ratio and the critical punching shear parameter. Rizk (2013) developed a formula to calculate minimum shear reinforcement to prevent brittle failure in the vicinity of concentrated loads in thick plates, concrete walls and slab-column connections . Calculation of minimum shear reinforcement was required to prevent brittle shear failure for thick concrete plates and walls in the vicinity of concentrated loads, as presented by two models. The first model was a modification of compression field theory, while the second was based on the diagonal shear cracking load. Both model versions for the slab size are affected by the principles of fracture mechanics. In their conclusion, Rizk (2013) added the recommendation to use shear reinforcement for the slab in the vicinity of a connection with columns. Moreover, Caldentey (2013) investigated different stirrup dispositions in eight concrete slab samples considering four different rebar disposition typologies. The slabs were rested on eight supporting points at 1.25 m from the centre of each slab. The samples tested were concrete slabs with dimensions of 2.8 m length, 2.8 m width and 0.25 m depth. Columns were 0.45 m long and 0.45 m wide. Reinforcement was used in different positions and links with the diameter sizes of 8 mm at a distance of 150 mm c/c, while the main flexural steel was 20 mm at 200 mm c/c. The main objective was to present the results and conclusions from the punching shear tests. Moreover, Caldentey (2013) showed the importance of stirrup detailing in the ultimate punching shear strength, and practically added common construction disposition. It was concluded that there are similarities in deflection and stiffness behaviour for all

slabs. Moreover, there was good agreement between failure loads with the values calculated using design codes EHE-2008, ACI 318-08, Eurocode 2, and FIB Model Code 2010. Due to the number of structural specimens done in laboratory using either materials, steel or FRP as structural reinforcement, the behaviour of steel reinforcement in concrete structures is more familiar compared to that of FRP reinforcement. However, steel presents corrosion problems, especially if exposed to the environment. The principal reason for using another material for concrete reinforcement has emerged during the last two decades. FRP rebar was the most candidate materials to replace the steel reinforcement in concrete because of its mechanical properties and corrosion resistance.

2.5 Punching shear of FRP reinforced concrete flat slabs

Several research campaigns have been conducted because of the differences in properties between steel and FRP bars, which aid in the investigation of the behaviour of concrete structures reinforced with FRP bars. However, few tests were carried for FRP reinforced concrete flat slabs connected to a column; hence, further research is required to find more reliable and practical ways to predict punching shear capacity. In the following sections, evaluating the different parameters that influence the behaviour of FRP reinforced flat slabs will be discussed with respect to the available research in the open literature. The reinforcing volume fractions examined fall into the limited range from 30-70 %, while reinforced concrete in general rarely has been tested at greater than 5 % (Bernard Potyrala 2011). On the other hand, the thickness of the investigated specimen slabs ranged from 75 mm to 350 mm. Furthermore, the concrete compressive strength is one of the dominant parameters affecting the value of punching shear strength of flat slabs. The minimum value of concrete compressive strength used in previous studies was 26 MPa, while the maximum

was 76 MPa. The effect of column shape and slab span length on the punching shear strength has not been sufficiently investigated for flat slabs.

Some studies demonstrate that the differences between FRP bars and steel bar-reinforced concrete flat slabs can affect the slab punching behaviour (Ospina et al. 2003), whereas, some have examined the punching shear behaviour of FRP reinforced concrete flat slabs. These studies include parameters such as FRP reinforcement ratio, concrete strength, slab thickness, column area and FRP types. Only two types of FRP bars have been used in all the existing studies (CFRP and GFRP). In addition, two structural types were investigated by previous researchers in this field: concrete flat slabs, and concrete deck slabs. The principle of both types of structure is the same, with the main difference being the column geometry. A square column dimension was used for two-way flat slabs, while rectangular column dimensions were used in the case of concrete deck slabs to simulate the footprint of truck tyres. Besides, most of the previously investigated specimens in the case of concrete deck slabs were supported in one direction. A square column connected to FRP reinforced concrete flat slab is considered in the current study.

2.5.1 Effect of FRP flexural reinforcement ratio

FRP has a brittle elastic response and, compared to steel, a lower elastic stiffness and distinctive binding feature which leads to wider cracks and reduced depth to the neutral axis. This led to smaller compression region of the cross-section with wider crack widths. Consequently, a smaller shear resistance provided by both aggregate interlock and compressed concrete. Research indicated that the stiffness of the tensile reinforcement has an influence on the shear capacity of flexural members without shear reinforcement (Nagasaka et al. 1993; Zhao et al. 1995; Michaluk et al. 1998; Tureyen and Frosch 2002). The contribution of

flexural reinforcement FRP reinforced concrete flat slab without shear reinforcement on punching shear capacity in term of dowel action has not been yet determined (ACI Committee 440 2015), because of the lower stiffness of FRP bars in the transverse direction as mentioned previously. However, the contribution of FRP reinforced concrete structure is assumed to be less than that of an equivalent steel reinforced area; hence further research is required to compute this effect. The influence of tensile reinforcement on punching shear capacity is also induced in flat slab structures. It has been an evidence that the axial stiffness of the FRP reinforcement is significantly affects the transverse shear response of FRP reinforced concrete flat slab connected by interior column (Ahmad 1993; Banthia 1995; Matthys and Taerwe 2000; El-Ghandour et al. 2003; Ospina et al. 2003; Lee 2009; Dulude et al. 2013; Hassan et al. 2013a; Hassan et al. 2013b; Sayed 2015). Experimental results of isolated FRP reinforced concrete flat slabs specimens subjected to a concentric load for punching shear strength shows lower punching shear capacity, lower stiffness in the cracked state (post-cracking stiffness), and greater crack width than those of their counterparts reinforced with steel bars when the same flexural reinforcement amount was used. This result from smaller dowel action and smaller uncracked compression zone as a result of a lower modulus of elasticity of FRP bars comparing with that of steel bars (Theodorakopoulos and Swamy 2007). Banthia (1995) reported that all concrete slabs reinforced with FRP grids absorbed less energy than slabs reinforced with a steel grid. This was attributed to the brittle nature of the FRP composites. It is worth mentioning that the greatest drawback of Ahmad (1994) and Banthia (1995) studies was that specimen sizes were very small compared to that of the latest studies in the punching shear strength of FRP reinforced concrete flat slab. An experimental study of larger specimens was

needed to simulate realistic slabs found in practice. Matthys and Taerwe (2000) investigated the effect of variable longitudinal tensile reinforcement ratio of a total seventeen GFRP and steel reinforced interior slab-column connections. They concluded that slabs reinforced with a similar flexural stiffness as that of steel reinforced slabs, the behaviour of the slabs were similar to that of steel reinforcement slabs. They observed a strong interaction between shear and flexure was noted for most of the tested slabs. They also mentioned in order to achieve the same punching shear strength as that exhibited by the steel reinforced flat slab, the reinforcement ratio and slab depth for FRP-reinforced slabs must be increased. El-Ghandour (2003) carried out an experimental program investigating the punching shear behaviour of FRP reinforced concrete flat slabs using two material types, CFRP bars and GFRP. Results showed a significant load capacity increase for slabs reinforced with CFRP flexural bars due to the higher modulus of elasticity of the CFRP material, which led to a larger area of concrete in compression. Moreover, El-Ghandour (2003) recommended smaller flexural bar spacing to eliminate the problems of concrete splitting and prevent bond slip failure in the case of slabs. Punching shear failure in FRP reinforced flat slabs is brittle and sudden, although Ospina et al (2003) show that two-way concrete flat slab reinforced with FRP grids rather than bars do not exhibit a sudden drop at punching shear failure. However, the punching shear capacity provided by FRP grids may not the same as the FRP bars due to the difference in bond behaviour and the concentration of stresses in the grids at the locations of the cross ribs led to more slip in the elastic cracked stage and more gradual load drop at ultimate rather than sudden. Moreover, due to the high tensile strength of FRP bars, the behaviour of FRP concrete slabs is controlled mainly by shear rather than flexure. Zaghloul (2003b) investigated the effects of

flexural reinforcement ratio, moment to shear ratio, the type of reinforcement, and the slab thickness in the behaviour of internal slab-column connections reinforced with CFRP grids tested under eccentric load. A notice was made by Zaghloul (2003b) that an increase in reinforcement ratio increases both strength and stiffness of the column-slab connection but the relationship is not linear. On the other hand, Theodorakopoulos and Swamy (2007) developed a method to evaluate the punching shear capacity of internally FRP reinforced slab-column connections without shear reinforcement which incorporates the effects of the FRP elastic modulus, bond characteristics, and ultimate tensile strength, which are appropriately different to those of steel. Theodorakopoulos and Swamy (2007) were found no concern about the differences between specified and test characteristics of the FRP reinforcement with reference to the predicted punching load. It should be quantifying the effects of the difference between nominal and test properties of FRP reinforcement to determine which values should be used when the proposed theoretical analysis is employed to predict the results of FRP slab tests. Lee (2009) investigated the effects of concentrating the reinforcement in the immediate column region and the conclusion was made a higher punching shear strength, more uniform distribution of strains in the top flexural bars, and better crack control a achieved when the top concentrating mat of flexural reinforcement was used within a distance of 1.5 times the slab thickness from the column faces compared to the companion slab with a uniform distribution of the same amount of reinforcement. Hassan et al (2013a) investigated eight specimens with different reinforcement ratio and depths. The first comparison was between two counterpart samples in series one and two. The two series had same slabs thickness but varied in reinforcement ratio and column size. Regardless of concrete strength, the results of the first two series with 200 mm

thickness showed that there was an increase in load capacities of about 18% and 14% for slabs with reinforcement ratios of 0.7% and 1.6%, respectively. In the case of a slab thickness of 350 mm, the results showed an increase of about 9% and 14% in load capacities for reinforcement ratios of 0.3% and 0.7%, respectively. Hassan et al (2013a) stated that an increase in the FRP reinforcement tension ratio led to a stiffer response in the elastic-cracking stage, increases punching shear capacity, lower reinforcement and concrete strains, reduces the ultimate slab deflection. Hassan et al (2013b) examined 10 more full-scale interior slab-column connections to two-way slabs reinforced with GFRP. At the failure Hassan et al (2013b) showed that the punching shear stress was proportional to the effective reinforcement ratio ($\rho_f \, E_f / E_s$) to the power of 0.34, which agrees with CSA S806 CSA S806 (Canadian Standards 2012) and BS8110 (British Standard 1997). Furthermore, Nguyen-Minh (2012) carried out a new fracture-mechanics-based empirical formula to estimate the punching shear resistance of interior GFRP reinforced slab-column connections. Both the size factor and the effect of the span to effective depth ratio (L/d) ware calculated by Nguyen-Minh (2012) and recommended to be taken into account in calculating the punching shear resistance of the FRP reinforced concrete flat slab. On the other hand, a series of developmental investigations were conducted by Dulude et al (2011); and (2013) to study the structural behaviour of GFRP-reinforced concrete in two-way slabs. The results showed that increasing the reinforcement ratio of the GFRP-reinforced by half for the two depths (200 mm and 350 mm) increased the normalized punching shear stress by 39% and 49%, respectively, for the counterpart specimens. The Dulude et al (2013) reinforcement ratio investigation showed a comparable normalized punching shear stress when the reinforcement ratio increased by two compared to the results of Ospina (2003),

Zaghloul (2003a), and Nguyen-Minh (2012). On the other hand, Sayed (2015) studied the FRP reinforced concrete interior slab-column connections subjected to eccentric load. The deflection and strain in the reinforcing bars increased due to unbalanced moment, the variation increment was between 9 to 12% and 7 to 8% at service and ultimate stages, respectively. Hassan et al (2017) showed by statistical analysis that the punching shear capacity was nonlinearly proportional to flexural reinforcement axial stiffness to the power of 0.336.

2.5.2 Effect of concrete compressive strength

High-strength concrete (HSC) is categorised by higher compressive strength, higher tensile strengths, and higher modulus of elasticity than normal-strength concrete (NSC). HSC improve the punching shear capacity by allowing a higher force to be shifted through the slab-column connection due to the increase of HSC tensile strength (Mendis 2003). There were a limited number of specimens reinforced with FRP bars fabricated using HSC. Banthia (1995) determined the influence of concrete strength and the use of fibre-reinforced concrete. There was no significant change in punching shear strength between two counterpart slabs with normal concrete strength and high concrete strength. This result was expected to be very close where the margin values of concrete strength used for comparison between the two specimens was 12 MPa. Moreover, Matthys and Taerwe (2000) and Zhang (2003) investigated specimens with the concrete compressive strength of 118 MPa and 71 MPa, respectively. In addition, the effects of concrete strength were considered in Hassan et al (2013b) study. Hassan et al (Hassan et al. 2013a; 2013b) stated that using high strength concrete for the GFRP reinforced concrete flat slab improved punching shear capacity, reduced concrete strains, and increased strains in the GFRP reinforcement. In the case of the specimen thickness of 200 mm, the ultimate

punching shear capacity increased by 27% when the concrete compressive strength rose from 38.6 to 75.8 MPa, when compared with that of the counterpart normal strength concrete flat slab. The specimen with the thickness of 350 mm increased the punching shear capacity by about 7% compared with that of the counterpart normal strength concrete flat slab. The Hassan et al (2013b) concrete strength investigation showed a reduction effect of the concrete compressive strength on the punching shear strength when slab depth increased. In the current research, the concrete compressive strength effect remained constant on the punching shear strength when the slab depth increased from 150 mm to 250 mm. On the other hand, usually the application of concrete compressive strength in the equations of punching shear strength is limited to a certain range in the most design of FRP codes and guides line, for example, CSA S806 (2012) which 60 MPa is the maximum concrete strength that must be used in calculating punching shear strength. Concrete strength was one of the parameters included in Sayed (2015) research. The study revealed that increasing concrete compressive strength slightly enhanced the punching shear capacity. It was also recorded that when the actual high concrete compressive strength value for one of the specimens used in the equation of the CSA S806 (2012) code yielded better results despite the limitation of 60 MPa by the code. Thus, further investigation for a wider range of HSC should be examined, with concentrated loading acting in the middle of the flat slab geometry to quantify effect HSC on punching shear strength and verifying the accuracy with the current punching shear prevision.

2.5.3 Effect of FRP flexural reinforcement arrangement

Lee (2009) investigated the effects of concentrating slab reinforcement around the column area. Six specimens were divided into two series: a series of slabs

reinforced with conventional steel bars and another reinforced with GFRP bars. The reinforcement ratio and arrangement were considered at a distance of 1.5 times the slab thickness from the column face. Two of the specimens were reinforced by uniformly distributed reinforcement ratio of 1%: the first was reinforced by steel bars and the second was reinforced by GFRP bars. The other two counterpart specimens reinforced by a banded concentrated reinforcement ratio of 2% at 1.5 times the slab thickness from the column face. The fifth specimen was reinforced with a banded distribution of approximately 3%. The last specimen was reinforced with 3% reinforcement, but steel fibre was added to the concrete.

Due to the lower modulus of elasticity of GFRP bars, the test results showed that GFRP reinforced concrete flat slab had a considerably lower punching shear capacity than the slabs reinforced with steel reinforcing bars. Moreover, it should lower post-cracking stiffness and greater deflections than the slabs reinforced with steel reinforcement bars. It recorded a lower punching shear of slabs reinforced with GFRP by 22 and 26% from the counterpart slabs reinforced by the steel reinforcing bars. In addition, more cracks were produced in the immediate column region than that of the slabs reinforced with steel bars. On the other hand, the test results also revealed that concentration of the flexural reinforcement within a distance 1.5 times the slab thickness from the column faces resulted to some extent in higher punching shear strength and greater post-cracking stiffness compared to that of the counterpart slab reinforced by a uniform distribution of the same amount of reinforcement. It is also concluded that the flexural bars resulted in a more uniform distribution of strains and improved crack control. Banded distribution of the reinforcement resulted in an increase in punching resistance by 5% in the case of steel reinforcement specimens,

whereas, the GFRP reinforcement specimens resulted in a rise of 11%. However, it is an ineffective way if excessive concentrations of the slab reinforcement were used to increase punching resistance of GFRP reinforced concrete flat slabs.

2.5.4 Effect of column dimensions

Hassan et al (2013a) included two cross-section column sizes (300 and 450 mm) in their study. The failure surfaces were increased due to an increase in the column dimensions which led to a reduction in the punching shear stress at failure. At failure, the decreases ratio in punching shear stress were varied between 7% to 24%. Dulude et al (2013) used the same specimens like that of Hassan et al (2013a) in their comparison of column sizes. Dulude et al (2013) mentioned in their conclusions that the column dimensions have a noticeable effect on the tested samples, especially the samples with low reinforcement ratios, which is not the same case in Hassan et al (2013a). They also added in their conclusion that increasing of column dimensions also results in an increase of failure surfaces and, consequently, the punching shear stress at the failure was reduced. Increasing the square column dimensions from 300 to 450 mm decreased the normalized punching shear stress at failure of the four counterpart specimens ($G_{(0.7)}$45/20, $G_{(1.6)}$45/20, $G_{(0.3)}$45/35, and $G_{(0.7)}$45/35 prototypes by 29%, 14%, 37%, and 12% compared to their counterparts ($G_{(0.7)}$30/20, $G_{(1.6)}$30/20, $G_{(0.3)}$30/35, and $G_{(0.7)}$30/35, respectively).

Matthys and Taerwe (2000) involved different load patch diameters in their investigation of slabs reinforced with FRP bars under concentric load. The results showed an increase in failure load due to the rise in load patch diameter. However, this effect was less pronounced (less than 7% increase in maximum failure load recorded) than the influence of the reinforcement and thickness of the

slab. On the other hand, Hassan et al (2017) declared the same observations for steel reinforced concrete slabs in the literature that the variation of column sizes decreased the punching shear stress on a control perimeter at $d/2$ from the column face with increased column size (Figure 2-3).

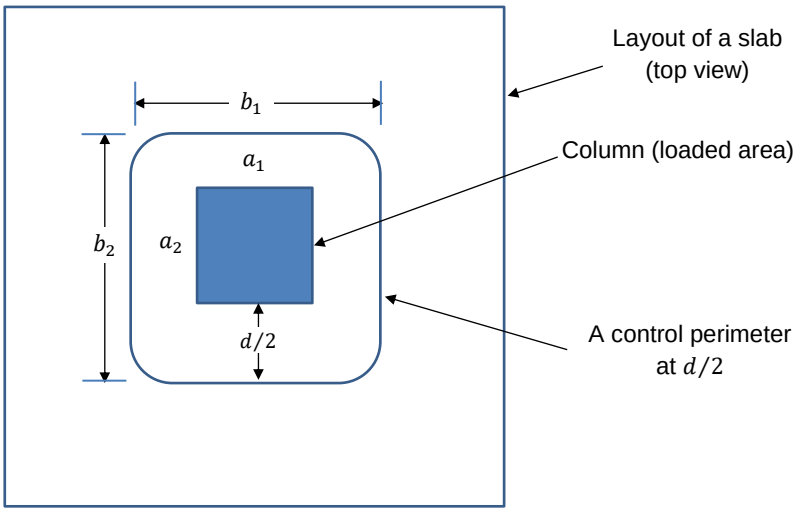

Figure 2-3. Basic control perimeter for $d/2$ from the loaded area

2.5.5 Effect of effective depth

Matthys and Taerwe (2000) investigated the effect of slab depths. Their conclusion showed that for slabs with similar flexural stiffness and concrete compressive strength, the effect of an increased slab thickness on the punching shear resistance was more pronounced than the effect of an increased reinforcement ratio and patch dimension. On the other hand, Zaghloul (2003a) and (2003b) considered only the main parameters such as reinforcement ratio, type of reinforcement, slab thickness and column aspect. Based on Zaghloul's evaluation of the test results, the thickness of the FRP reinforced slabs should be increased by 25 % to achieve both higher stiffness and strength, despite a lower reinforcement ratio.

Dulude et al (2013) studied the effect of slab thickness on the punching shear capacity and concluded that this parameter significantly affected punching shear

capacity. The normalised punching shear stress increased by an average of 63% at failure, when keeping the same reinforcement ratio and increasing the effective depth by approximately 115%. Dulude et al (2013) also mentioned in their conclusions that due to more and wider cracks in the case of low reinforcement ratios, the reduction in the shear span-depth ratio contributes to reducing the deflection, as it reduces the moment at the same applied load. However, the deflection was not significantly reduced in the case of slabs with high reinforcement ratios, as the flexural cracks were fewer and their widths were smaller. Consequently, the slight changes in the shear span-depth ratio did impact the measured deflection.

2.6 Concrete Bridge Deck Slabs Reinforced with FRP bars

Due to the fast deterioration of concrete bridge decks, FRP reinforced concrete has become one of the most suitable alternative solutions to the conventional SRC bridge deck. Extensive studies have been carried out to investigate the behaviour of concrete bridge deck slabs reinforced with different types of FRP composite bars by researchers such as Bouguerra et al (2011); El-Gamal et al (2005); and El-Gamal et al (2007). Six full-scale slabs of size 3 m length × 2.5 m width × 0.2 m depth (Figure 2-4) were constructed and tested to failure by El-Gamal et al (2005). Three deck slabs were reinforced with GFRP bars, while two slabs were reinforced with CFRP bars. A final slab was reinforced with steel bars as a control specimen. El-Gamal et al (2005) included two parameters in the test, the reinforcement type and ratio in the bottom transverse direction.

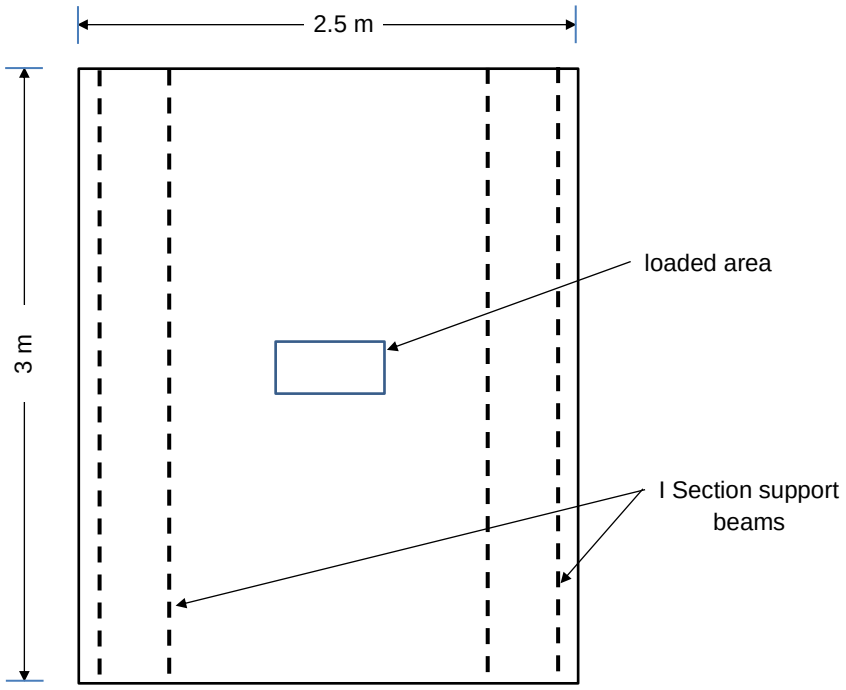

Figure 2-4. Typical dimension and loaded area bridge deck slab (El-Gamal et al. 2005)

The mode of failure for all deck slabs was punching shear, but the carrying capacity was three times the design factored load specified by the Canadian Highway Bridge Design Code. In addition, El-Gamal et al (2005) introduced a new empirical model to predict the punching shear capacity of restrained FRP-reinforced bridge deck slabs. The empirical model was verified and showed good agreement with the test results. El-Gamal et al (2007) added four full-scale concrete deck slabs of the same dimensions as the previous slab specimens to investigate the influence of each FRP reinforced layer on the behaviour of concrete bridge deck slabs reinforced with FRP bars. It was concluded that the bottom reinforcement in the transverse direction had a significant effect on the behaviour and strength of concrete bridge deck slabs, while the top and bottom longitudinal reinforcement did not have a substantial impact on the deflection, strains and strength of the tested deck slabs. However, more tests are required to examine concrete bridge deck slabs reinforced with FRP bars to include more parameters. Bouguerra et al (2011) tested several new parameters, such as slab

thickness, concrete compressive strength, bottom transverse reinforcement ratio, and type of reinforcement. A total of eight full-scale concrete slabs were constructed by Bouguerra et al (2011) with the same dimensions as El-Gamal et al (2007) concrete deck slabs dimensions, except that the thickness of the slabs was varied between 150 – 200 mm. The conclusion of the experimental work considered the effect of the main parameter, i.e. transverse reinforcement, in the cracking width. Besides, reduction of deck slab thickness can be recovered by increasing the concrete strength, while the punching shear of the investigated slabs was dramatically affected by the slab thickness and concrete compressive strength.

2.7 Computational nonlinear analysis

In the last two decades, consecutive studies have been carried out on the punching shear of flat slabs reinforced with GFRP bars. Recent codes and standards have been improved according to the significant progress in researches and the use of FRP as construction materials. Despite this significant improvement, more research is required to increase the possibility of deployment of FRPs and reduce some restrictions due to the lack of scientific knowledge.

Punching shear in flat slabs has some essential parameters effecting dramatically in the value of ultimate punching shear capacity like effective depth, reinforcement ratio, concrete strength and column parameter (Banthia 1995; Matthys and Taerwe 2000; Zaghloul 2003a; Hussein et al. 2004). Laboratory tests of punching shear on the area of column connection with flat slab are essential for observing the actual behaviour and failure mode. Experimental tests are mostly expensive, especially structural elements reinforced or strengthened with any types of FRP. On the other hand, punching shear behaviour is influenced by various parameters. The time needed to cover all parameters limits the

progress of experimental research. Very few parametric studies have been performed by nonlinear analysis. Advance the knowledge of nonlinear behaviour with the development of computational capacities; the parametric studies became possible and more deployable.

A few previous studies had been developed to create a parametric analysis of material factors effecting punching behaviour in RC flat slabs (Menetrey 1994; Hallgren 1996; Ozbolt et al. 2000; Eder et al. 2010; Mamede et al. 2013; Genikomsou and Polak 2015; Wosatko et al. 2015). Five of them performed their analysis by using a three-dimensional finite element model (Ozbolt et al. 2000; Eder et al. 2010; Mamede et al. 2013; Genikomsou and Polak 2015; Wosatko et al. 2015) whereas, Menetrey (1994) and (Hallgren 1996) applied two-dimensionally modelled systems. Menetrey (1994) and Hallgren (1996) used rotationally symmetric elements with ring reinforcement and adopted special conditions to simulate partial bond between steel and concrete. Both studies (Menetrey 1994; Hallgren 1996) showed stiffer curves in the finite element analysis compared to the experimental ones and explained that it was because of the simplified modelling of the two-way reinforcement as 1/4 quadrilateral axisymmetric mesh. Nowadays, with more powerful computers than in the past, the 3D finite element analysis of punching shear of two-way reinforced slabs is more achievable.

Eder et al (2010) carried out a model by nonlinear finite element analysis of punching shear failure for RC flat slabs. The proposed modelling was validated with a large scale RC flat slab without shear reinforcement that failed in punching shear. A parametric analysis was carried out to determine the influence of the critical parameters which govern performance. The results showed that the procedure was capable of predicting the measured response of a large-scale

punching shear test of a slab without shear reinforcement accurately. Tension softening was found to have a higher effect on the predicted load-displacement response than the concrete tensile strength.

Mamede et al (2013) worked on punching shear by conducting some experimental work and modelling 3D nonlinear finite element analysis. The finite element model was compared with the experimental ones, and afterwards, a parametric study on punching shear was carried out to cover parameters of reinforcement ratio, slab thickness, concrete strength and column dimensions. The results of the non-linear 3D finite element analysis showed a satisfactory agreement with the experimental results by comparing the deflections and punching shear strength. In addition, the parametric study showed an increase of the reinforcement ratio by a cubic root with punching load predicted by finite element modelling analysis. The punching shear capacity was also increased as the reinforcement increased but with less ductility. The finite element analysis predicted punching load with an average proportional root of 0.41 of concrete strength. Mamede et al (2013) noted that higher concrete strength resulted in higher cracking loads. It was also said that increasing the thickness of the slab and the column dimensions led to an increase in punching shear strength predicted by finite element analysis.

Another study was carried out by Genikomsou and Polak (2015) on punching shear behaviour of interior slab-column connections by implementing nonlinear finite element three-dimensional software. The finite element analysis modelling was constructed under static and pseudo-dynamic loading to investigate the RC flat slab-column connection failure modes in terms of ultimate load and cracking patterns. Based on the test results of an interior slab-column connection, the material parameters of the damaged plasticity model in ABAQUS were calibrated.

The accurate material modelling especially the concrete modelling was the most challenging aspect of the finite element modelling of concrete structures (Genikomsou and Polak 2015). Both ABAQUS/Standard and ABAQUS/Explicit were used for parametric investigations to calibrate the material model given in ABAQUS. Genikomsou and Polak (2015) studied many material parameters, but the most critical for the accurate definition of the concrete modelling appeared to be the dilation angle and the use of the damage parameters. To adopt a proper mesh size, the cracking propagation together with the load-displacement response should be taken into consideration. The final results of the finite element analysis of Genikomsou and Polak (2015) study confirmed the ability of the proposed model for predicting the punching shear failure in concrete slabs without shear reinforcement.

Wosatko et al (2015) presented a numerical simulation of punching shear behaviour of RC flat slab connected to a column. An asymmetric quarter of the test specimens configuration was implemented. A three-dimensional finite element model was considered with elastic reinforcement embedded as truss elements in the concrete. The study was limited to the simulation of the static response from monotonically increasing the imposed displacement of the column. Wosatko et al (2015) mentioned that proper calibration of damage-plasticity models could be used for predicting shear behaviour and failure in RC slabs. It was expected, the FE analysis is susceptible to the adopted representation of the tensile concrete behaviour. Wosatko et al (2015) also stated that even with proper modelling of tension, premature failure is predicted due to localised deformation related to flexural and shear cracking.

2.8 Artificial Neural Network

The main limitation of previous studies (Matthys and Taerwe 2000; Rahman et al. 2000; Abdalla 2002; El-Ghandour et al. 2003; Ospina et al. 2003; Zaghloul 2003a; El-Gamal et al. 2005; El-Gamal et al. 2007; Li et al. 2007; Lee 2009; Bouguerra et al. 2011; Dulude et al. 2011; Nguyen-Minh and Rovňák 2012; Zheng et al. 2012; Dulude et al. 2013; Hassan et al. 2013a; Hassan et al. 2013b; Metwally 2013) was the uncertainty highlighted by the contrast between the predictions and the experimental results. This is due to the absence of a general function for predicting the punching shear capacity which can work more accurately in predicting the punching shear capacity of the flat slab reinforced with FRP bars. For these reasons, Metwally (2013) used test results available in the open literature to evaluate the punching shear strength of concrete flat slabs reinforced with different types of FRP. Data from 59 full-size slabs and the bridge deck were collected from the literature of concrete slabs reinforced with FRP bars. Six parameters were used in the study; FRP reinforcing ratio, Young's modulus of FRP bars, slab thickness, loaded areas, concrete compressive strength and slab specimen length. Metwally (2013) applied for the first time the ANN Technique to obtain the best prediction of punching shear capacities. In addition, a new empirical model was introduced in the study which was a modification of the El-Gamal et al (2005) equation. The prediction results from ANN of Metwally (2013) were the most consistent, with a standard deviation (STD) of 0.11 and coefficient of variation (COV) 11.2 %, whereas the proposed equation gave an STD of 0.16 and 16 % COV. In any case, the results of the proposed equation showed uncertainty in some parts of the comparison study, especially in the experiment tests results of Matthys (2000) and El-Ghandour et al (2003). The same issue is applicable to the tests results of Lee et al (2009).

The proposed equation underestimated the punching shear capacity of the slabs. The uncertainty of the ANN results in Metwally (2013) study was due to inconsistency in the data collection being used in this study. The samples being used in ANN training were a mixture of two-way reinforced flat slabs and concrete bridge decks. The main differences between the concrete bridge deck slab and two-way reinforced flat slab are the supporting system and the geometry of the loaded area. All the bridge deck samples used in the study of Metwally (2013) were simply supported in only two sides of each specimen. Moreover, the geometry of the loaded area in the bridge deck specimens was rectangular instead of square to simulate the footprint of the truck tyres. To be more consistency in clustering data, all bridge decks were excluded from data analysis of the current research and all two-way concrete flat slabs reinforced with FRP bars were included in the ANN. The number of parameters which were used in the study with the number of tests was found to be a critical parameter enabling ANN to give the best prediction. From this point of view, ANN technique was used in this research to get the best prediction of punching shear capacities but with larger numbers of data collection options, numbers, and consistency. 69 tests results were examined, including all punching shear results for different types of scale specimens. Moreover, from the current parametric study, five parameters were identified which were most effective in the punching shear results. These were used to evaluate the ANN modelling results against the experimental test data and code of practice CSA S806 (2012). Also, it is assessed against best-modified equation in the prediction of punching shear capacity proposed by Ospina et al (2003).

2.9 Membrane action in the punching shear capacity specimen tests

Most of the previous specimens were supported vertically by steel beams located at four-sided edges of the specimens as seen in Figure 2-5. Additionally; no restrictions were provided for the specimen dimensions in the previous experimental studies to deal with the effect of membrane action which may happen from the type of support applied before. Most of the codes of practice consider the punching shear stress parameter at a distance of 0.5d or 1.5d from the face of the column CSA S806 (2012), BS 8110 (1997) and ACI 440. 1R-15 (2015). On the other hand, the zero moment is likely to occur at a distance of 0.2L to 0.22L of the slab span length between two columns. Yitzhaki (1966) considered a specimen with a depth to length ratio d/a of about 1/14 to 1/16. This ratio was used for concrete slabs with steel bar reinforcement, and almost the same ratio was used for the latest experimental punching shear strength tests using FRP reinforcement bars. Therefore, the range of specimen sizes was selected by considering these ratios and fracture size effects as explained by Bazant et al (1994). The general expression of the size effect law did not include the way and the type of support effect in the small or large scale specimens' tests. Bailey (2001) verified the behaviour of the membrane action by considering a two-way spanning slab (Figure 2-6) which was supported vertically around its edges and had no horizontal restraint. This behaviour is an interaction which occurs between strips creating tensile stresses and compressive stress. With this type of slab and restraint, the slab can carry a higher load than that calculated using normal yield-line theory in case of SRC (Bailey 2001). In the case of concrete reinforced with FRP bars, the normal yield-line theory can be applied by including the concept of an equivalent plastic moment capacity for FRP concrete section (Pirayeh Gar et al. 2014), because FRP doesn't obey the yielding

behaviour. The failure mode of flat slab specimens reinforced with FRP bars in Figure 2-6 is more likely to follow the same crack pattern that induced by membrane forces in a slab with no in-plane restraint. Keyvani et al (2014) showed that the lateral restraint in the flat slab is available from the slab itself and there is no requirement for any other restraining of the slab edges. The restraint of flat slab laboratory specimens reinforced with FRP bars originates from four vertical sided edges (Figure 2-5, Figure 2-7 and Figure 2-8). Compressive membrane forces in the slab will be formed as a result of its tendency to grow in-plane, enhancing the punching shear strength. Therefore, the same theory of membrane action can be applied to specimen slabs which failed under punching shear but with some modifications to consider the type of supports and loaded area.

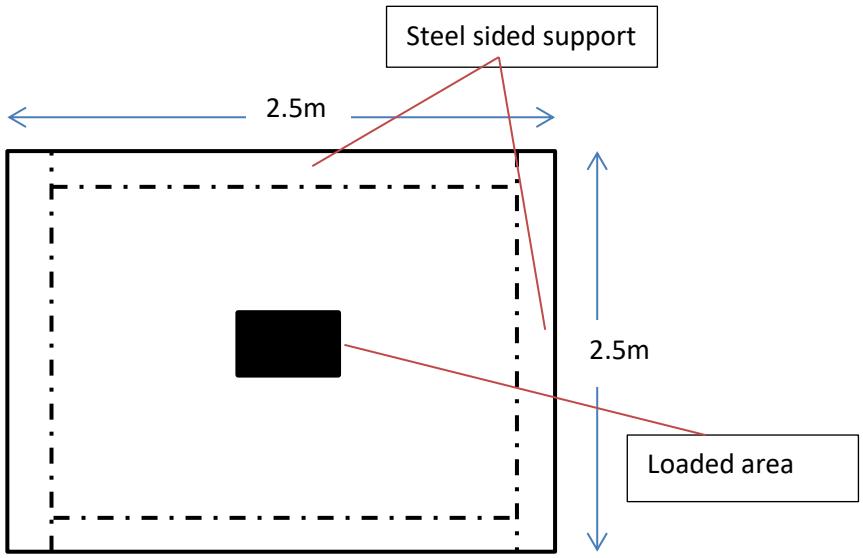

Figure 2-5. Example layout of simply supported slab in the laboratory test samples.

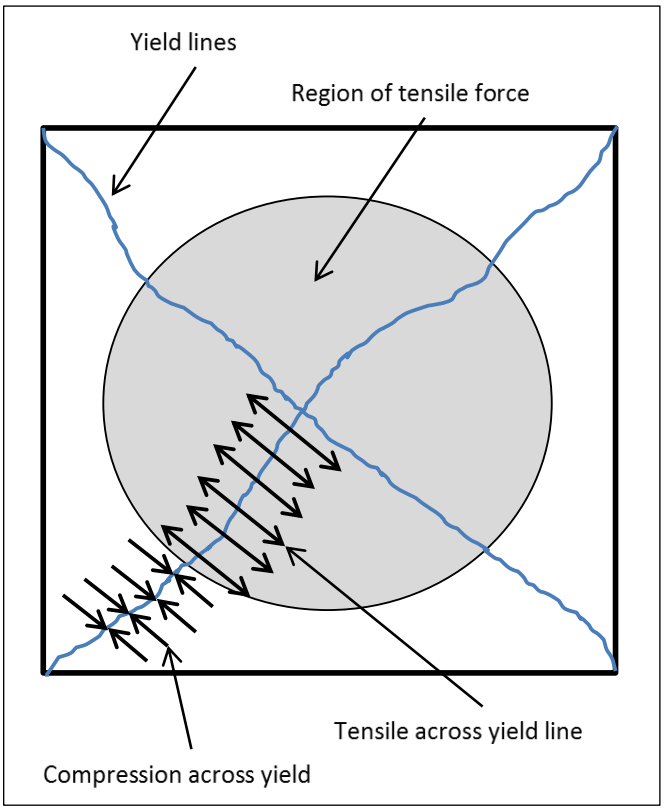

Figure 2-6. In-plane membrane forces in a slab with no in-plane restraint (Bailey 2001)

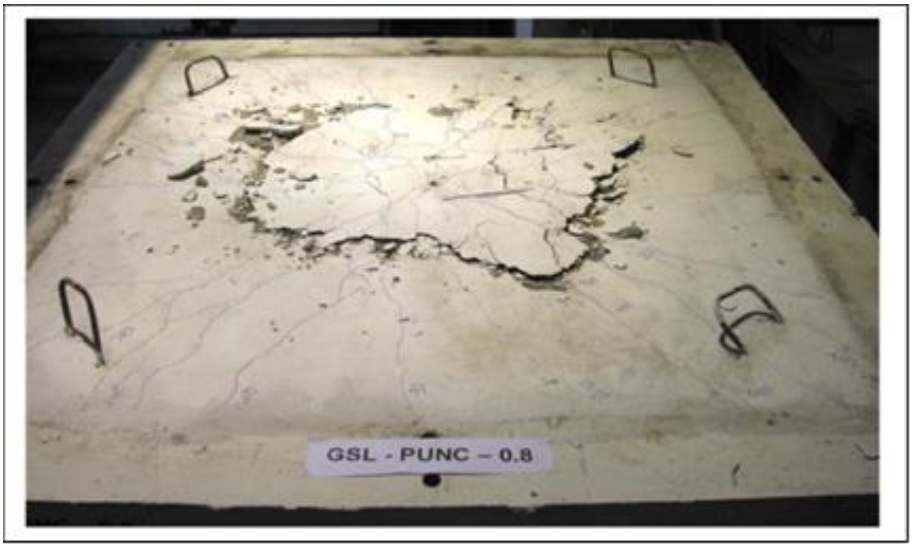

Figure 2-7. Failed one of GFRP reinforced slabs (Nguyen-Minh and Rovňák 2012)

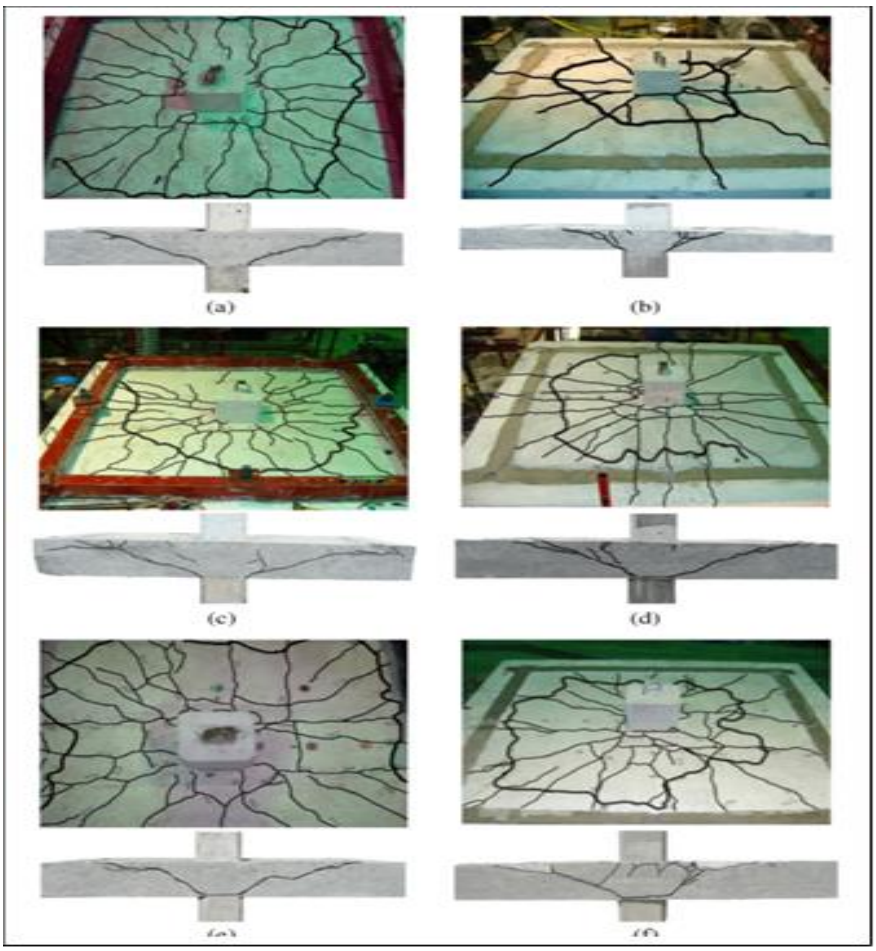

Figure 2-8. Typical punching-shear failure and main shear crack for some Specimens (Hassan et al. 2013b)

2.10 The fracture mechanics approach

In general, the formulas based on the fracture mechanics approach would lead to more accurate results for predicting the resistance of structural members compared to the empirical approach (Nguyen-Minh and Rovňák 2012). The existing formulas for estimation of the punching shear resistance of FRP reinforced concrete slabs either are empirical (Ospina et al. 2003) or are based on modified equations for steel reinforced slabs (Matthys and Taerwe 2000; El-Ghandour et al. 2003; Theodorakopoulos and Swamy 2008; Lee 2009).

Alexander (1992) described the punching shear behaviour model of a steel-reinforced interior slab-column connection by subdividing the shear transfer within the connection. The slab is divided into four quadrant strips. Each quadrant

strip is assumed to transfer the load to the radial strips by beam action and these, in turn, transfer the load to the column through arching action Figure 2-9.

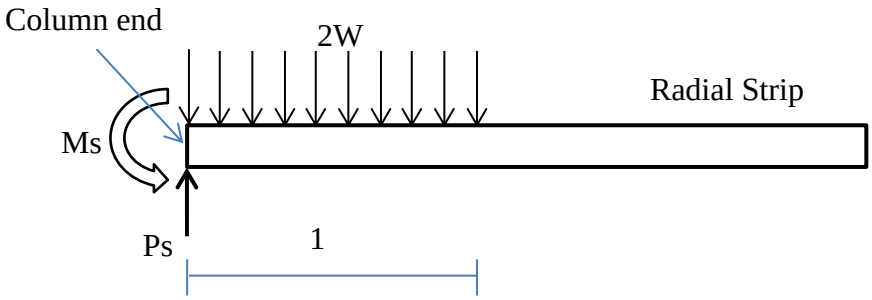

Figure 2-9. Loading geometry for strip model.

Nguyen-Minh (2012) used the same concept of a quadrant strip to obtain the punching shear model. The calculation is started by determining punching shear resistance V_u of a slab-column connection;

$$V_u = V_{u,1} + V_{u,2} \qquad 2\text{–}1$$

Where $V_{u,1}$ and $V_{u,2}$ = shear resistance of two orthogonal beams of spans L_1 and L_2 respectively (Figure 2-10).

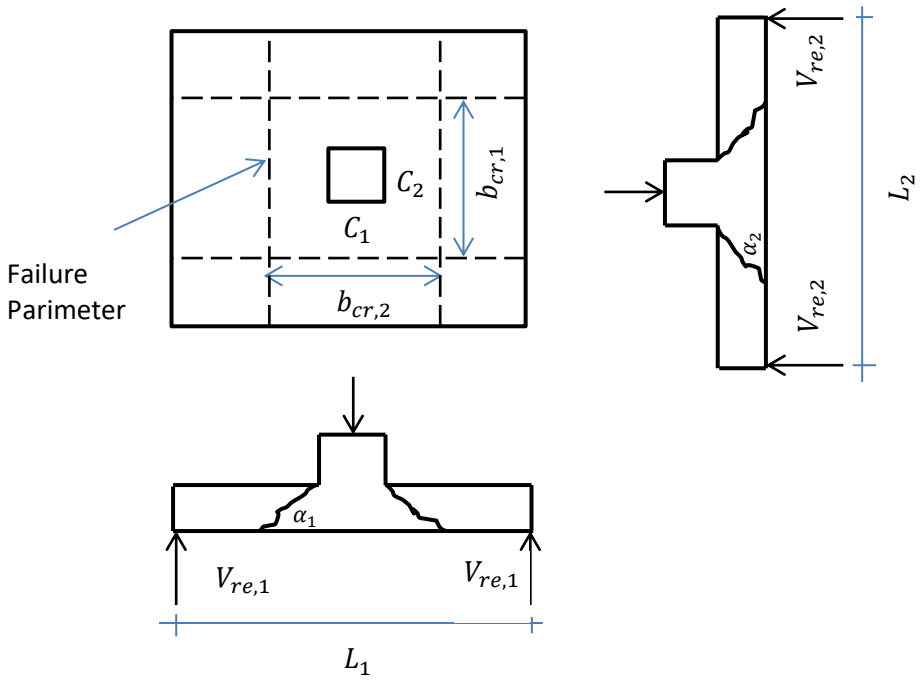

Figure 2-10. Idealized beam model (Nguyen-Minh and Rovňák 2012)

The final proposed equation for estimating punching shear resistance was derived for only square column cross section.

$$V_u = \sqrt{\frac{400}{d}}\left[\frac{0.8}{\left(\frac{L_1}{d}-\frac{c_1}{d}\right)}\right]\left(\frac{\rho_f}{100}\right)^{0.33} E_f^{0.33}(f_c')^{0.33} b_{cr,1} d \qquad 2\text{–}2$$

Where $d\ (mm)$ = effective depth of the slab; $L\ (mm)$ = span of idealized beam; $c\ (mm)$ = dimension of the square column cross section; $\rho\ (\%)$ = FRP reinforcement ratio; $E_f\ (MPa)$ = modulus of elasticity of the FRP reinforcement; $f_c'\ (MPa)$ = mean cylinder compressive strength of concrete; and $b_{cr} = c + \left(\frac{2d}{tan\propto}\right)$ (mm) = is the edge length of the failure perimeter.

The results showed very good punching shear strength estimation in the case of square column connections. The comparison was extended to include flat slab with a circular column, but there were overestimates for some results. This equation needs more study to overcome this issue.

2.11 Conclusions

An introduction to punching shear behaviour of slabs reinforced by FRP bars was given in this chapter. A brief outline of FRP properties and mechanical properties were addressed. An explanation was given regarding failure types of concrete flat plates with the issue of punching shear failure. Literature covering punching shear of steel reinforced flat slabs and FRP bars reinforced flat slabs were reviewed. An explanation of the membrane action concept and the fracture mechanics approach were given in relation to the expected influence of the supporting system of the tested slab under punching shear.

The main conclusions which can be drawn from the study described previously in this chapter are summarised as follows:

- Based on the results of the previous research achievement detailed in the literature review, there is a need for more experimental investigation with an extended range of parameters that effect punching shear resistance of RC flat slabs with different types of FRP bars.
- Some of the studies have been conducted on a small scale of concrete flat slab specimens under laboratory conditions, which do not sufficiently simulate realistic slabs found in practice.
- Many parameters are controlling the punching shear strength in FRP reinforced concrete flat slabs; the most important among them are reinforcement ratio and slab thickness.
- An increase in reinforcement ratio will increase punching shear strength, but the relationship is not linear and varied according to the depth of slabs.
- The literature shows that most of the study focused on investigating the effects of reinforcement ratio on punching shear capacity, but none of these studies was carried out to examine the impact of reinforcement diameter on punching shear capacity.
- The effect of concrete strength on punching shear strength and ultimate deflection is highly sensitive to the depth of the slab.
- A uniform reinforcement distribution in a reinforced concrete flat slab is ideal for real construction applications as the effect of FRP flexural reinforcement in different arrangements is minor and hence adding a complicated field work without a significant advantage.
- The difficult relationship between various parameters considered in the punching shear phenomena and the time needed to cover all parameters limits the progress of experimental research. Civil engineers have raised concerns regarding computing software modelling of complex structures.

Using Matlab tools (ANN) and nonlinear computational analysis (ABAQUS) can deliver reliable results, saving time and reducing the loss of materials.

- Most of the finite element modelling showed acceptable predictions of punching shear capacity in concrete flat slabs.
- A predictable influence of the supporting system on the punching shear capacity of the tested flat slabs reinforced with FRP bars failed under punching shear.

CHAPTER THREE

EXPERIMENTAL INVESTIGATION OF GFRP FLAT SLAB

3.1 Introduction

The main aim of the experimental investigation designated in this chapter is to study the structural behaviour of FRP reinforced concrete flat slabs subjected to a concentric load. The effect of slab thicknesses, concrete compressive strength, and, the effect of flexural reinforcement diameter on the punching shear strength. Deflection of the slabs was measured and recorded at various locations. The results of the experimental work are presented in terms of failure modes, punching shear capacity, and load-deflection response in this chapter, and used to assess the accuracy of the available punching shear equations for flat slabs reinforced with FRP bars in various codes of practice. In addition, the experimental results will also be used in both chapter four and five to validate the numerical model proposed to predict the behaviour and the punching shear capacity of FRP reinforced concrete flat slabs.

3.1.1 Material Properties and Test Setup

3.1.1.1 *Concrete*

All concrete used for specimens tests was ready-mixed with a compressive strength of 35 MPa and 55 MPa at 28 days and maximum aggregate size of 10 mm. The compressive strength was measured using control cubes, while the tensile strength (f_t) was measured by a splitting test cylinder. The following control specimens were prepared during the casting of each slab: three 100 mm cubes and three 300 mm high by 150 mm diameter cylinders.

3.1.1.1.1 Concrete strength and fresh properties

The slump test was performed on the fresh concrete to measure the flowability. The cone was placed in a square metal sheet with a dimension of 700 mm × 700 mm × 1 mm. This cone was filled with fresh concrete which came directly from the mixture in three stages. All stages were distributed evenly in three layers of fresh concrete, and each layer was tempted 25 times with a 600 mm long bullet-nosed metal rod with 16 mm in diameter. At the end of the third stage, any extra concrete on the top of the mould was removed to be level with the top surface of the mould. Then, the mould was lifted very carefully upwards to avoid any concrete disturbance inside the cone. The slump of the concrete was measured by measuring the distance from the top of the slumped concrete and the top surface of the mould. A medium degree of workability was estimated between 50 mm and 90 mm, which are typical measurements for the normal RC placed with vibration. The slumped concrete samples were simply subsiding, keeping more or less to the slump cone shape (Figure 3-1).

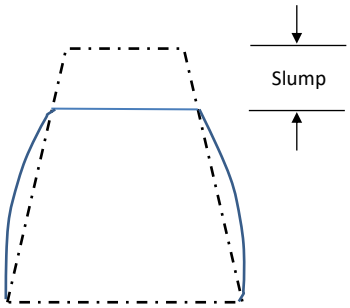

Figure 3-1. True slump

The following control specimens were prepared during the casting of each slab: three 100 mm × 100 mm × 100 mm cubes and three 300 mm high by 150 mm diameter cylinders. The size of the cubical moulds was sufficient for the aggregate size used in the concrete. Firstly, the moulds were prepared by cleaning and the inner surface of the moulds was slightly lubricated with a special

oil for this purpose. Secondly, the fresh concrete was poured into the mould, whereas, electrical vibration table was used to compact the concrete. The top surface of each cubic specimen was levelled and smoothened with a trowel Figure 3-2.

Figure 3-2. Cubing moulds and cylinder moulds concrete samples

Then, after three hours from the concrete casting, a polyethene sheet was used to cover all cubic specimens. Subsequently, after 24 hours the specimens were removed from moulds and kept covered by the polyethene sheet for curing purposes. The test was applied in two separate periods; the first one was after three days, whereas, the second one was after 28 days. After that, the bearing surface of the test machine was cleaned, and each specimen was placed centrally in the device in such manner that each load was applied to the two opposite sides of the cubic mould.

The tensile strength of concrete is an important property. Splitting tensile strength test of the concrete cylinder is the method used in the current thesis to determine the tensile strength of concrete as mentioned before. The procedure of the splitting tensile test was first carried out after 28 days. Firstly, the compression testing machine for the specimen was prepared and set to the required range.

Then, the specimen was placed on the top of the plywood strip of the lower plate, after that, the other plywood strip was placed above the specimen. Finally, the upper plate was lowered down to touch the plywood trip, and then the load applied continuously with a rate of 10kN/sec until it reached failure load.

3.1.1.2 *Reinforcement properties*

Sand-coated GFRP bars (Pultrall 2013) and steel bars were used to reinforce the slabs tested. Their properties are listed in Table 3-1 based on values provided by the manufacturer and lab tests. The tensile strength and the cross-sectional properties of FRP bars were determined by selecting five representative bars from each diameter for testing in accordance with B.1 and B.2 Test Method of (440.3R-4), whereas, Figure 3-3 to Figure 3-7 shows the specimens during the tensile tests and cross-section measurements.

Table 3-1. Properties of reinforcing bars based on values provided by the manufacturer

Bar Material	Diameter (mm)	Area (mm^2)	Tensile Modulus (GPa)	Ultimate Strength (MPa)	Ultimate Strain (%)
Sand-Coated #5 GFRP	15.9 (16.7)	198 (220)	52.5 ± 2.5 (52.0)	1130 (1208)	2.15 (2.3)
Sand-Coated #6 GFRP	19.1 (19.4)	285 (295)	52.5 ± 2.5 (50.8)	1110 (1178)	2.11 (2.3)
Steel	10	79	200	580	0.24
Values between brackets based on lab tests					

Figure 3-3. Preparing GFRP bars for tensile tests

Figure 3-4. GFRP bar specimen and extensometer

Figure 3-5. Typical tensile failure of GFRP bar specimen

Figure 3-6. Preparing GFRP bars for diameter measurements

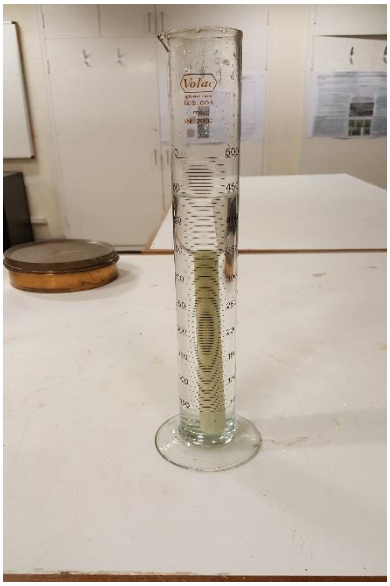

Figure 3-7. GFRP bar specimen volume measurements

3.1.1.2.1 Cross-section properties of GFRP bars

To determine the cross-sectional area, an equivalent diameter test method was used. This method is required to determine the cross-sectional area because FRP bars are made in variable forms; sand coated, ribbed and braided shapes. A graduated measuring cylinder was used to measure the volume of the specimen with a gradient of 5 mL (Figure 3-7). In addition, a calliper with a precision of 0.0025 mm is used to measure the dimension of the specimen. The test was started by preparing five GFRP bars specimens of approximately 200 mm long for each diameter (Figure 3-6). Care was taken to ensure the perpendicularity of the cutting face to the longitudinal direction of the specimen, then the cut surface of the specimen was coated with a thin layer of paraffin wax. Then, all cutting GFRP bars specimen were stored in the standard laboratory atmosphere for about 24 h before testing (23 ± 3 °C and 50 ± 10% relative humidity). Subsequently, the dried graduated cylinder was filled with water to appropriate height. Next, the length of each specimen was measured three times, and the average of the three measurements was rounded up to the nearest 0.1 mm. The volume of the water was measured before and after immersing the specimen. The cross-sectional area A is determined by applying equation 3-1:

$$A = \frac{\Delta V}{L} \times 1000 = \frac{V_1 - V_0}{L} \times 1000 \qquad 3\text{-}1$$

where

ΔV = change in the cylinder volume reading when the specimen is immersed in the water or ethanol, mL;

V_0 = volume of water or ethanol in the cylinder before immersing the specimen, mL;

V_1 = volume of water or ethanol when the specimen is immersed in the water or ethanol, mL; and

L = length of the specimen, mm.

3.1.1.2.2 Longitudinal tensile properties of GFRP bars

In the laboratory, tests were planned to determine the tensile strength, modulus of elasticity and ultimate stain. The test was carried out by preparing the specimen which is a representative of the batch being tested. The length of the specimen is the full length of the test section and the lengths of the anchoring sections. The total length was 50 mm, 10 mm is the length of the test section, and 20 mm is the length of each anchoring section at both end of each specimen Figure 3-3. The number of test specimens for each diameter and type was five. All GFRP bars specimens were stored in the standard laboratory atmosphere before testing (23 ± 3 °C and 50 ± 10% relative humidity). Next, the specimen was mounted on the testing machine with care to ensure that the longitudinal axis of the specimen matches with the line joining the two anchorages fitted to the testing machine (Figure 3-4). Then, the data acquisition system was connected before starting the load. The rate of the load was kept constant increments during the test (5 kN with a rate of 0.03 mm/sec) in such a way that the specimen failed within approximately five minutes (Figure 3-5). The load was increased until tensile failure occurred, whereas, the strain measurements were recorded up to 50% of the expected tensile capacity.

The tensile strength was calculated by Equation 3-2:

$$f_u = \frac{F_u}{A} \qquad 3\text{-}2$$

where

f_u = tensile strength, MPa;

F_u = tensile capacity, N; and

A = cross-sectional area of specimen, mm²

The tensile modulus of elasticity was calculated between two points of a linear regression of the data taken from 20% to 50% of the bar tensile strength. The tensile modulus of elasticity is calculated according to equation 3-3:

$$E_L = \frac{F_1 - F_2}{(\varepsilon_1 - \varepsilon_2)A} \quad \text{3-3}$$

where

E_L = axial (longitudinal) modulus of elasticity, MPa;

A = cross-sectional area, mm²;

F_1 and ε_1 = load and corresponding strain, respectively, at approximately 50% of the ultimate tensile capacity or guaranteed tensile capacity, N and dimensionless, respectively; and

F_2 and ε_2 = load and corresponding strain, respectively, at approximately 20% of the ultimate tensile capacity or guaranteed tensile capacity, N and dimensionless, respectively

3.1.2 Experimental programme

Six full-scale two-way slab specimens were constructed and tested under concentric loading up to failure. The main parameters studied were the effect of flexural reinforcement spacing on the punching shear strength while the effective reinforcement ratio (ρ_f) was kept constant in all specimens. For this reason, the experimental investigation combines two reinforcement diameters with the other parameters: depth of slab (d), and compressive strength of concrete (f_c). The experimental investigation comprises two parts, which include construction and testing of six full-scale interior slab-column connections, reinforced with GFRP and steel bars. Three slab-column connection specimens reinforced with GFRP bars will be tested in Part 1. The concrete strength was kept constant in this part at around 50 MPa, whereas the other parameters were varied according to the

planned objectives. The remaining slabs were included in Part 2 with a concrete strength of 37 MPa including the controlled specimen reinforced with steel bars. All specimen slabs were reinforced in the flexural side with one orthogonal assembly. Testing the specimens was done in the inverse position with reference to the actual position in most buildings. A contra-flexure line surrounded the interior column at an assumed distance of $0.2\,l$ of the full length from the centerline of the column. All the slab specimens represent a full-scale slab of dimension 3.8 m span. The concluded specimens were a square of 1,700 mm long in both directions with a depth of 150 mm or 250 mm. Simple support was used for all specimens acting on all four edges with a clear span of 1,500 mm. A concentric load was then applied to the slab by loading a square steel cap of cross-section 200mm from the top.

The first two specimens (G_{150}(200)47 and G_{250}(160)52) in Table 3-2 were mainly designed to investigate d of the slabs of 150 mm and 250 mm, respectively, whereas the second and third specimens (G_{250}(160)52 and G_{250}(100)53) were meant to measure the effect of flexural reinforcement spacing of 160 mm and 100 mm, respectively. The fourth and fifth specimens (G_{150}(200)35 and G_{250}(160)37) were constructed to compare concrete compressive strength f_c with the test specimens G_{150}(200)47 and G_{250}(160)52, respectively. The sixth specimen (S_{150} (200)37) is the controlled SRC slab with a depth of 150 mm and concrete strength of 37 MPa.

3.1.2.1 *Specimen Labelling and reinforcement configuration*

The test specimens are labelled with a letter denoting the reinforcement type (G for GFRP and S for steel bars) followed by slab thickness, the reinforcement spacing in brackets and ending with the concrete strength. For example, the specimen $G_{150}(200)47$ is a slab reinforced with GFRP bars with a depth of

150mm, reinforcement spacing centre to centre of 200 mm in each orthogonal direction and ends with a concrete strength of 47 MPa. The test specimens are presented in Table 3-2.

Table 3-2. Details of test specimens

No	Specimen	Slab thickness mm	d mm	Column Dimension mm	Tension GFRP	ρ_f %	f_c MPa	f_t Cylinder MPa
1	G_{150}(200)47	150	94	200	8 No. 5	0.96	47	2.9
2	G_{250}(160)52	250	191	200	11 No. 6	0.93	52	3.1
3	G_{250}(100)53	250	191	200	16 No. 5	1.01	53	3.0
4	G_{150}(200)35	150	94	200	8 No. 5	0.96	35	2.8
5	G_{250}(160)37	250	191	200	11 No. 6	0.93	37	2.8
6	S_{150} (200)37	150	100	200	9-10M	0.40	37	2.8
f_c compressive concrete strength in the tested day								

According to the depths, the specimens were categorised geometrically into two main parts. Part one is 150 mm deep, including two GFRP reinforced slabs G_{150}(200)47, G_{150}(200)35 and one steel reinforcement slab S_{150}(200)37, with a reinforcement ratio of 1%, and reinforcement spacing measured 200 mm (Figure 3-8(a) and Figure 3-8(d)). The second part is 250 mm deep including three GFRP reinforced slabs; G_{250}(160)52 and G_{250}(100)53, with the same reinforcement ratio of 1% and varied reinforcement spacing measured between 100 mm to 160 mm (Figure 3-8(b) and Figure 3-8(c)). The actual concrete strength was varied under normal concrete strength measured between 37 MPa to 53 MPa. Two GFRP reinforcement diameters were used in the slab specimens 19.1 mm and 15.9 mm. The reinforcement ratio was maintained constant ($\rho_f = 1\%$)) for all GFRP tested specimens.

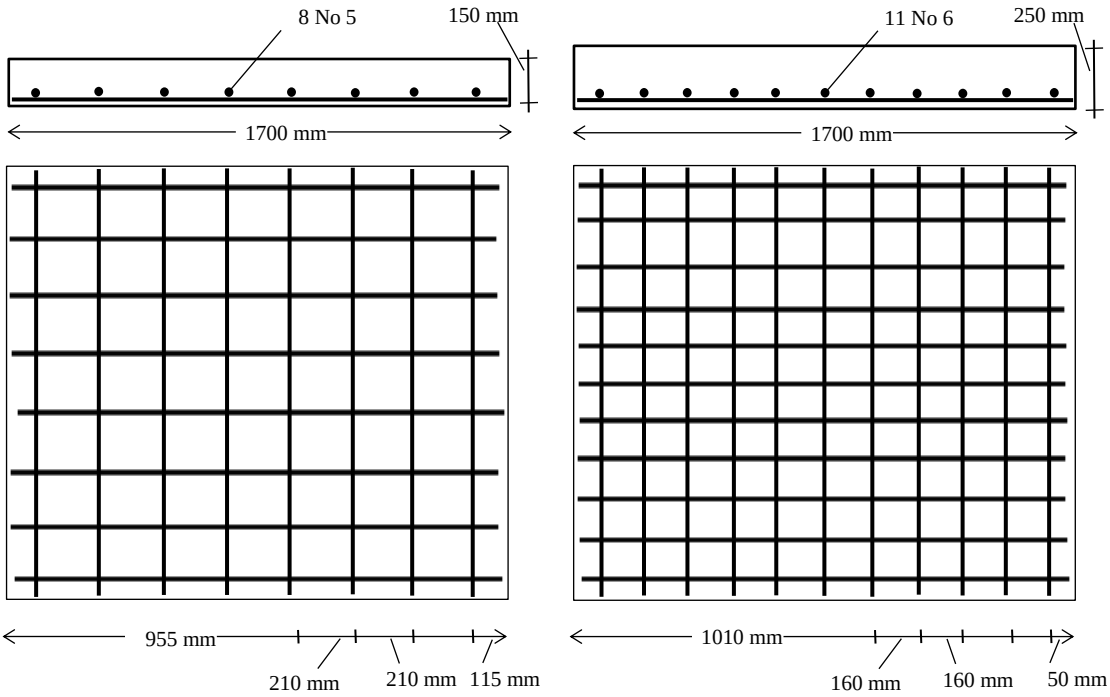

a. $G_{150}(200)47$ & $G_{150}(200)35$

b. $G_{250}(160)52$ & $G_{250}(160)37$

c. $G_{250}(100)53$

d. $S_{150}(200)37$

Figure 3-8. Geometry and reinforcement configuration of specimens

3.1.2.2 *Fabrication of test formwork and specimens concrete casting*

The formwork used to cast the test specimens is shown in Figure 3-9 (a). All formworks were coated with oil before concrete casting to prevent concrete sticking to the formwork after hardening. Then, the reinforcement meshes for the slabs were placed with the concrete cover of small cubes prepared previously for this purpose Figure 3-9 (b).

Each specimen was cast in one stage to simulate the construction of the real flat slabs on site. Then a steel panel of about 2.5 m length was used to remove any excess concrete from the top surface of the samples, whereas, trowels were used to smoothening the concrete finishing surface of each specimen Figure 3-10.

(a)

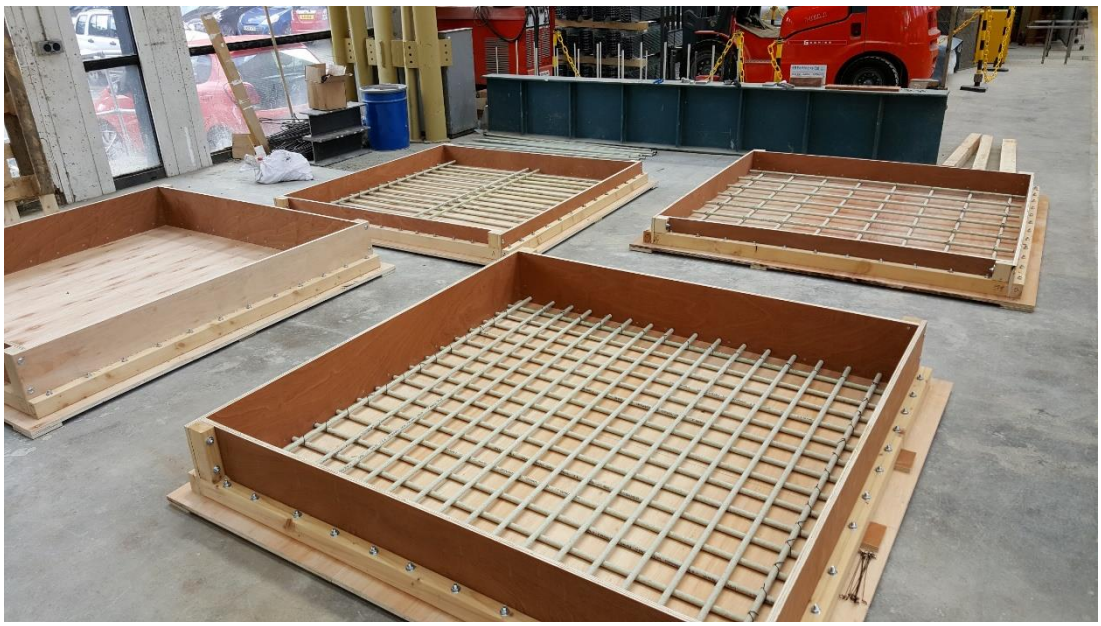

(b)

Figure 3-9. Preparing specimens: (a) formwork: (b) GFRP bars reinforcement rebaring

Figure 3-10. Specimens after concrete casting

3.1.2.3 *Instrumentation and Test Setup*

A concentrated load was applied to a loading steel cap of 200 mm × 200 mm × 50 mm acting from the top of the specimen slab until failure. A 10 mm thickness of mortar was used between the steel cap and the surface loaded area of the slabs. All tested specimens were simply supported in all four sides at a distance of 1.5 m centre to centre of I-section steel frame of 100 mm width laid on the flat, strong floor. A mortar layer of 15 mm thickness was also used on the steel section surface before placing of the adjusted specimen to allow an even load distribution from all four sides of the specimen and steel section to the rigid floor (Figure 3-11). Consequently, a hydraulic jack of 1000 kN connected to two pumps working simultaneously was used to apply load based on the expected capacity of each specimen with a rate of 5 kN/min.

Six linear voltage differential transformers (LVDTs) were used to capture the deflection during the running test as shown in (Figure 3-11). All LVDTs were connected to a data-logger system to record the readings during each running test. The concrete cover was greater than the reinforcement diameter of 19.1mm and 15.9mm by 70% and 100%, respectively, to ensure a good bond between concrete and reinforcements in accordance to Canadian Standards (2012).

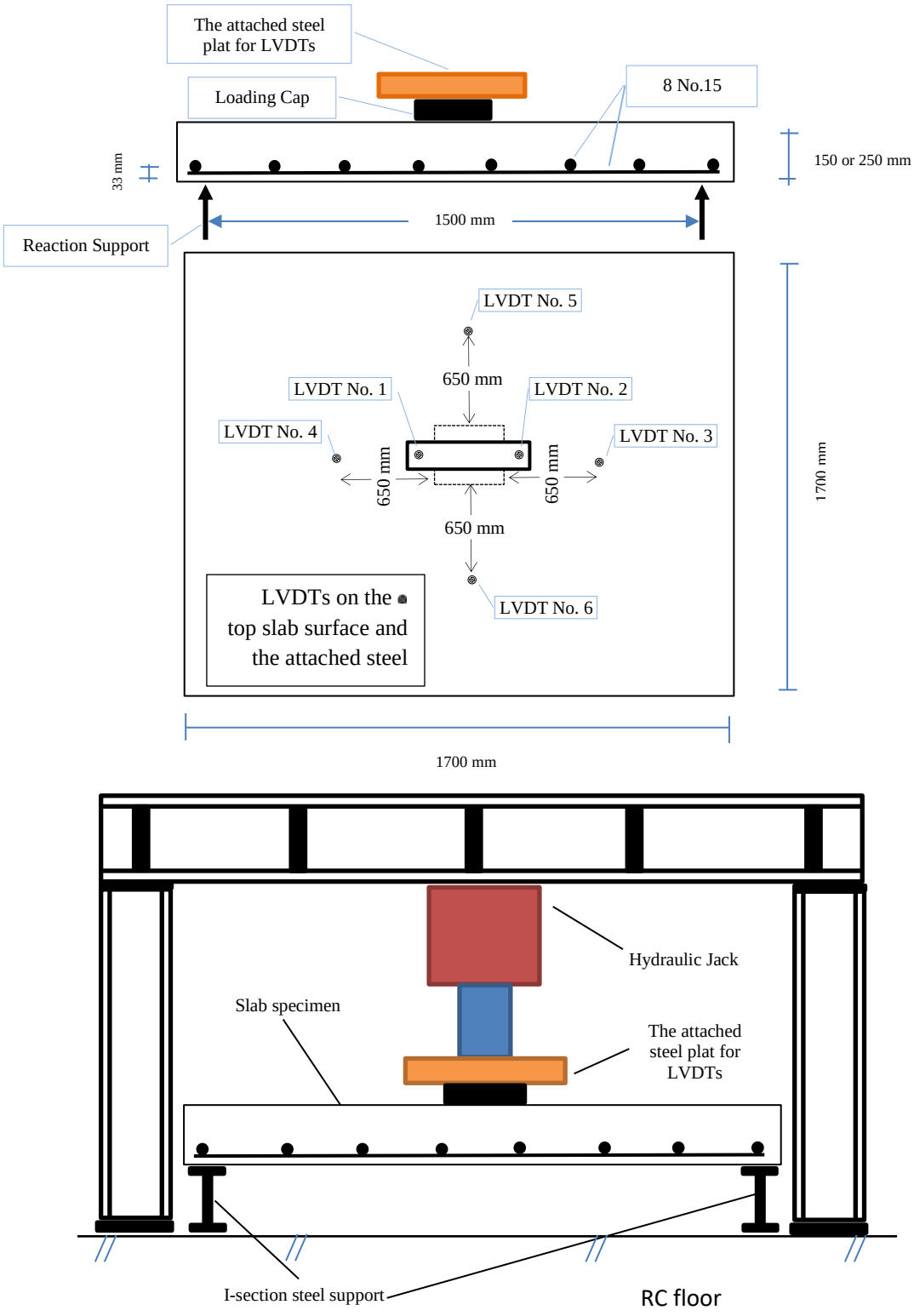

Figure 3-11. Test setup and instrumentations

3.2 Test Results and Discussion

3.2.1 Failure Modes

All specimens failed under the punching shear mode of failure except specimen G_{250}(100)53. No initial cracking was spotted on the test specimens as the loading system was applied from the top and it was not possible to monitor crack formation (Figure 3-12).

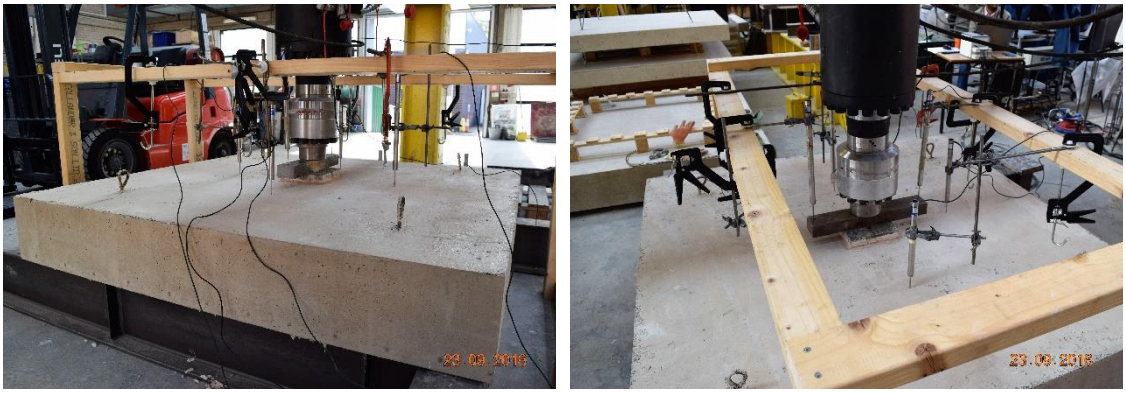

a b

Figure 3-12. Test specimens: (a) testing of a specimen; (b) LVDTs location

Some cracks were spotted at the edge of the slabs at a higher load, which means they were extended beyond the slab supports. Most of the cracks appeared at approximately 50% of the ultimate load, in this stage circumferential cracks expected to exist around the column and connected with flexural cracks. Finally, a punching failure through the slab was developed by the loaded area steel cap.

Punching shear was the mode of failure for all the specimens, irrespective of the reinforcement used. This mode of failure was demonstrated by a sudden drop in the applied load, accompanied by the appearance of a clear crack defining the failure surface of the specimen around the column (Figure 3-13).

Figure 3-13. Typical failure surface around the column

The two specimens, G_{150}(200)47 and G_{150}(200)35, showed large deflections prior to failure and more flexural cracks around the column after the punching-shear failure (Figure 3-15 and Figure 3-16(a)).

Failure cracks were close to the support in all specimens. The maximum and minimum angle of failure surface in most previous experimental specimens were between $22.5°$ and $45°$, but this is not the case in the current research specimens. If the shear stress calculated for failure surface with an angle of $22.5°$ in the specimen G_{150}(200)47 (Figure 3-14), the result will be 1.23 N/mm^2. Whereas the prediction of shear stress using equation 3-20 is 1.09 N/mm^2, and it is the most accurate prediction shear stress compared with the experimental result of specimen G_{150}(200)47 (A-3). The predicted shear stress in equation 3-20 calculated in a larger area compared to the case shown in Figure 3-14 which in turn need a smaller angle of failure surface ($18°$) compared to the proposed minimum angle of failure ($22.5°$). The case study of the specimen G_{150}(200)47 is an indication that shear cracks are more likely to start at a distance close to the support, and this is also the same case for the rest of the specimens in current research which is also an evidence in the sample G_{250}(160)52 when modelled by finite element (Figure 4-11).

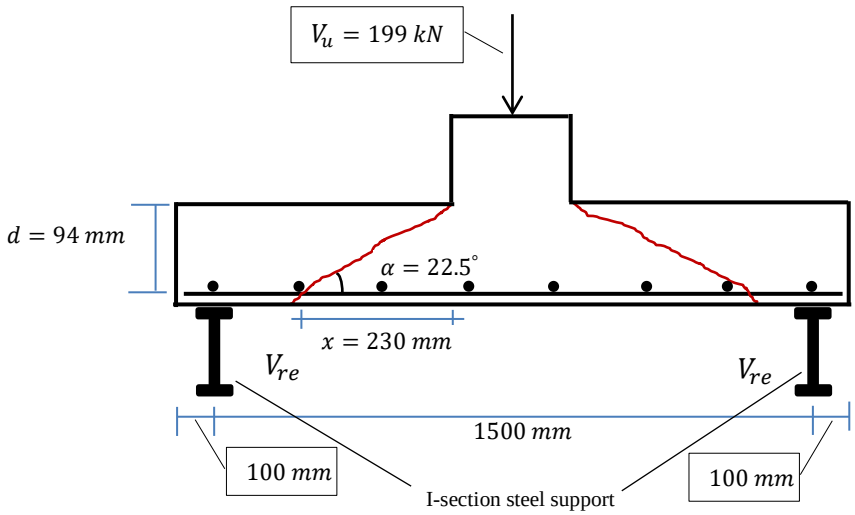

Figure 3-14. Failure surface area (G_{150}(200)47)

3.2.2 Punching Shear Capacity

The results of the ultimate punching shear capacities and the corresponding deflections ware presented in Table 3-3. The GFRP reinforced concrete slab (G_{150}(200)47), with the same slab specimen depth, but with higher concrete strength by 21% and higher reinforcement ratio by 41.6%, gave almost the same punching shear capacity with the counterpart of SRC slab (S_{150}(200)37), because the GFRP bars have smaller values of moduli of elasticity compared to steel bars (about quarter of that of steel). On the other hand, specimen G_{150}(200)35, with the same concrete strength, failed at a lower punching shear capacity compared with specimen S_{150}(200)37. A lower modulus of elasticity of GFRP reinforcement compared to that steel ($E_f/E_s = 0.26$) was one of the main reasons for this result. Besides, GFRP bars have a higher strain, which causes more extensive cracks at the same load level in the elastic range, compared to the specimen reinforced with steel bars. The wider cracks will lead to a smaller neutral-axis depth which in turn will reduce the contributions of the uncracked concrete zone (compression side). Moreover, the aggregate interlock will also decrease as a result of a wider crack action, which, in turn, yielded lower punching shear capacity.

The results also show that decreasing the concrete strength from 47 MPa to 35 MPa and 52 MPa to 37 MPa in specimens with depths of 150 mm and 250 mm, respectively, will reduce punching shear capacity by 16% for both specimens which also agree with Sayed (2015) results (clause 1.6.3). In addition, slab thickness is one of the significant parameters that dramatically affected the punching shear capacity which was also approved experimentally by other researchers (Matthys and Taerwe 2000; Dulude et al. 2013). This was evidenced by increasing the slab thickness of two counterpart specimens – G_{150}(200)47, G_{250}(160)52 and G_{150}(210)35, G_{250}(160)37 – from 150 mm to 250 mm (effective depth from 94 mm to 191 mm), while the reinforcement was maintained to be at the same ratio. The punching shear capacity was increased in both counterpart specimens by 67.8% which agrees with Dulude et al (2013). Regardless of the concrete strength difference of the two counterpart specimens, there was no difference in the ratio of the shear capacity.

The use of different reinforcement spacings along with keeping the same reinforcement ratio have adverse effects on the punching shear capacity. Although reducing the reinforcement spacing (by changing bars' diameter) for the same p_f was intended to increase the punching shear capacity, the result in the current research showed an inverse value. The value of the shear capacity in the specimen G_{250}(100)53 (479 kN) was less by 22.4% compared to the specimen G_{250}(160)52. Unexpected behaviour of the specimen G_{250}(100)53 compared to the counterpart G_{250}(160)52 and other specimens, for this reason, G_{250}(100)53 can't be compared with specimens failed with punching shear.

Table 3-3. Test specimens and the test results

Specimen	Slab Dimension mm	d mm	Column Dimension mm	f_c MPa	f_t Cylinder MPa	ρ_f %	V_{cr} kN	Δ_{cr} mm	V_u kN	Δ_u mm
G_{150}(200)47	$1700 \times 1700 \times 150$	94	200	47	2.9	0.96	89.3	1.86	199.0	18.8
G_{250}(160)52	$1700 \times 1700 \times 250$	191	200	52	3.1	0.93	218.1	0.79	617.2	10.4
G_{250}(100)53	$1700 \times 1700 \times 250$	191	200	53	3.0	1.01	143.1	0.78	479.3	10.4
G_{150}(200)35	$1700 \times 1700 \times 150$	94	200	35	2.8	0.96	66.4	1.17	167.8	18.2
G_{250}(160)37	$1700 \times 1700 \times 250$	191	200	37	2.8	0.93	206.2	0.59	520.9	8.4
S_{150}(200)37	$1700 \times 1700 \times 150$	100	200	37	2.8	0.40	84.9	1.3	194.9	24.9

G_{150}(200)47

G_{250}(160)52

G_{250}(100)53

G_{150}(200)35

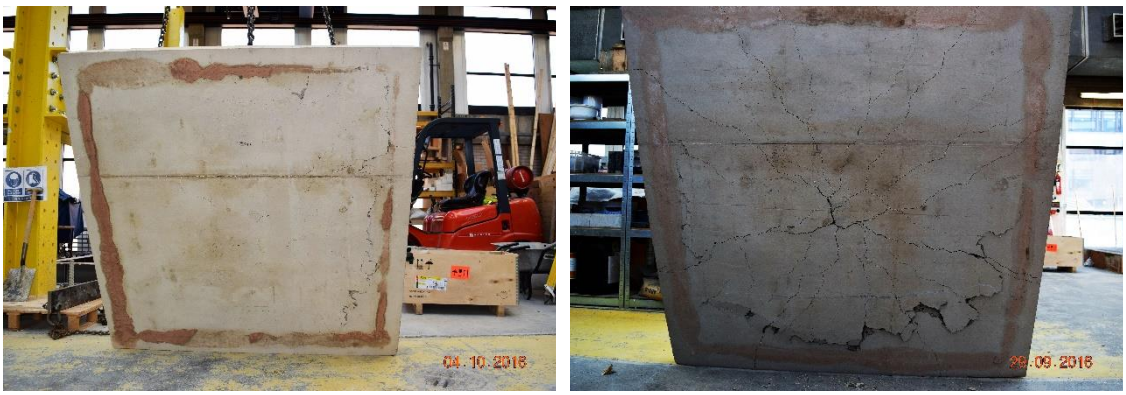

G_{250}(160)37 S_{150}(200)37

Figure 3-15. Punching shear failure and shear crack for all specimens

3.2.3 Load-Deflection Response

Figure 3-16 shows the load-deflection relationships for all tested specimens measured from the LVDTs placed at metal plate connected directly to the loaded area plate cap. All specimens exhibited typical bilinear load-deflection behaviour until sudden failure due to punching shear. The first portion reflects the stiffness of the uncracked section up to the occurrence of the first crack, whereas, the second portion represents the post-cracking stiffness decreasing until failure (Figure 3-16). Despite lower reinforcement of specimen S_{150}(200)37 with counterparts G_{150}(200)35 and G_{150}(200)47, it showed higher deflection values at the same load level. At service load level, specimen G_{150}(200)35 showed 10% lower deflection compared to specimen S_{150}(200)37. At failure, this percentage increased to 26.9% due to the SRC flat slab ductile behaviour in the specimen S_{150}(200)37 compared to G_{150}(200)35. In the specimen G_{150}(200)47 showed 30% higher deflection at service load level compared to S_{150}(200)37, this is due to the higher concrete compressive strength in specimen G_{150}(200)47 compared to S_{150}(200)37. Higher concrete strength can lead to better use of the high strength properties of FRP bars and which is also can increase the stiffness of the cracked section (ACI Committee 440 2015). Specimen G_{250}(100)53, shows less stiffness

and very gradual transition from the uncracked section to the post-cracking stiffness compared to the same depth slab specimens G_{250}(160)52 and G_{250}(160)37 (Figure 3-16(b)). The first crack in specimen G_{150}(200)47 started at a load of 89.38kN whereas, specimen G_{150}(200)35, started at a lower load of 66.38kN as shown in Table 3-3 and Figure 3-16(a). In contrast, the specimens having a depth of 250 mm (G_{250}(160)52 and G_{250}(160)37) exhibited higher first cracking load of about three times of that measured for specimens having a depth of 150 mm. It was also observed that increasing thickness of slab leads to an increase in the initial stiffness. Moreover, with the differences of 12 MPa of concrete strength, specimen G_{150}(200)47 had greater initial stiffness than specimen G_{150}(200)35. In addition, specimen G_{150}(200)47 showed a higher first cracking load by 26% more than that recorded for specimen G_{150}(200)35. However, both specimens showed an identical decrease in the post-cracking stiffness until failure. Moreover, specimens, G_{150}(200)47 and G_{150}(200)35, have very close final deflection values of 18.8 mm and 18.2 mm, respectively. In the case of greater depth of 250 mm slab specimens, the initial cracked stiffness was almost identical with minimal marginal differences. In contrast, specimen G_{250}(160)37 displayed lower post-cracking stiffness with minimal margin differences compared with specimen G_{250}(160)52 (Figure 3-16(b)). Regardless of the effects of concrete strength, it has a minor influence on the post-cracking stiffness for all GFRP reinforced flat slabs. Specimen G_{250}(100)53, with less spacing between reinforcement bars, acts differently in case of initial uncracked stiffness with lower initial stiffness and exhibit the same post-cracking stiffness compared to G_{250}(160)52.

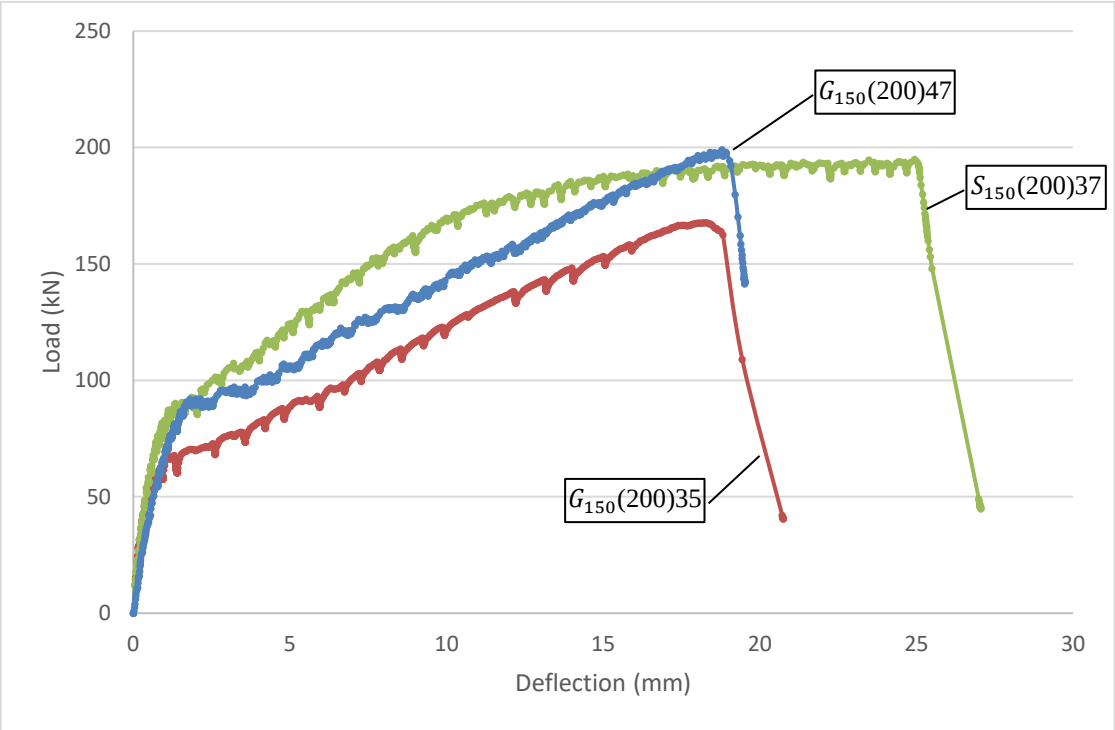

a

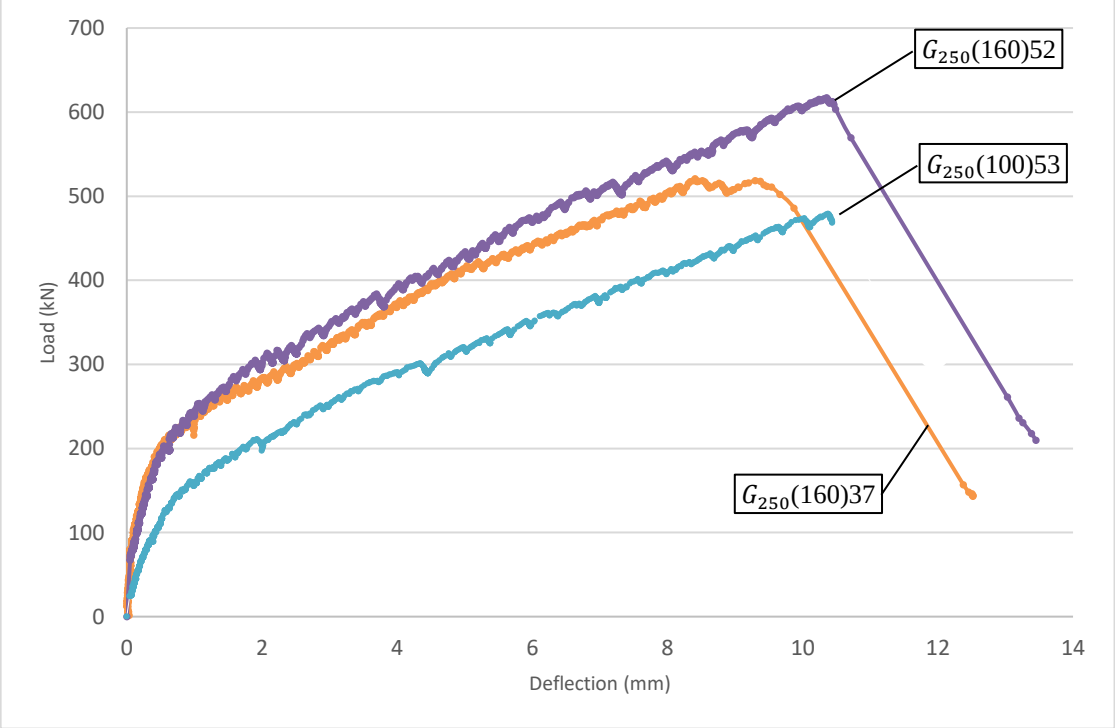

b

Figure 3-16. Load versus deflection (a) Slabs depth 150 mm; (b) Slabs depth 250 mm

The deflection-profile of specimens $G_{150}(200)35$ and $S_{150}(200)37$ are shown in Figure 3-17 and Figure 3-18, respectively, whereas, the other specimens

deflection-profile are shown in Appendix Figure B-1 to Figure B-4. Comparing the measurement of deflection on the centrelines of the slab where the LVDTs were installed (Figure 3-11), it can be seen that there is a balanced deflection in all direction due to vertical shear force (Figure 3-17(a)). In each opposite two LVDTs, the load deflection measurements are shown in opposite trend for each LVDT as shown in Figure 3-17(a) and Figure 3-18(a). Both deflection-profile in the specimen G_{150}(200)35 and the specimen S_{150}(200)37 (Figure 3-17(b) and Figure 3-18(b)) are a nonlinear relationship with distance. The deflection of 60% of failure load and at 325 mm from the face of the column for the specimen G_{150}(200)35 is 57% of that measured in the mid of the slab specimen, whereas, in case of 100% of failure load the deflection is 54% compared to that of middle span. On the other hand, the SRC flat slab specimen was close to the average range of G_{150}(200)35, 54% and 52% at 60% and 100% of the failure load, respectively. At 60% of the failure load and within a distance of 325 mm specimen G_{150}(200)35 achieved a deflection that was 42% of the deflection at the failure load, whereas, in the middle of the slab the deflection at 60% of the failure load was about 40% of the deflection that occurred at 100% of the failure load. On the other hand, the specimen S_{150}(200)37 has a lower ratio range compared to that of specimen G_{150}(200)35. In case of specimen S_{150}(200)37 at 325 mm and with 60% failure load, deflection is about 19% lower than that at the full failure load, whereas, at the mid-point deflection a deflection of 18% is higher at 100% failure load compared to that of 60% failure load deflection.

The deflection-profile in most GFRP reinforced concrete flat slab specimens are not a linear relationship with a distance (except for specimen G_{150}(200)47 compared to the specimen S_{150}(200)37 (Figure B-1(b) to Figure B-4(b)). At 100%

failure load and within distance of 325 mm specimen G_{150}(200)47 achieved 32% higher deflection than of that at 60% failure load, whereas, at mid of the slab the deflection is about 34% of the 60% failure load compared to that of 100% of the failure load. Specimen G_{250}(100)53 is the most varied deflection ratio between the deflection at a distance of 325 mm from the face of the column and the deflection at the mid of slab. At a length of 325 mm from the face of the column, the 60% of the failure load showed lower deflection by 44% from that of 100% of the failure load, while, at the mid of the slab specimen the deflection is 39% greater for the 100% failure load compared with that occurred at 60% of the failure load. On the other hand, the two specimens G_{250}(160)52 and G_{250}(160)37 showed the same deflection profile behaviour with about 36% greater deflection than that of 100% for the 60% failure load and at 325 mm from the face of columns. However, at the 100% of the failure load, the deflection ratio is about 33% higher than of that 60% failure load at the mid of slab specimens.

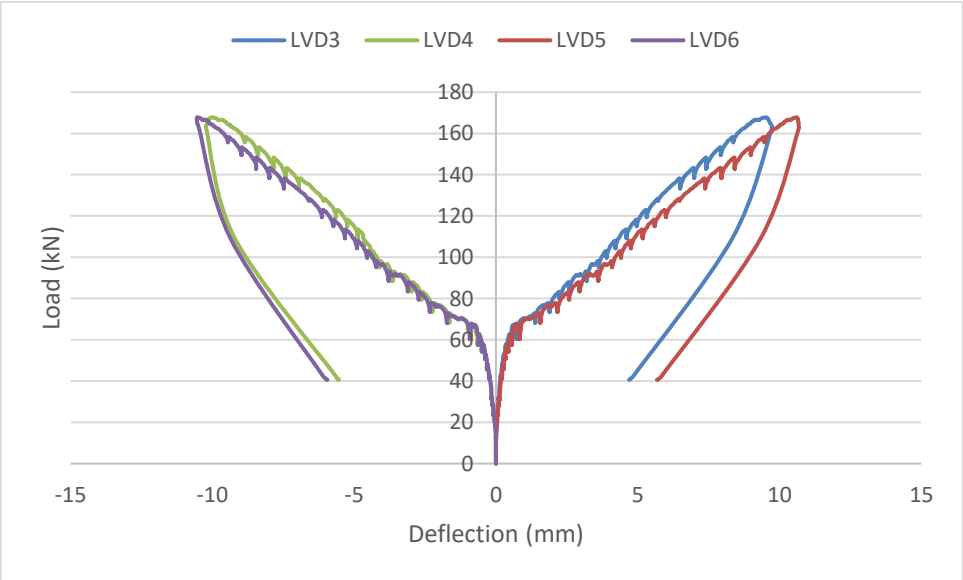

(a) Balanced deflection in the two-opposite direction LVDTs

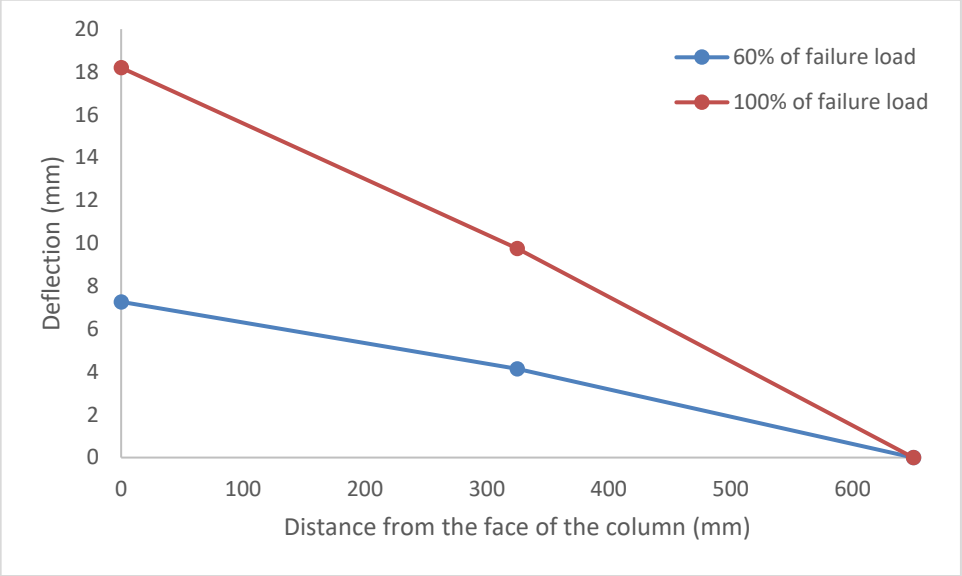

(b) average values of all direction LVDTs

Figure 3-17. Deflection-profile for specimen G_{150}(200)35

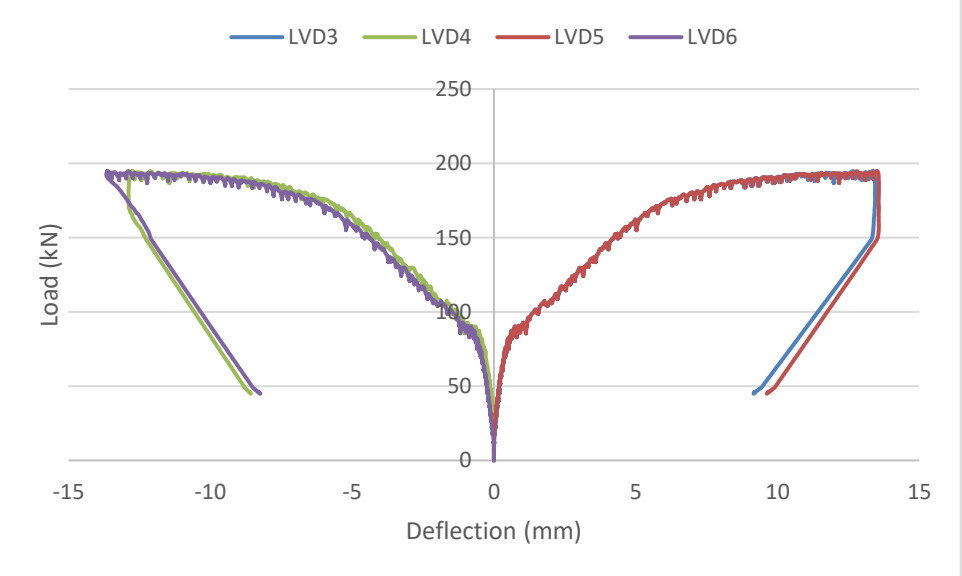

(a) Balanced deflection in the two-opposite direction LVDTs

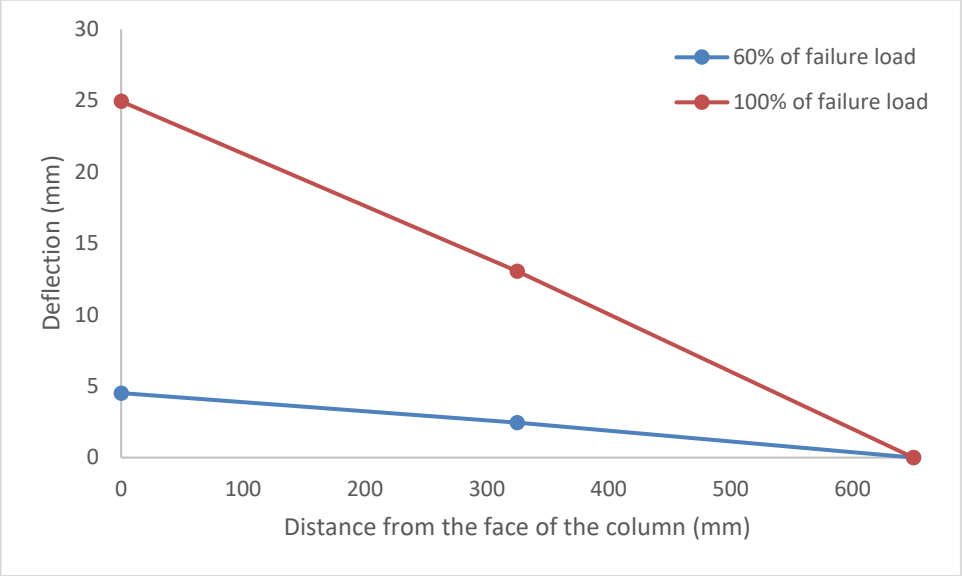

(b) average values of all direction LVDTs

Figure 3-18. Deflection-profile for specimen S_{150}(200)37

3.3 Assessment existing design provisions for punching shear

3.3.1 Introduction

All the existing formulas for estimation of the punching shear resistance of FRP reinforced concrete slabs in several codes and design guidelines are based on modified formulas for conventional steel reinforced slabs. Most of these design provisions are based on the process of adding the concrete contribution (V_c) and the FRP stirrup contribution (V_f) for shear design. The current formulas do not account for the effect of the ratio of slab span to thickness ratio except the study carried out by Nguyen-Minh (2012), which is also limited by the angle of the failure surface (α). Some of them do not consider the size effect (Nguyen-Minh and Rovňák 2012). However, the difference between steel and FRP reinforcement properties were modified to be applied in the design formula. For example, El-Ghandour (2003) applied a correction factor E_f/E_s that takes into account the difference in the elastic modulus between FRP, E_f, and steel reinforcement, E_s.

An overall understanding of shear behaviour is well established since the truss analogy theory (Mörsch 1909). The complexity of the previously proposed theories makes them hard to implement directly into design equations.

3.3.2 Design principles

The understanding fundamental principle behind the current recommendations of FRP reinforced structure designs is that the bond between concrete and reinforcement is assumed to be enough to allow forces and strains acting on the concrete section regardless of the type of reinforcement utilised. Hence, any practical design including FRP sustains the same strain as would be in the equivalent steel reinforcement ($\varepsilon_{FRP} = \varepsilon_S$) and the same design forces are developed ($F_{FRP} = F_S$), then that design will lead to the same safe result as when steel reinforcement is applied. This approach is well known by the name of strain approach Guadagnini et al (2003). According to this assumption (Pilakoutas et al. 2011), the equivalent area of flexural reinforcement A_e can be determined from Equation (3-4):

$$F_f = \varepsilon_f \times E_f \times A_f = \varepsilon_s \times E_s \times A_s = F_s \quad \text{3-4}$$

$$A_e = A_f \frac{E_f}{E_s} \quad \text{3-5}$$

Where ε_f is FRP reinforcement strain, ε_s is the steel reinforcement strain, E_f is the Young Modulus of FRP, E_s is the Young Modulus of steel reinforcement, A_f is FRP reinforcement area, and A_s is steel reinforcement area.

3.3.3 Predictions of Punching-Shear Capacity

This section is concerned with assessing the accuracy of the available punching shear equations for flat slabs reinforced with FRP bars in various codes of practice, namely CSA S806 (Canadian Standards 2012), ACI 440 (ACI Committee 440 2015) and JSCE (JSCE et al. 1997). Moreover, other equations

from other researchers (Matthys and Taerwe 2000; El-Ghandour et al. 2003; Ospina et al. 2003; El-Gamal et al. 2005; Nguyen-Minh and Rovňák 2012) were also addressed in this chapter for a comprehensive study overall current methods used to calculate punching shear capacity of flat slab reinforced with FRP bars. The accuracy of the design equations was assessed by comparing their predictions against the experimental results.

- **CSA S806-12 (CSA 2012)**

CSA S806 (2012) adopted the punching shear strength by selecting the smallest of three Equations (*3-6*) to (*3-8*). The value of concrete punching shear strength V_c of FRP-reinforced concrete can be computed by:

$$V_c = \left[1 + \frac{2}{\beta_c}\right]\left[0.028\lambda\emptyset_c(E_F\rho_F f_c')^{\frac{1}{3}}\right] \quad 3\text{-}6$$

where β_c is the ratio of the long side to short side of the column, concentrated load, or reaction area, λ is a factor to account for concrete density = 1.0 for normal density concrete, $\emptyset_c$ is the material resistance factor and was taken 1.0, E_F is the Young Modulus of FRP, ρ_F is FRP reinforcement ratio, and f_c' is the specified compressive strength of concrete.

Equation (*3-6*) considers the shape of the loaded area by given the factor ratio β_c. The second equation can be computed by:

$$V_c = \left[\left(\frac{\alpha_s d}{b_o}\right) + 0.19\right]\left[0.147\lambda\emptyset_c(E_F\rho_F f_c')^{\frac{1}{3}}\right] \quad 3\text{-}7$$

Where α_s = 4 for interior columns, 3 for edge columns, and 2 for corner columns. In Equation (*3-7*), the loaded area was considered for two intersect panels' direction in flat slabs of internal columns which included four critical parameters sided of punching shear resistance, d is the effective depth of flat slab, whereas, b_o is the critical punching shear parameter. Equation (*3-7*) considers general

shape effect of the loaded area rather than distinguish between square or rectangular shapes. The loaded area ratio was ignored in Equation (*3-8*), and a factor of 0.056 was given instead as seen in Equation (3-8).

$$V_c = 0.056\lambda\emptyset_c(E_F\rho_F f_c')^{\frac{1}{3}} \quad 3\text{-}8$$

All three Equations (*3-6*), (*3-7*), and (*3-8*) have the cubic root of multiplied parameters E_F, ρ_F, and f_c' to reduce the effective change in the punching shear values.

- **ACI 440. 1R-15 (ACI 2015)**

The ACI 440. 1R-15 (2015) equation is a modification of the ACI 318 (2005) equation for steel reinforcement which includes a factor to account for the axial stiffness of FRP reinforcement. The contribution of longitudinal FRP reinforcement in terms of dowel action is assumed to have less effect than that of an equivalent steel area. The concrete shear capacity V_c of a flexural member using FRP as main reinforcement can be calculated by Equation (3-9) (SI units):

$$V_c = \frac{4}{5}\sqrt{f_c'}b_o c \quad 3\text{-}9$$

Where f_c' is the specified compressive strength of concrete, b_o is the perimeter of the critical section for slabs and footing, and c is cracked transformed section neutral axis depth. For the singly reinforced, rectangular cross sections, the neutral axis depth c can be computed by Equation (*3-10*):

$$c = kd \quad 3\text{-}10$$

Where k is the ratio of the depth of neutral axis to reinforcement depth and d is the effective depth. k ratio can be determined by the following Equation (*3-11*):

$$k = \sqrt{2\rho_f n_f + (\rho_f n_f)^2} - \rho_f n_f \quad 3\text{-}11$$

where ρ_f is the FRP reinforcement ratio$\left(\frac{A_f}{b_w d}\right)$,$A_f$ is the area of FRP reinforcement, and n_f is the ratio of modulus of elasticity of FRP to the modulus of elasticity of concrete. The Equation (*3-9*) can be written as:

$$V_c = \left(\frac{1}{5}k\right) 4\sqrt{f_c'} b_o c \qquad 3\text{-}12$$

Equation (*3-12*) is simply the ACI-318 (2008) shear equation for steel reinforcement modified by the factor $(\frac{1}{5}k)$, which accounts for the axial stiffness of FRP reinforcement.

- **Japanese Design Recommendations (JSCE 1997)**

The design punching shear capacity V_{pcd} can be determined by equation (*3-13*):

$$V_{pcd} = \beta_d \beta_p \beta_r f_{pcd} \frac{u_p d}{\gamma_b} \qquad 3\text{-}13$$

$$f_{pcd} = 0.2\sqrt{f'_{cd}} \quad ; f_{pcd} \text{ shall be} \leq 1.2\ N/mm^2 \qquad 3\text{-}14$$

$$\beta_d = \sqrt[4]{1/d} \quad ; \text{if } \beta_d > 1.5 \text{ then } \beta_d = 1.5 \qquad 3\text{-}15$$

$$\beta_p = \sqrt[3]{\frac{100pE_{fu}}{E_0}} \quad ; \text{if } \beta_p > 1.5 \text{ then } \beta_p = 1.5 \qquad 3\text{-}16$$

$$\beta_r = 1 + \frac{1}{1(1+0.25^{u}/_{d})} \qquad 3\text{-}17$$

Where f'_{cd} is the design compressive strength of concrete N/mm^2, u is the peripheral length of loaded area, E_{fu} is the Young's modulus of tensile reinforcement, E_0 is the standard Young's modulus $(200\,kN/mm^2)$, u_p is the peripheral length of the design cross-section at *d*/2 from the loaded area, d effective depth, p is the reinforcement ratio, and $\gamma_b$is the member standard safety factor generally equal 1.3.

❖ **Matthys and Taerwe (2000)**

The formula by Matthys and Taerwe (2000), proposed Equation (*3-18*) according to the British standard BS 8110-1 (1997). A recommendation for modification of British Design Codes BS8110: “Structural use of concrete Part 1” (BSI 1990) and BS5400 suggested by Institution of Structural Engineers “Interim guidance on the design of RC structures using fibre composite reinforcement” (IStructE 1999). The proposed modifications are coinciding with the strain approach (3.3.2), and it is modification factor given in Equation (*3-5*).

$$V_u = \left(\frac{1.36}{d^{1/4}}\right)\left[100 \times \rho_f \left(\frac{E_f}{E_s}\right) \times f_{cm}\right]^{1/3} b_o d \qquad 3\text{-}18$$

Where E_F is the Young Modulus of FRP, ρ_f is FRP reinforcement ratio, d is the depth of flat slab, f_{cm} is the mean concrete compressive cylinder strength, b_o is the perimeter of the critical section for slabs and E_s is Young Modulus of steel reinforcement. In Equation (*3-18*), the shape effect in the punching shear stress wasn’t considered. The calculation of punching strength is based on the stressed area governed by the multiplication of critical punching shear parameter by the depth of flat slabs d.

❖ **El-Ghandour et al (2003)**

Clarke (1996) recommended the use of an equivalent area of steel $\mathrm{A_e}$ by multiplying the actual area of FRP reinforcement $\mathrm{A_{FRP}}$ by the modular ratio of FRP $\mathrm{E_{FRP}}$ to that of steel $\mathrm{E_S}$. The modular ratio $^{\mathrm{E_{FRP}}}/_{\mathrm{E_S}}$ is used in most of the current formulae with different power ratios. The correction factor is also modified by El-Ghandoor (2003), which is based on $^{\varepsilon_{\mathrm{FRP}}}/_{\varepsilon_{\mathrm{S}}}$.

El-Ghandour et al (2003) used a correction factor based on FRP stiffness $\left(\frac{E_f}{E_s}\right)$ instead of ρ_s in the equation of punching shear capacity in ACI code for steel.

$$V_u = 0.33\sqrt{f_c'}\left(\frac{E_f}{E_s}\right)^{1/3} b_o d \qquad 3\text{-}19$$

Where f_c' is specified compressive strength of concrete, E_F is the Young Modulus of FRP, d is the depth of flat slab, b_o is the perimeter of the critical section for slabs and E_s is Young Modulus of steel reinforcement.

- **Ospina et al (2003)**

Ospina et al (2003) modified the equation used by Matthys and Taerwe (2000), Equation (*3-18*). The modification was based on the power of correction factor $\left(\frac{E_f}{E_s}\right)$. The power of 1/2 is given instead of 1/3 to increase the effect of the FRP stiffness.

$$V_u = 2.77\left(\rho_f f_c'\right)^{1/3}\left(\frac{E_f}{E_s}\right)^{1/2} b_o d \qquad 3\text{-}20$$

Where f_c' is specified compressive strength of concrete, E_F is the Young Modulus of FRP, ρ_F is FRP reinforcement ratio, d is the depth of flat slab, b_o is the perimeter of critical section for slabs, and E_s is Young Modulus of steel reinforcement.

- **EL-Gamal et al (2005)**

El-Gamal et al. (2005) proposed equation take into consideration the effects of the flexural stiffness of the main bottom reinforcement and the effect of the continuity in the longitudinal and/or in the transverse direction. The following Equation (*3-21*) is the modification of ACI equation.

$$V_u = 0.33\sqrt{f_c'}\left[0.62\left(\rho_f E_f\right)^{1/3}\left(1+\frac{8d}{b_o}\right)\right]1.2^N b_o d \qquad 3\text{-}21$$

Where N represents the continuity effect of the slab on the punching capacity,

$N = 0$ (for one span slab in both directions);

$N = 1$ (for slab continuous along one direction);

$N = 2$ (for slabs continuous along their two directions);

Where f_c' is specified compressive strength of concrete, E_f is the Young Modulus of FRP, ρ_f is FRP reinforcement ratio, d is the depth of flat slab, and b_o is the perimeter of the critical section for slabs.

- **Nguyen-Minh (2012)**

Nguyen-Minh and Rovňák (2012) derived Equation (*3-22*) under the assumption of a constant angle of the failure surface. In fact, the angle may vary as a result of the action of several factors (concrete strength, reinforcement ratio, reinforcement material). Varied angle assumption was made only by the span-to-slab effective depth ratio$\left({}^{L}/_{d}\right)$.

$$V_u = \sqrt{\frac{400}{d}}\left[\frac{0.8}{\left(\frac{L_1}{d}-\frac{c_1}{d}\right)}\right]\left(\frac{\rho_f}{100}\right)^{0.33} E_f^{0.33}(f_c')^{0.3} b_{cr,1} d \qquad 3\text{-}22$$

Where f_c' is specified compressive strength of concrete, E_f is the Young Modulus of FRP, ρ_f is FRP reinforcement ratio, $c\ (mm)$ is dimension of the square column cross section, d is the depth of flat slab, b_o is the perimeter of critical section for slabs, and $b_{cr} = c + 2d/\tan\alpha$ (mm) is the edge length of the failure perimeter. The angle of the failure surface α can be calculated as $\alpha = 729(L/d)^{-1.26}$, within the limit of $22.5^o \leq \alpha \leq 45^o$.

3.4 Database collection

The database of 69 specimens of flat slabs examined for punching shear strength were collected from previous studies (Hussein et al.; Matthys and Taerwe 2000; Rahman et al. 2000; Abdalla 2002; El-Ghandour et al. 2003; Ospina et al. 2003; Zaghloul 2003a; Hussein et al. 2004; El-Gamal et al. 2005; El-Gamal et al. 2007; Li et al. 2007; Lee 2009; Bouguerra et al. 2011; Dulude et al. 2011; Nguyen-Minh and Rovňák 2012; Zheng et al. 2012; Hassan et al. 2013a; Hassan et al. 2013b;

Metwally 2013) and the current study (Table A-1). Tests examined six parameters: span length of slabs L, height of slabs H, concrete strength f_c, reinforcement strength f_u, Young Modulus of the reinforcement E_f, reinforcement ratio ρ_f, and the reinforcement diameter d_f. Most of the specimens from previous studies (El-Ghandour et al. 2003; Ospina et al. 2003; Zaghloul 2003a; Hussein et al. 2004; Lee 2009; Bouguerra et al. 2011; Dulude et al. 2011; Nguyen-Minh and Rovňák 2012; Zheng et al. 2012; Metwally 2013) have L greater than 1000 mm, whereas, 37 slabs out of 69 have depth measured between 60 mm and 150 mm (Figure 3-19; Figure 3-20). Moreover, concrete strength considered in the tested specimens was normal strength concrete with a value between 30 MPa and 50 MPa (Figure 3-21). In addition, a large amount of f_u from the tested slabs was limited between 500 MPa and 1500 MPa with corresponding E_f between 40 GPa to 100 GPa which is about ¼ of steel Young Modulus value and in the best case ½ of steel Young Modulus (Figure 3-22; Figure 3-23). On the other hand, ρ_f has a wide range of value distributed between 0.15 and 2.0% (Figure 3-24). Most of the tested lab specimens were considered to be in the large-scale specimen tests.

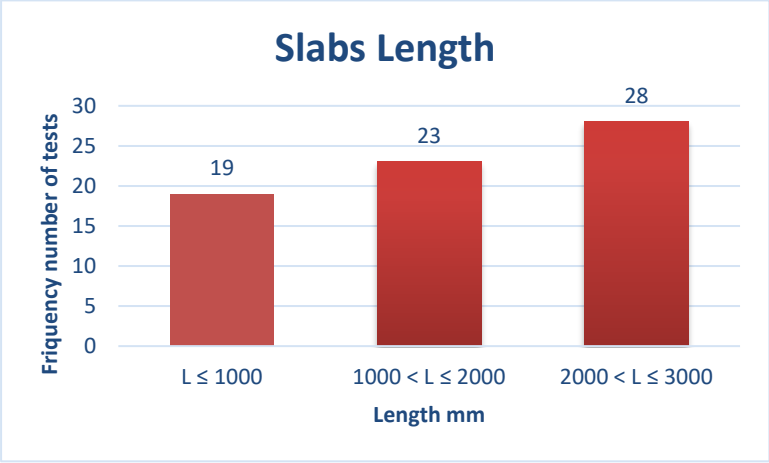

Figure 3-19. Distribution of slabs length in the database

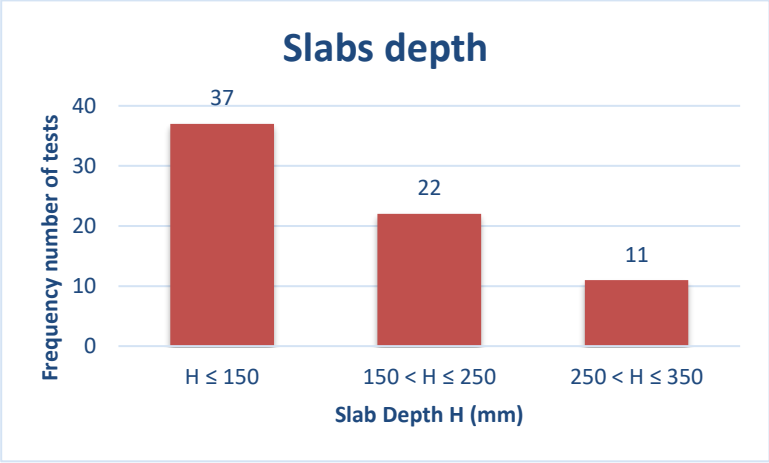

Figure 3-20. Distribution of slabs depth in the database

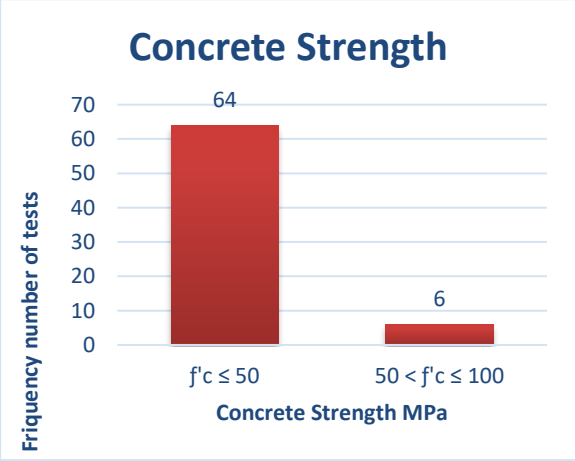

Figure 3-21. Distribution of concrete strength in the database

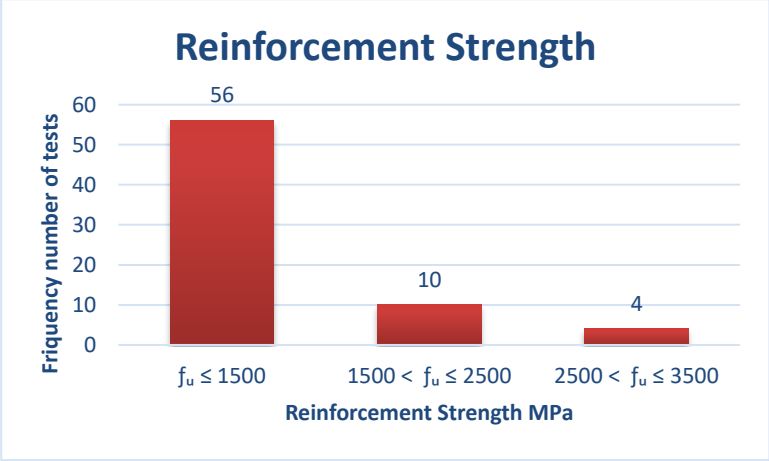

Figure 3-22. Distribution of reinforcement strength in the database

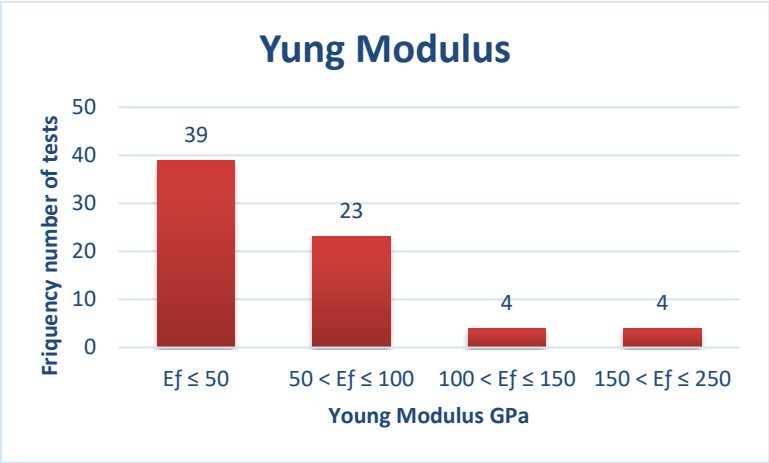

Figure 3-23. Distribution of Young Modulus in the database

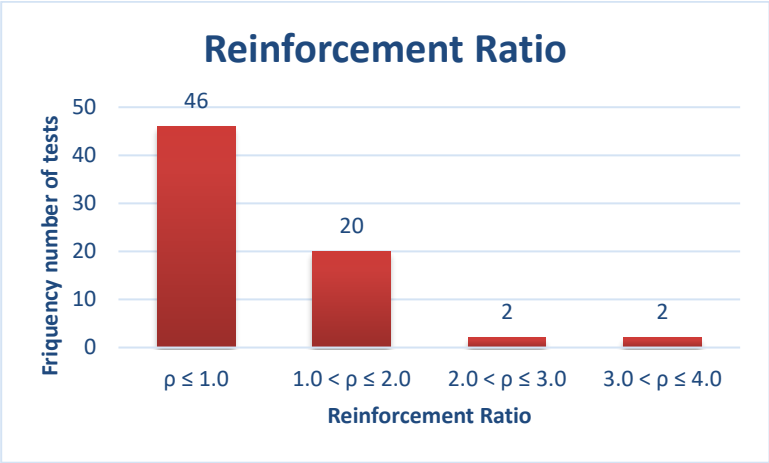

Figure 3-24. Distribution of Reinforcement Ratio in the database

3.4.1 Comparison Between Theoretical Prediction and Test Results

Numerical results for three codes of practice (JSCE et al. 1997; Canadian Standards 2012; ACI Committee 440 2015) and five other formulas (Matthys and Taerwe 2000; El-Ghandour et al. 2003; Ospina et al. 2003; El-Gamal et al. 2005; Nguyen-Minh and Rovňák 2012) were compared with the 69 test results in the database collection. A wide spectrum of material and geometrical properties was covered in the 69 reference experimental results. It should be noted that all safety factors in the existing formulas were assigned to 1.0. Mean value (M), SD, COV and mean absolute percentage error (MAE) of the experimental punching shear resistance to predicted ratios $V_{u,exp}/V_{pred}$ (Table A-3) are summarised in Table 3-4.

Shear design equations were presented and verified by plotting the predicted shear strengths against the experimental values for all specimens in Figure 3-25 to Figure 3-32. Overall, a good agreement of the shear resistance values calculated by the proposed formula with the test results is evident in Figure 3-25 to Figure 3-32. In each figure, a straight line was also drawn to represent the scenario of experimental results of punching shear strength matching the predicted shear strength. Equation 3-18 shows the smallest scatter in the results (Figure 3-28), giving COV = 0.16 and M = 1.14, which has an average of 12.3% lower predicting results values than the targeting test results values. Since Equation 3-20 is the modification of the weight contribution of FRP stuffiness in the Equation 3-18, results were most likely identical but with a noticeable advantage of M = 0.97 (3% higher predicting results values than the targeting test results values) for the Equation 3-20 predictions. On the other hand, Equation 3-22 shows good results (Figure 3-32) with COV = 0.17, but with a quite high

MAE = 1.03. Moreover, the Equation 3-22 results were also showed that if the dimension of the specimens is increased, the results of $V_{u,exp}/V_{pred}$ became more conservative (Figure 3-32 and Table A-3). The theoretical calculated angle of failure surface ($\alpha = 729(\frac{L}{d})^{-1.26}$) in Equation 3-22 is limited between a minimum angle of 22.5˚ and a maximum angle of 45˚ whereas, most of the specimen from the database were have a calculated α either greater than 45˚ or less than 22.5˚ according to equation $\alpha = 729(\frac{L}{d})^{-1.26}$. This angle of failure limitation in equation $\alpha = 729(\frac{L}{d})^{-1.26}$ affects the prediction of punching shear resistance adversely. Since the calculation of α in equation $\alpha = 729(\frac{L}{d})^{-1.26}$ is directly related to the L/d results, most of the specimens in the collected data have calculated L/d values measured between 8 and 18 (Hassan et al. 2013a; Hassan et al. 2013b). Among the codes of practice, the most conservative results were ACI 440.1R-15 (Equation (3-9)), although, no any factor of safety was used in the equations, whereas, two of codes CSA- S806-12 (Equation (3-6), Equation (3-7) and Equation (3-8)), and JSCE (1997) (Equation (3-13)) gave more accurate results than ACI 440.1R-15 (Equation (3-9)). JSCE (1997) equations (Equation (3-13)) showed less scattered results than CSA- S806-12 equations (Equation (3-6) to Equation (3-8)) with COV = 0.19, whereas, MAE = 0.71 greater value than CSA-S806-12 equations values (0.65). Both codes, JSCE (1997) and CSA- S806-12 have an average of 19% lower predicting results values than the targeting test results valu

Table 3-4. Summary of statistical results for shear design methods.

Design method	M	SD	COV%	MAE%
CSA- S806-12	1.20	0.25	0.21	0.65
ACI 440.1R-06	2.17	0.50	0.23	2.10
JSCE (1997)	1.21	0.23	0.19	0.71
Mattys and Taerwe (2000)	1.14	0.18	0.16	0.65
El-Ghandour et al (2003)	1.23	0.47	0.38	0.98
Ospina et al (2003)	0.97	0.18	0.19	0.61
El-Gamal et al. (2005)	0.98	0.26	0.27	0.96
Nguyen-Minh and Rovňák	1.28	0.21	0.17	1.03

M: Mean value
SD: standard deviation
COV: coefficient of variation
MAE: mean absolute percentage error

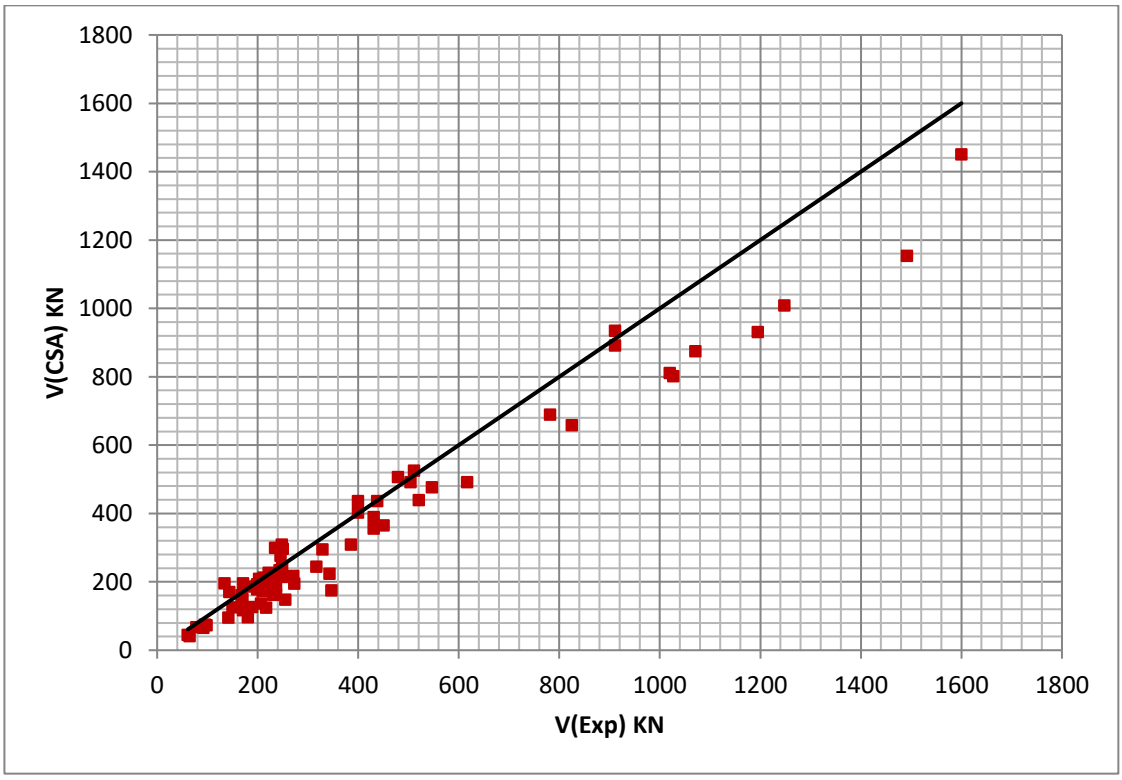

Figure 3-25. CSA- S806-12 predicted vs experimental punching shear capacities.

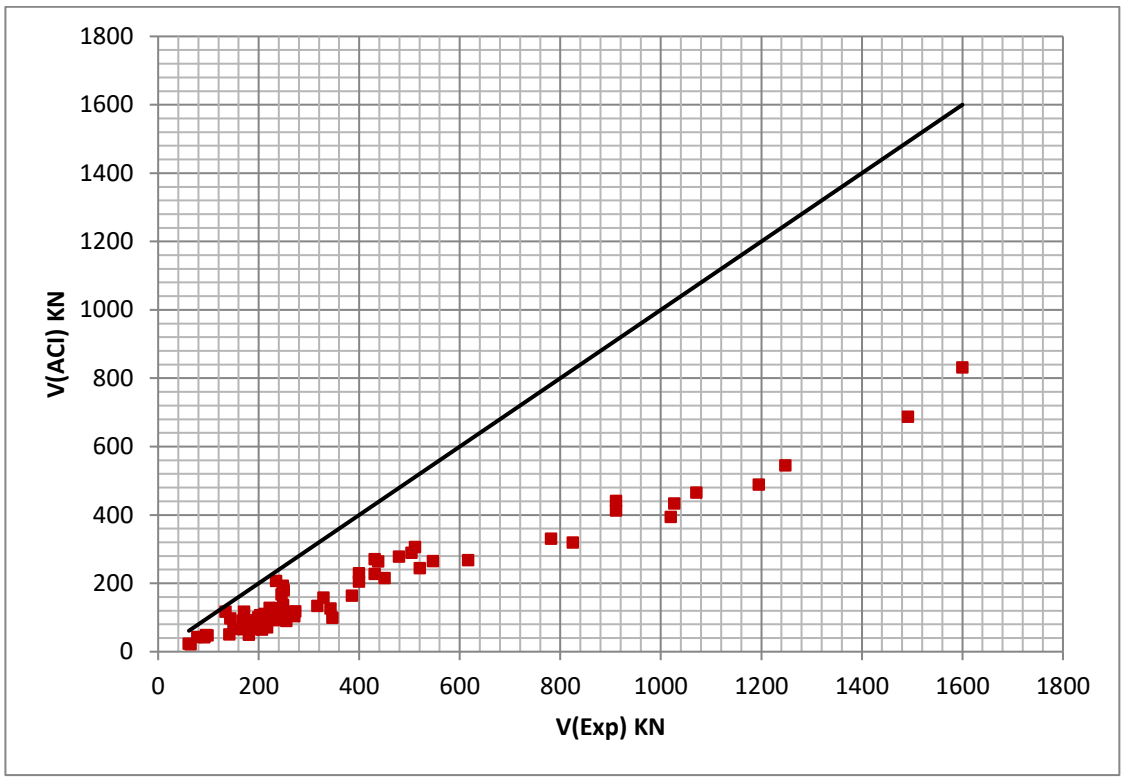

Figure 3-26. ACI 440.1R-06 predicted vs experimental punching shear capacities.

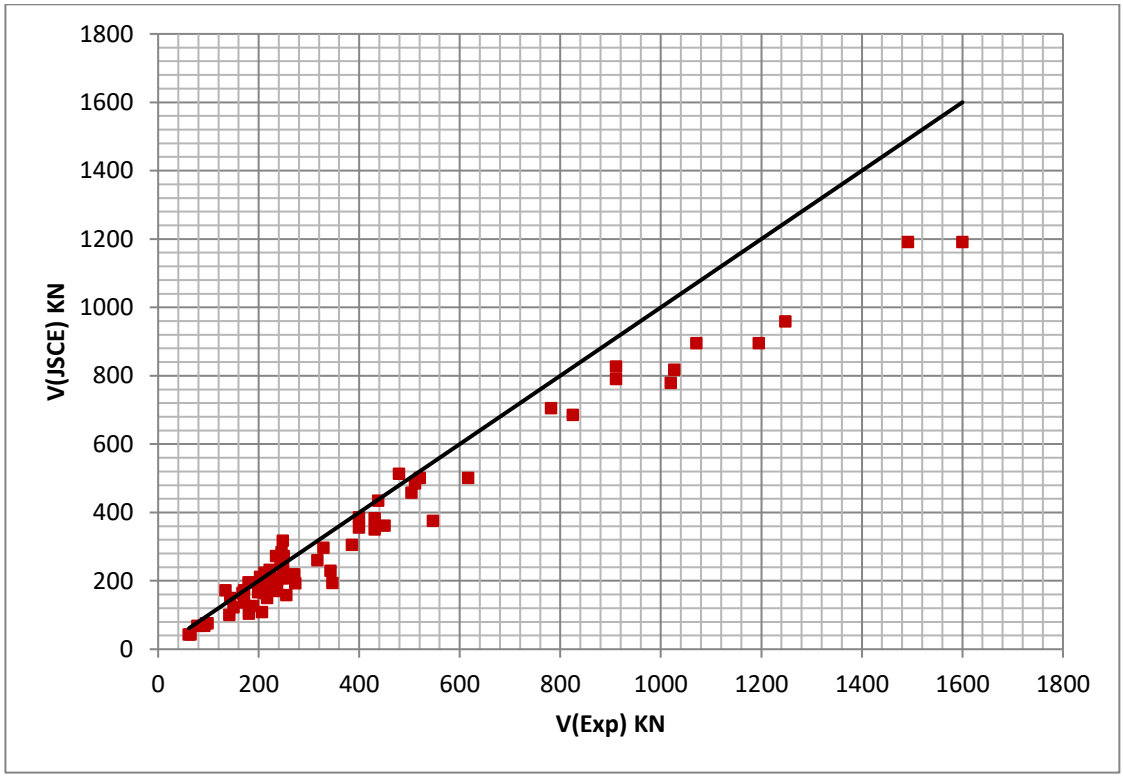

Figure 3-27. JSCE 19997 predicted vs experimental punching shear capacities.

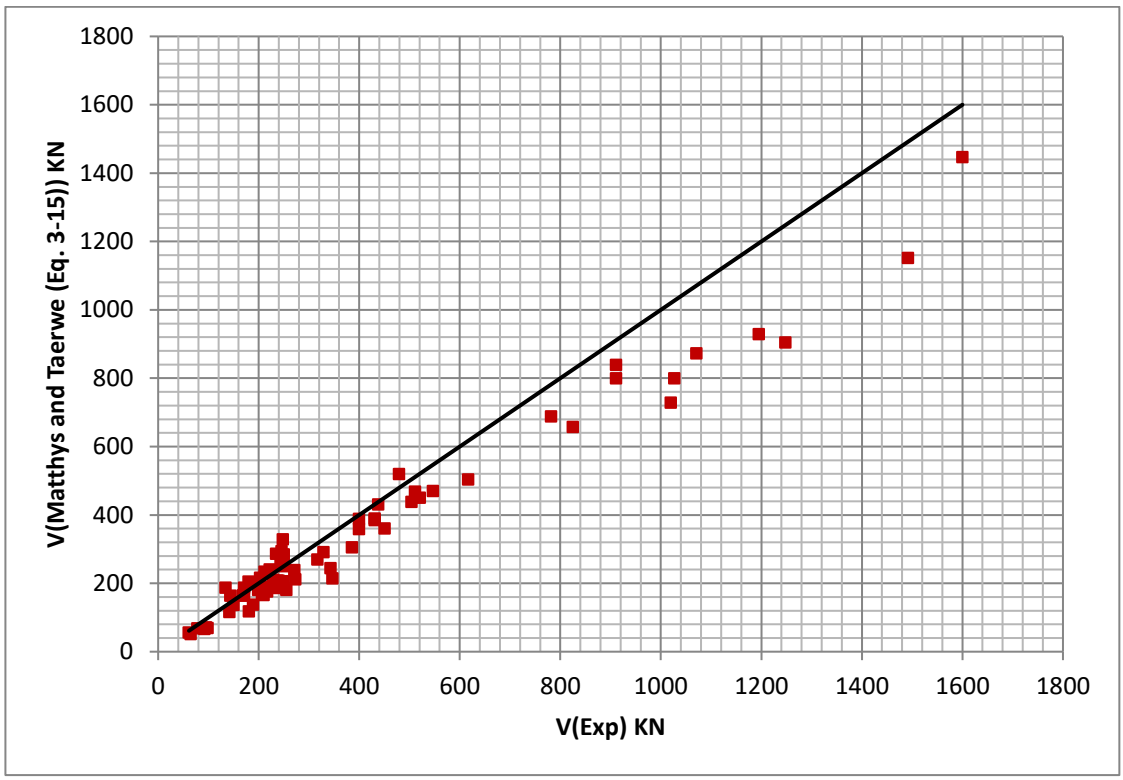

Figure 3-28. Mattys and Taerwe (2000) predicted vs experimental punching shear capacities.

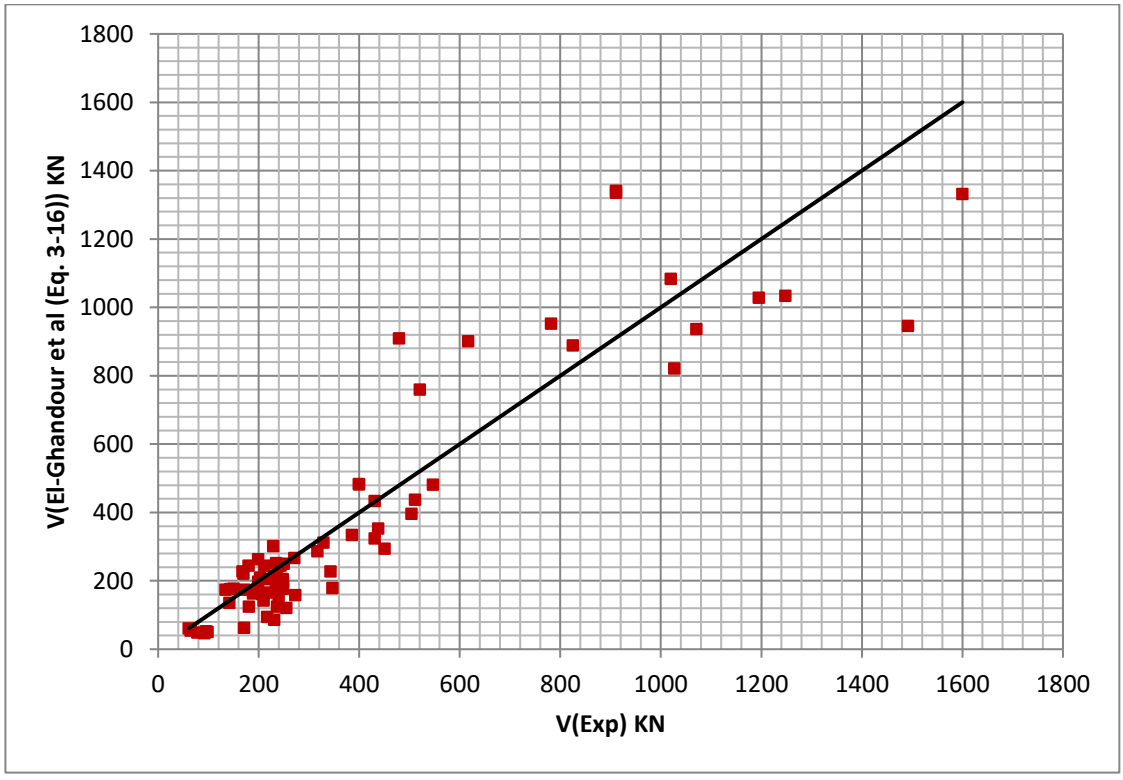

Figure 3-29. El-Ghandour et al (2003) predicted vs experimental punching shear capacities.

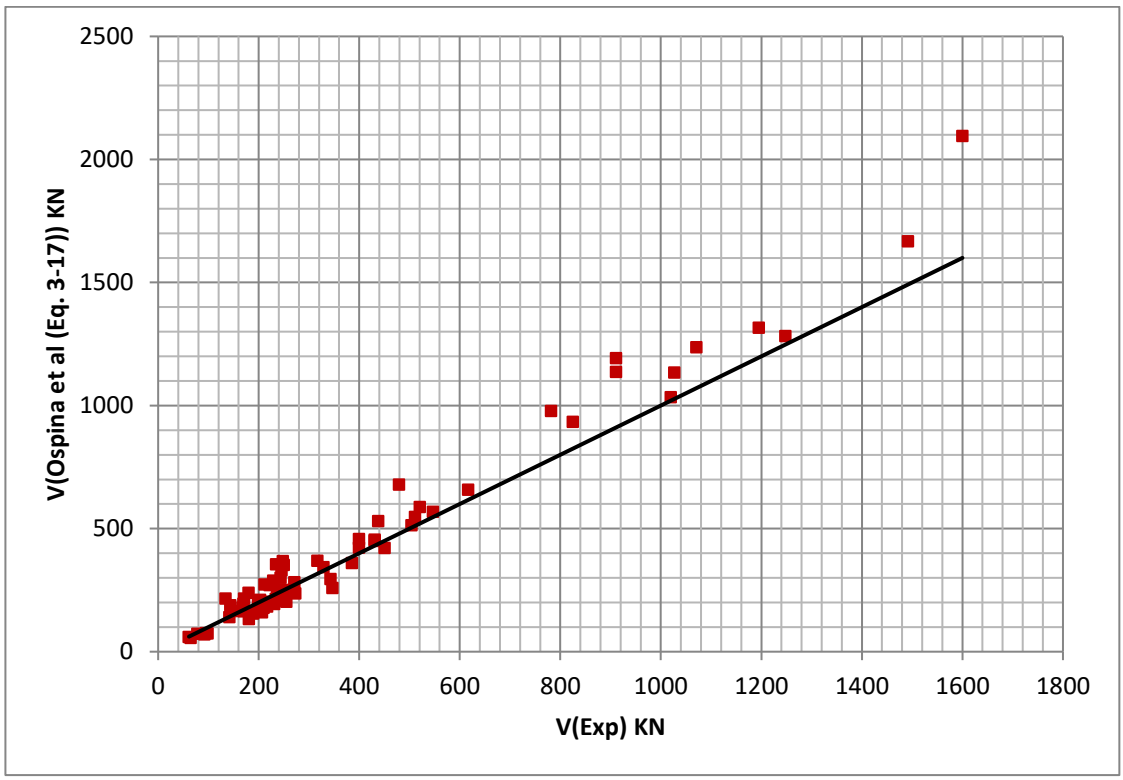

Figure 3-30. Ospina et al (2003) predicted vs experimental punching shear capacities.

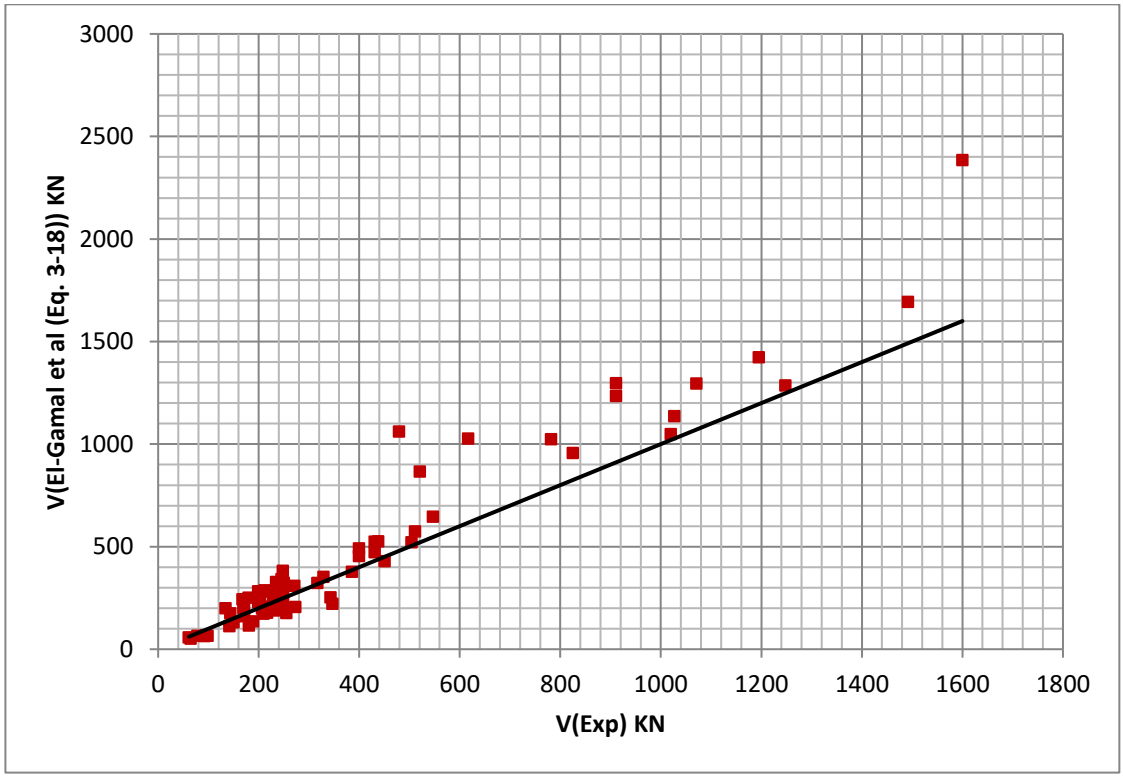

Figure 3-31. El-Gamal et al. (2005) predicted vs experimental punching shear capacities.

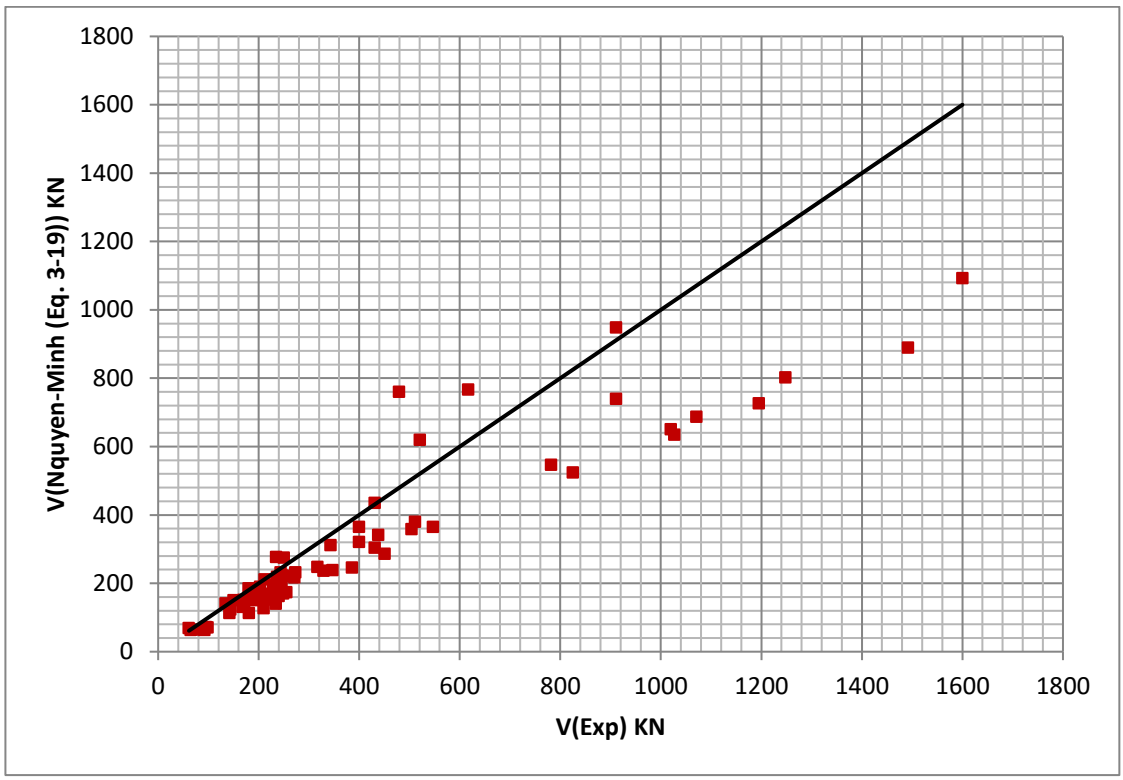

Figure 3-32. Nguyen-Minh and Rovňák (2012) predicted vs experimental punching shear capacities.

3.5 Conclusions

Six full-scale two-way slab specimens were constructed and tested under concentric loads up to failure. Punching shear capacities of slabs examined in the current investigation and elsewhere were also compared against the predictions from various equations available in the literature. The main conclusions, which can be drawn from the study described previously, are summarised below:

- Despite a lower reinforcement ratio of steel reinforcement slab by 58%, it can give a higher punching shear capacity by 14% of the counterpart GFRP reinforced slab.
- The effect of concrete compressive strength remained constant on the punching shear strength when the depth of slab increased from 150 mm to 250 mm, which is not the case for Hassan et al (2013b).

- It was recorded that if the depth of the slab specimens increased, the effects of concrete compressive strength is reduced in the post stiffness despite the similarity in the linear initial stiffness.
- With the lower specimen depth and same reinforcement ratio, the final deflection will more likely to be identical despite the difference in concrete strength failure load, whereas, in case of deeper specimen depth, it has an influence on the deflection with a margin of 19%.
- Overall, both Equations by (Matthys and Taerwe 2000; Ospina et al. 2003) give better predicted punching shear capacity values than other equations considered in the comparisons.
- ACI 440. 1R-15 (2015) gives a highly conservative prediction of punching shear strength compared to the other two codes of practice CSA S806 (2012) and Japanese Design Recommendations (JSCE 1997).
- Most equations of punching shear strength prediction are highly inaccurate with large-scale flat slab specimens tested and fall under experimental punching shear capacity values.
- A modification approach for the determination of the equivalent reinforcement area in Equation 3-18 (Matthys and Taerwe 2000) has shown an adequate estimation of punching shear resistance of slabs with larger scale and higher reinforcement ratio.

- Effect of slab span length (L) is considered for the first time in Equation 3-22 (Nguyen-Minh and Rovňák 2012), but the result of punching shear resistance is affected adversely by the limitation of the angle of the failure surface ($22.5^o \leq \alpha \leq 45^o$).

CHAPTER FOUR

FINITE ELEMENT MODELING (ABAQUS)

4.1 Introduction

Finite element method provides a convenient, adaptable and accurate way of solving and analysing highly complicated structural engineering problems, such as the analysis of RC. The complex structural engineering comprises nonlinear stress-strain response of concrete, concrete cracking, reinforcing bars rupture, the interaction between concrete and reinforcing bars, creep and concrete shrinkage.

This chapter aims to use finite element software ABAQUS Hibbitt et al (2014) for the numerical analysis part. The modelling space used 3D solid extrusion, deformable components. In addition, the damaged plasticity model for concrete in the ABAQUS material library was implemented for the concrete modelling response considering the material nonlinearity of concrete in addition to the perfect elastic behaviour of the GFRP bars. The productivity and precision of the created model were verified against the experimental results presented in the current chapter (Chapter four) and two more specimens selected from the open literature.

4.2 Finite element model

The work described in this chapter is a three-dimensional (3D) analysis modelling of concrete slab-column connections. There are some sources of difficulty in performing nonlinear finite element models summarised in material modelling, element type selections and the way of solution procedure included in models. The finite element simulations are based on utilising constitutive models. The

most common models are nonlinear elasticity, plasticity, damage mechanics and coupled damage and plasticity (Chen and Han 1988; Simo and Ju 1989; Hansen and Schreyer 1994; Lemaitre and Chaboche 1994; Holzapfel 2000). Finite Element software ABAQUS Hibbitt et al (2014) was used for the numerical analysis part. ABAQUS model was developed using the coupled damage-plasticity which is offered by the program for 3D finite element analysis. Modelling was started by defining flat slab concrete material and the reinforcement materials (GFRP) in the two-orthogonal direction, whereas, the load and the roller support considered in individual sections.

The modelling space used 3D solid extrusion, deformable components. In addition, the damaged plasticity model for concrete in the ABAQUS material library was implemented for the concrete modelling response.

4.2.1 Concrete Model

Concrete is one of the most heterogeneous materials, which displays a complicated nonlinear mechanical behaviour. The common mode of concrete member failure is cracking in tension and crushing in compression and is characterised by softening which is defined stress decreasing combined with increasing of deformation. This softening is irreversible deformations and degradation of the material stiffness (Grassl and Jirásek 2006). However, the concrete damaged plasticity model was implemented to describe concrete material modelling in this research, which, consists of an isotropic damage mechanics models used to define the tensile and low confined compression stress states. The damaged plasticity model can be used for a plain concrete and RC structures subjected to monotonic, cycling, and dynamic loading under low confining pressure (Hibbitt et al. 2014).

4.2.1.1 Concrete damaged plasticity parameters

The definition of concrete damaged plasticity is based on the five parameters requested to be considered for any modelling in ABAQUS. Two of these parameters have constant values in ABAQUS, whereas, the other variable parameters are limited between two values according to the structural modelling. The two constant parameters the hyperbolic flow potential eccentricity (ε) and the ratio of the concrete strength in the biaxial state to the concrete strength in the uniaxial state (σ_{bo}/σ_{co}) and, the default values were chosen 0.1 and 1.16, respectively, from the ABAQUS (2014) documentation values. It is defined by a small positive number that represents the rate at which the hyperbolic flow potential approaches its asymptote (Hibbitt et al. 2014).

On the other hand, other three variable parameters weren't given specific values in the ABAQUS. The first parameter is dilation angle (ψ) which stands for a material parameter that controls the plastic strain of concrete. In another meaning, dilation angle controls an amount of plastic volumetric strain developed during plastic shearing and is assumed constant during plastic yielding. Physically, ψ can be interpreted as a concrete internal friction angle. It is a fact that the low value of ψ will yield to brittle behaviour whereas higher value will yield to more ductile behaviour (Malm 2009). Concrete is a brittle material which suffers from a considerable change in volume resulting from inelastic strains. This changing in volume is called dilatancy (α_p). Dilatancy is a parameter in Drucker-Prager potential function 4–1:

$$G = \alpha_p I_1 (2J_2)^{\frac{1}{2}} \qquad 4–1$$

Where I_1 is first invariant of stress tensor, J_2 is second invariant of the stress deviator, and α_p is dilatancy.

Concrete damage plasticity model uses equation 4–2 for the potential function, which derived from equation 4–1.

$$G_{(\sigma)} = \sqrt{(\varepsilon\sigma_{t0}\, tan\,\psi)^2 + \bar{q}^2} - \bar{P}\, tan\,\psi \qquad 4–2$$

Where ε is the strain tensor, $\bar{\mathrm{q}}$ is the Mises equivalent effective stress, and $\overline{\mathrm{P}}$ is the effective hydrostatic stress.

Dilatancy is modelled in the concrete damaged plasticity model by evaluating value for the Dilation Angle. Some of the researchers (Wu et al. 2006; Voyiadjis and Taqieddin 2009) determined the parameter α_p to range between 0.2 and 0.3, which gave an equivalent dilation angle of 31° to 42°, respectively. Therefore, the dilation angle variation in the current research is between these two limits with some trail models extended out of these limits and with respect to the maximum value given in the ABAQUS documentation (56.3°) to study in general the effects of dilation angle on the current modelling. The second parameter in the concrete damaged plasticity is the ratio of the second stress invariant in tension to that in compression (K_c). The value of K_c is limited between two values 0.5 and 1.0. There are very minimal differences in resultant values (in terms of force-displacement response) compared to the experimental results when the K_c is varied between the two limits. The best value founded of the K_c after comparison with experimental results is the default value of 0.667 provided by the ABAQUS. The last parameter included in the concrete damaged plasticity parameters is called viscosity (μ). The viscosity is representing the relaxation time of the viscoelastic system, and it is used to overcome some convergence problems. The parameter value is depending on the time increment step. The default value provided by ABAQUS is zero. The values of the trail modelling in the current research was kept in small values according to Genikomsou and Polak (2015) and Lee and Fenves (1998).

After a parametric study, which created to select the parameters used to define the concrete damage plasticity model, the concluded results were presented in the following table.

Table 4-1. Parameters of concrete damage plasticity used in the current ABAQUS model

Dilation angle	Eccentricity	σ_{bo}/σ_{co}	K_c	Viscosity Parameter
43°	0.1	1.16	0.667	0.0001
Where σ_{bo}/σ_{co} is the ratio of initial equibiaxial compressive yield stress to initial uniaxial compressive yield stress, *K*c is the ratio of the second stress invariant in tension to that in compression.				

4.2.1.2 Elastic behaviour

Linear elastic behaviour of concrete (E_c) value can be defined directly in ABAQUS. The behaviour of Elastic modulus in the linear elastic range was calculated by using equation according to Eurocode 2 (2004), whereas the Poisson's ratio v = 0.2.

$$E_c = 22000\left(\frac{f_c'+8}{10}\right)^{0.3} \qquad 4\text{–}3$$

where E_c is the elastic modulus of concrete in MPa and f_c' is the cylinder compressive strength of concrete in MPa.

4.2.1.3 Compression behaviour

Two main failure mechanisms were considered for the concrete material; tensile cracking and compressive crushing. In the current research, the brittle concrete behaviour under uniaxial compression is characterised by using the stress-strain relationship outside the elastic range according to Eurocode 2 (2004), which is also shown in Figure 4-1.

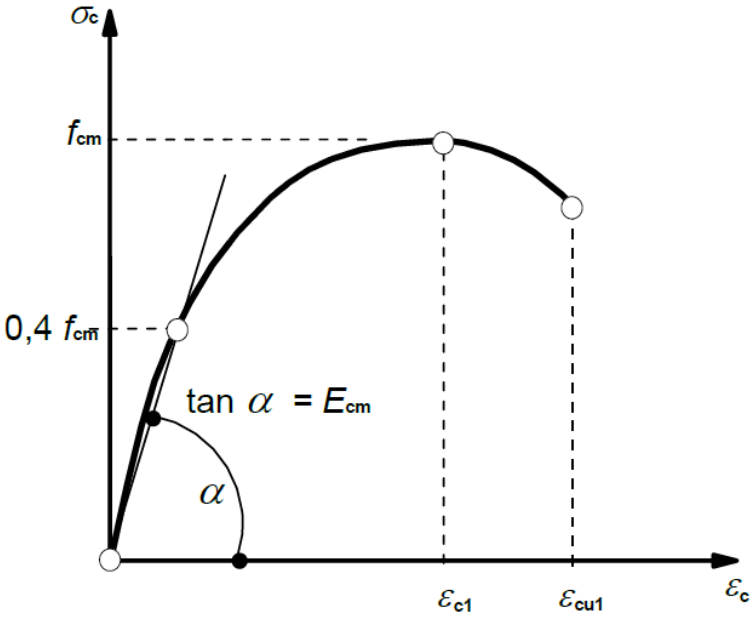

Figure 4-1. Stress-strain relationship of concrete in compression (BS EN 1992-1-1:2004)

In other meaning, the compressive stress is provided as a function with the inelastic strain in a tabular form. In Figure 4-1, three phases of behaviour can be observed in the stress-strain relationship. The linear part is continuing until reach a stress level of $\sigma_{cm} = 0.4f_c'$. The second part is nonlinear up to the maximum load f_{cm} corresponding strain level of ε_{c1}, which (ε_{c1}) can be obtained from Table 3.1 in the Eurocode 2 (2004). After the peak stress, the third part of the relationship is continuing with softening up to the ultimate strain of ε_{cu1}, which (ε_{cu1}) can be obtained from Table 3.1 in the Eurocode 2 (2004). The equations 4–4 to 4–7 of the compressive stress-strain relationship of concrete were presented as follows:

$$\sigma_c = f_c' \frac{K\eta - \eta^2}{1 + (K-2)\eta} \qquad 4\text{–}4$$

$$K = 1.05 \frac{E_c \varepsilon_{c1}}{f_c'} \qquad 4\text{–}5$$

$$E_c = 22000 \left[\frac{f_c' + 8}{10}\right]^{0.3} \qquad 4\text{–}6$$

$$\eta = \frac{\varepsilon_c}{\varepsilon_{c1}} \qquad 4\text{–}7$$

where σ_c is the compressive stress of concrete in MPa, f_c' is the mean value of concrete cylinder compressive strength in MPa, E_c is the elastic modulus of concrete in MPa, ε_c is the compressive strain of concrete at any stress σ_c, and ε_{c1} is the strain at peak stress.

4.2.1.4 Tension behaviour

Stress-strain approach was used to model the behaviour of normal concrete under tension. In the concrete damaged plasticity model of ABAQUS, three different methods can be used to define the behaviour of concrete under uniaxial tensile load. The first method is the stress-strain approach which required to specify the data of stress and strain in a tabular form. The second option method is the crack-opening-displacement approach. This approach is also requested the tensile stress and the crack-opening displacement input data in the tabular form. Whereas the third method is fracture energy approach which is defined the energy required to open a crack of unit area (Hillerborg et al. 1976). After a comparison modelling in ABAQUS, the stress-strain approach was found the most accurate method among the other two approach in the current study. The approach is considered the additional strength and stiffness that is resultant from the concrete and the bar interaction. These interacting is known as tension stiffening, and it can be modelled by applying a progressively descending post-peak tensile response. To contemplate this effect, the following stress-strain equations were listed from 4–8 to 4–12:

$$\text{for } \varepsilon_t \leq \varepsilon_{cr} \qquad \sigma_t = E_{co}\varepsilon_t \tag{4–8}$$

$$\text{for } \varepsilon_t > \varepsilon_{cr} \qquad \varepsilon_t = f_c' \left[\frac{\varepsilon_{cr}}{\varepsilon_t}\right]^{0.4} \tag{4–9}$$

$$E_{co} = 5000\sqrt{f_c'} \tag{4–10}$$

$$\varepsilon_{cr} = \frac{f_c'}{E_{co}} \tag{4–11}$$

$$f_t = 0.33\sqrt{f_c'} \qquad 4–12$$

where σ_t is the tensile stress of concrete in MPa, E_{co} is the initial elastic modulus of concrete in MPa, ε_{cr} is the strain of concrete at peak stress (at cracking). f_t' is the tensile strength of concrete at the peak value of concrete stress in MPa,

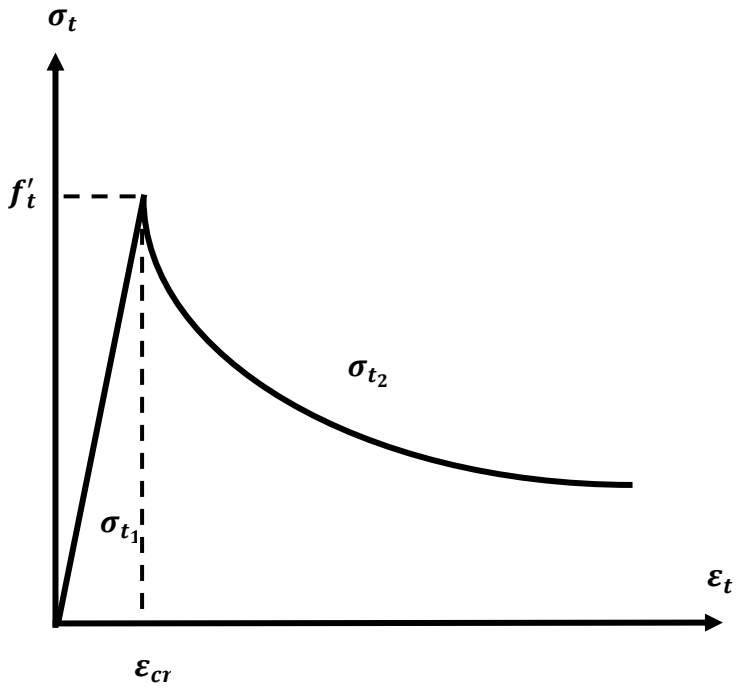

Figure 4-2. Uniaxial stress-strain tensile model

The elastic modulus (E_c) in the linear elastic range was calculated according to Eurocode 2 (2004), whereas the Poisson's ratio v = 0.2. Dilation angle ψ = 43˚ and potential eccentricity ε = 0.1 parameters were used in the part of plastic range damage parameter. In addition, the ratio of initial biaxial compressive yield stress to initial uniaxial compressive yield stress σ_{b0}/σ_{c0} was determined by default 1.16, while the ratio of the second stress invariant on the tensile meridian (shape factor) K_c = 0.667. Finally, the last parameter requested was viscosity parameter which set to zero. Mechanical properties of the previous experimental database were uploaded individually in the material manager of the ABAQUS Hibbitt et al (2014). Each of the mechanical properties of each experimental test was updated

accordingly for each model. Moreover, mechanical properties of the concrete for the present research were measured experimentally as shown in Table 3-2.

4.2.2 Reinforcement model

Glass Fiber Reinforcement polymer bars were modelled to be a linear elastic isotropic material with brittle failure at tension force. Reinforcements were created in the ABAQUS by selecting two-dimensional wire truss application. The two parameters f_f and E_f were uploaded in ABAQUS from the experimental results given in Table 3-2 to Table 3-1.

4.2.3 Load Bearing Plate

A steel plate size 200 mm × 200 mm × 50 mm was modelled to be a linear elastic isotropic material with two parameters E_s 400000MPa and Poisson's Ratio 0.3. The load that caused each displacement was evaluated as the vertical reaction associated with each step at the support location. Top plate surface with reference point was created to be a rigid plate, whereas, the bottom surface connected by a tie type connection with concrete surface to avoid any horizontal displacement of the plate during application of the load (Figure 4-3).

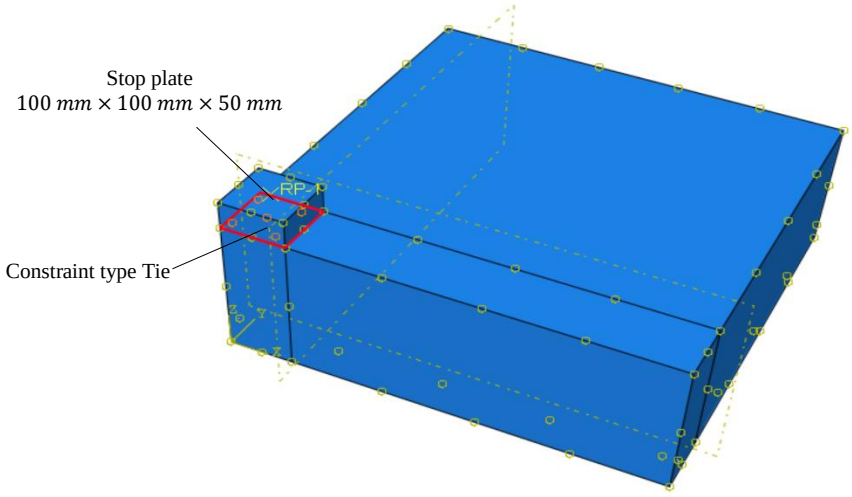

Figure 4-3. Constraint type Tie between load bearing plate and the surface of the concrete

4.2.4 Mesh and convergence issue

Three materials type were used in the current finite element analysis. Different definitions of mesh elements were given for each material type. A wide range of mesh elements is available in ABAQUS program for different geometries and analysis types. The type of element is selected according to the general knowledge of the theory and application of the ABAQUS (Hibbitt et al. 2014). The accuracy of the elements usually depends on the number of the nodes in each element and the order of the integration. In case of linear interpolation case, nodes are located at the end of elements, whereas in the case of quadratic or cubic interpolation functions, nodes located in-between and at the ends of each element. By adding more nodes to the elements, simulation of concrete can lead to more accurate results. Figure 4-4 is the basic understanding between the linear cubic element with fewer nodes and a quadratic cubic element with extra nodes in-between elements.

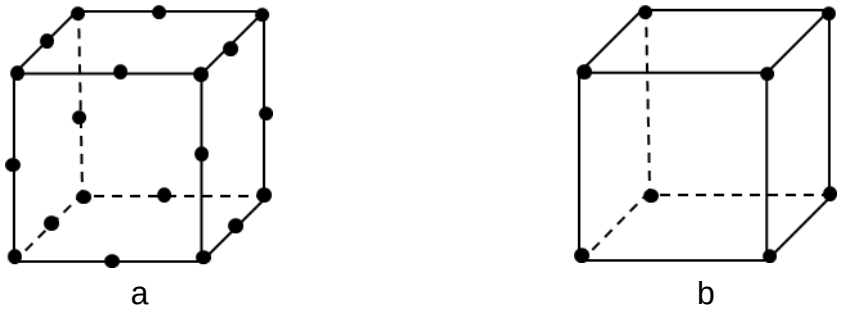

Figure 4-4. Elements and nodes (a) quadratic elements; (b) linear elements

Mesh size is one of the main aspect affecting the accuracy of the FE results and the simulation time analysis dramatically. It is a commune fact if the size of the mish is reduced, the more accurate result is attained. Though, applying finer elements requests more computational time and resources. In case of structural elements reinforced with GFRP bars, it is expected to have more, and wider

cracks compared to the structural elements reinforced with SR bars due to low young modulus and high strain. However, refining the mesh may cause more convergence problems resulting from narrower crack bands (Alih and Khelil 2012). In case of GFRP reinforced concrete slab, refining of the mesh is more convention than reducing mesh sensitivity. In order to select the best mesh size in this project, the model was applied with different mesh size and the results were compared with the experimental results.

4.2.4.1 Concrete mesh

It is difficult to model a structure made of brittle materials like concrete for common static solution approaches. Propagation of cracks which usually occur in a brittle material can cause unstable structural responses. Due to localised damage, nodes displacement around the damage zones dictates the average of the displacement increment which in turn the global model of displacement cannot be sensitively reflected by the failure process. A nonlinear analysis was applied with displacement mechanism type.

Solid (or continuum) elements was used to model all concrete specimens tested in this current project G_{150}(210)47, G_{250}(160)52, G_{250}(100)53, G_{150}(210)35, G_{250}(160)37, and S_{150} (210)37 in the ABAQUS (Hibbitt et al. 2014). The continuum modelling is the most common model for RC structures due to the ability to express most of geometries and model linear and nonlinear behaviour. C3D8R hexahedral elements and 8-noded were used for the concrete with reduced integration to avoid the shear locking (Hibbitt et al. 2014). The coarse mesh was used in the preliminary trail modelling results which showed inaccuracy results, due to the distraction of the hexahedral elements of C3D8R in the concrete tensile zone. Given the ability to select first-order of second-order

interpolation in ABAQUS, the first-order was selected to reduce running time of the analysis.

4.2.4.2 Load bearing plate mesh

Solid elements were used to model load bearing plate which had been used in the current project. The same hexahedral elements C3D8R of concrete elements are applied to the load bearing plate.

4.2.4.3 Reinforcement mesh

Linear truss elements T3D2 with 2-nodes represent the reinforcement mesh. Truss elements in ABAQUS can represent two or three dimensions of a slender structural element which has the ability to resist and transfers only axial forces. By adding the area of the cross-section of FRP bars with it is mechanical properties, GFRP reinforcement bars will be contributed with low effects in the shear resistance. Since the strain is considerable in case of FRP reinforced bars compared to the steel bars, truss elements can be used to model components which strain is computed from the change of it is length (Hibbitt et al. 2014). On the other hand, a truss element has the advantage of ease of using the perfect bond by defining embedded GFRP bars into concrete slab as a host region.

4.2.5 Concrete and Reinforcement Interaction

The interaction between different components materials is one of the vital factors for modelling any structure. The importance of interaction is reflected in the sensitivity of correct transfer of the forces between the different parts of a structure. The ABAQUS library considered a different variety of contact models for any interaction between various components of materials in each modelling. Therefore, the method of embedded reinforcement in the concrete was used to simulate the bond between the concrete and the reinforcement. Since all the

specimens used in the current research were failed by punching shear, the assumption of the perfect bond was chosen to represent concrete and reinforcement interaction.

4.2.6 Boundary Conditions

All the slabs specimen were modelled by a quarter size of the real specimen size in ABAQUS (2014) (Figure 4-5a). Two faces were chosen the option of symmetry in the ABAQUS to represent the continuity of the slab specimens into two direction x-access and y-access (plane surface z-x in the x-access and plane surface z-y in the y-access) (Figure 4-5b). Whereas, the other two represent the ending two sides of the slabs specimen and supported by simply support in the direction of z-access direction (Uz=0) (Figure 4-5b). The symmetry case is also applied to the stop plate in the two parallel the symmetry faces of the slabs specimen.

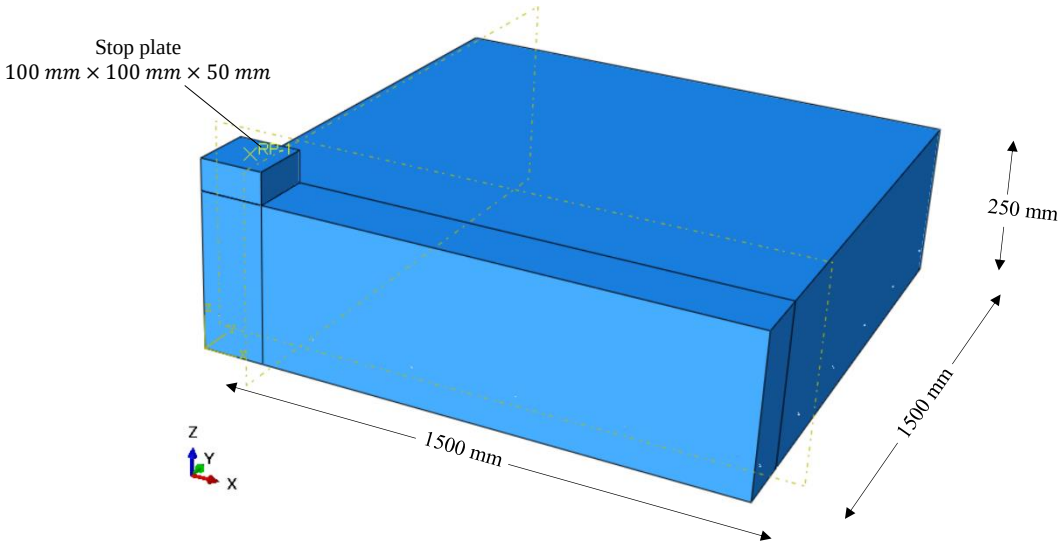

(a)

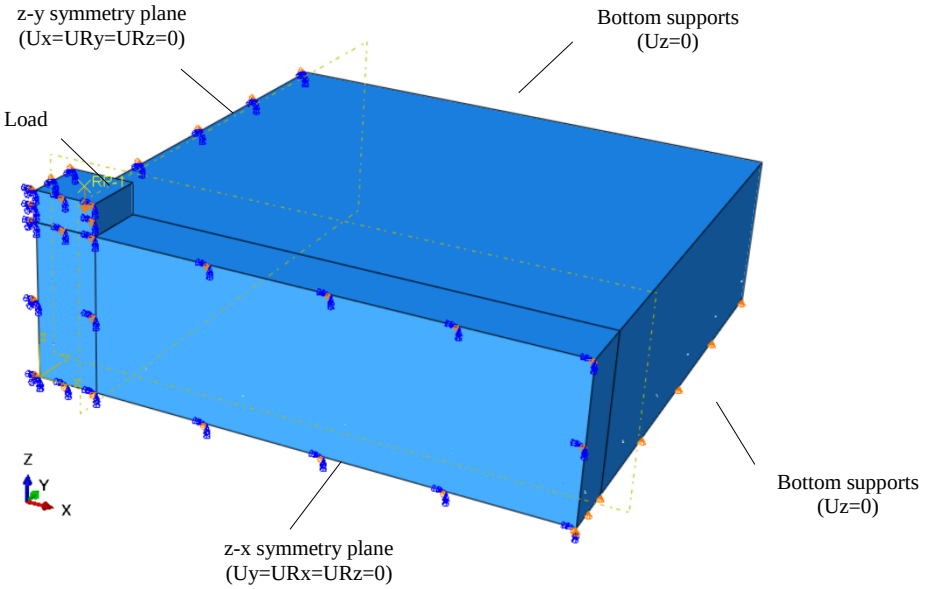

(b)

Figure 4-5. Geometry and boundary conditions (a) Geometry modelling; (b) boundary conditions

4.3 Parameters investigation of the Explicit Model

There are fewer parameters require a parametric study in case the Explicit Model compared to the Static Model. The parametric study was conducted to choose the most suitable value for each parameter. The case study was established by comparing the most accurate models' behaviour and result to the experimental ones. Moreover, the time requires running the model was considered in the case study. The study was started by selecting one of the lab specimens (G_{250}(160)37) from the current research and was modelled for several trails to investigate the overall effects of each parameter, whereas, the results were compared with the experimental ones by plotting load force and displacement graphically (Figure 4-10). It was concluded the most two effects parameters on the Explicit Model are Dilation Angle (ψ) and the size of the mesh.

4.3.1 Mesh Size

The mesh size sensitivity was examined by running several models with different mesh sizes, and other parameters were kept constant. It is well known if the mesh sizes were refined, the more accurate results are achievable. In case of explicit modelling, the sensitivity of the mesh sizing is more than static modelling (Yu et al. 2008). However, refining the mesh sizing will lead to more running modelling time. The mesh of 20 mm × 20 mm × 20 mm was selected to start the investigation of effects of the mesh sizing. Genikomsou and Polak (2015) were concluded the mesh of 20 mm × 20 mm × 20 mm size is the most suitable for their case study of modelling of punching shear of concrete slabs reinforced with steel bars. Larger mesh sizes were included in the investigation of the current research. Four mesh sizes applied for the investigating of the mesh sensitivity were: 20 mm × 20 mm × 20 mm, 27 mm × 27 mm × 27 mm, 30 mm × 30 mm × 30 mm and 35 mm × 35 mm × 35 mm (Figure 4-6). The comparison of the mesh sizes was plotted in Figure 4-7.

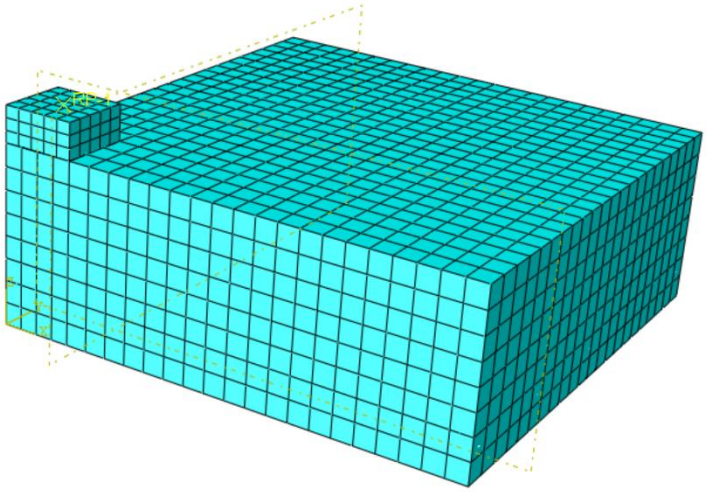

Figure 4-6. Slab mesh 30 and plat mesh 20

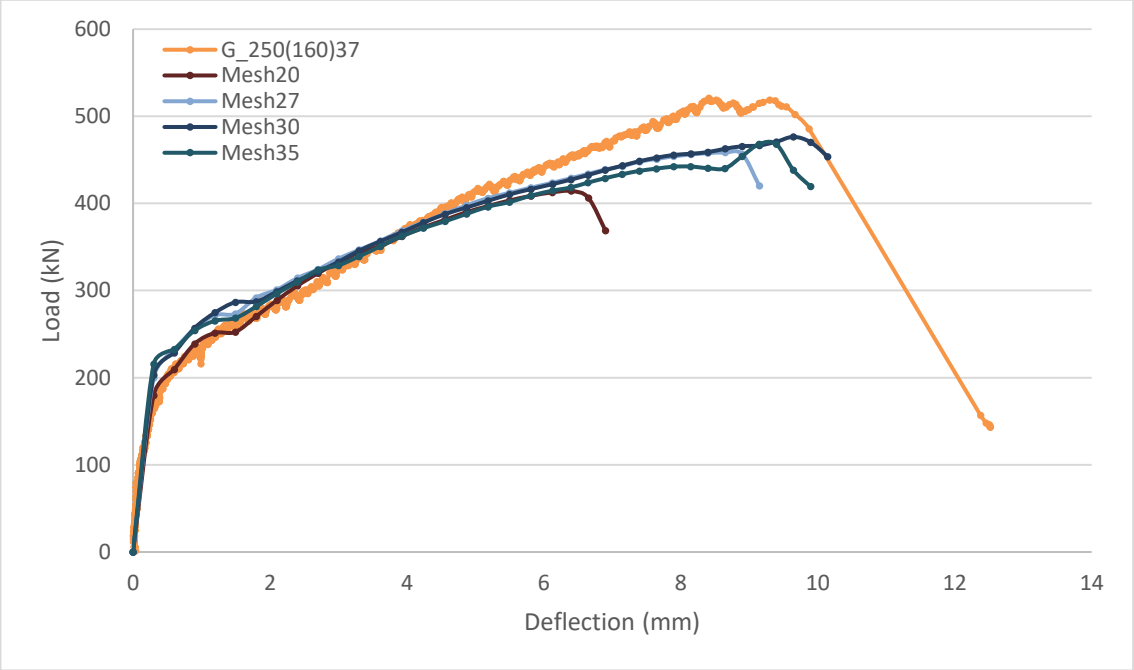

Figure 4-7. Load versus deflection for slab G_{250}(160)37(Mesh sizes 20,27,30 and 35)

4.3.2 Dilation Angle

The effect of dilation angle was examined by adopting three different values in ABAQUS: $\psi = 40^{\circ}$, $\psi = 43^{\circ}$, and $\psi = 45^{\circ}$. To select the appropriate dilation angle value in a modelling, the simulation was running for some models with the three mentioned ψ values and compared with the load-deflection response of the specimens G_{250}(160)37 (Figure 4-8). The effect of dilation angle is about $^{1}/_{3}$ end of each trend. When ψ values were kept increasing, the influence on the deflection is more than the load effects, whereas, no much impact on the initial stiffness of the load-deflection behaviour. It was noticed if the value of ψ increased from 40° to 43°, the load value increased by a percentage of 11% and the deflection is also increased but with 8%. Whereas, when the value of dilation angle risen from 43° to 45° the load failure was raised with small margin compared with the deflection. At the end of the analysis, the value of $\psi = 43^{\circ}$ was selected for best load-deflection behaviour compared with the experimental once (Figure 4-8).

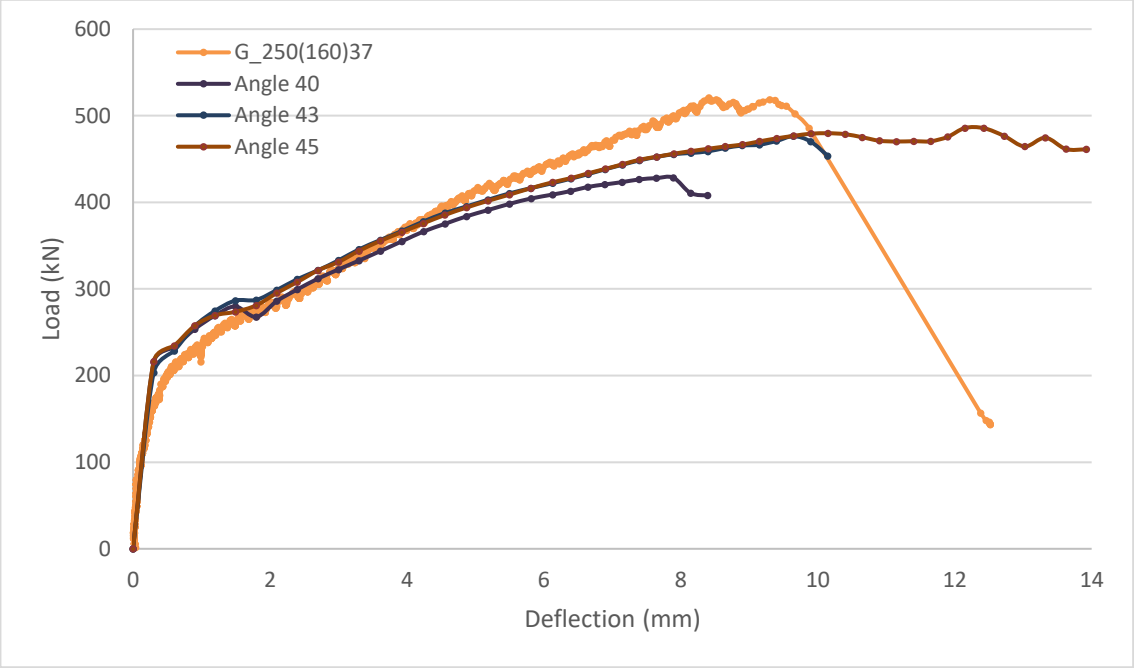

Figure 4-8. Load versus deflection for slab G_{250}(160)37(Dilation Angle 40,43, and 45)

4.4 Model validation

In this section, the parameters in the previous articles were investigated to select the most appropriate values to achieve a certain accuracy of load-deflection and general behaviour results. All proposed ABAQUS models were tested against the current experimental behaviour of GFRP reinforced concrete flat slabs. The validation is extended to cover two more specimens selected from open literature and comparing them with the proposed model.

4.4.1 Open literature Validation

The selection of the two specimens was according to the depth measurement value. It was aimed to select two different depth values with approximate variation not less than 40% and bearing in mind that they have the same dimensions of length and width. The two specimens were taken from Hassan et al (2013b) experimental work. The details of the two slab specimens are listed in Table 4-2. The two selected slab specimens were failed in punching shear due to evident

crack defining the failure surface of the specimen around the column which is similar to the failure of experimental specimens of the current study.

The comparisons of load versus deflection between the proposed modelling and the specimens of the open literature are plotted in Figure 4-9. It can be seen that the proposed modelling behaviour is very similar to the selected experimental specimens. It has been noticed a minor change in behaviour after concrete cracking. Overall, all proposed models have very reasonable predicting the load-deflection behaviour compared the selected two specimens.

Table 4-2. Details of test specimens from open literature (Hassan et al. 2013b)

No	Specimen	Slab thickness mm	d mm	Column Dimension mm	Tension GFRP	ρ_f %	f_c MPa
1	$G_{(0.7)}$30/20	200	134	300	12 No. 5	0.71	34.3
2	$G_{(0.3)}$30/35	350	284	300	12 No. 5	0.34	34.3

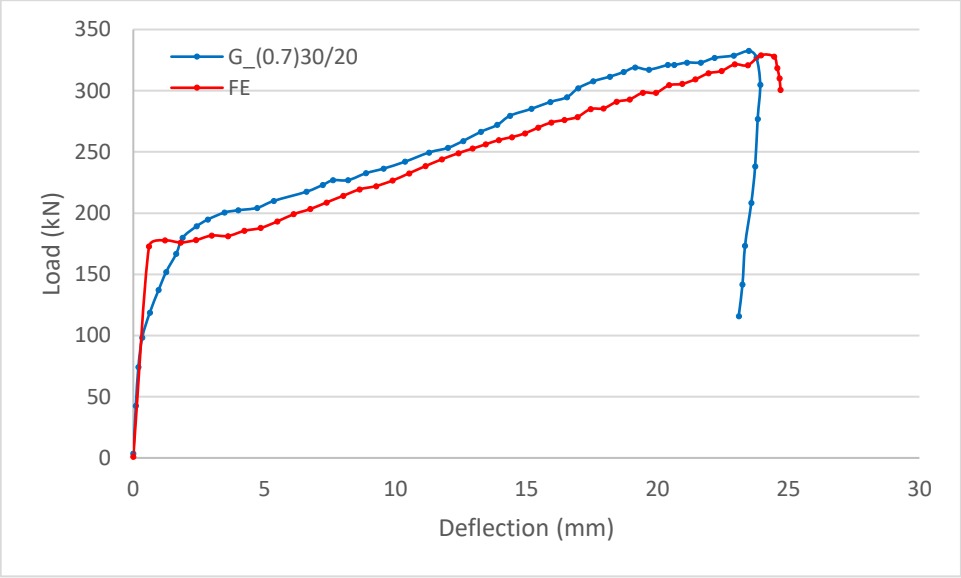

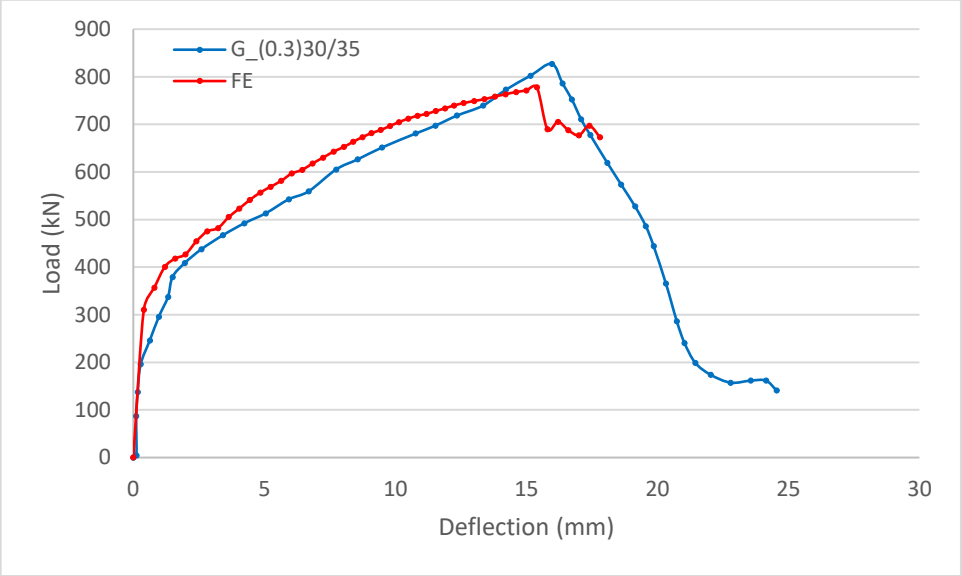

Figure 4-9. The proposed FE model load-deflection verses the open literature experimental work (Hassan et al. 2013b)

4.4.2 Experimental failure load validation

A comparison was carried out between the experimental failure load results from the current research and the failure load prediction results obtained from the proposed FE modelling (

Table 4-3). The finding is presented in

Table 4-3. The mean, SD and coefficient of variance are 0.98, 8.5%, and 8.67%, respectively. Specimen G_{250}(100)53 had unexpected load failure result from the experimental work as explained in section 3.3 of this work. Regardless of the different depths of flat slab used in the present computational analysis, the predicted load failure from the FE modelling gives acceptable results compared with the experimental results.

Table 4-3. Comparisons between the FE predicting load failure and the current experimental load failure load

Slab notation	Experimental failure load V_{Exp} (kN)	FE predicted failure load V_{FE} (kN)	$\frac{V_{Exp}}{V_{FE}}$
G_{150}(210)47	199.0	205	0.97
G_{250}(160)52	617.2	597	1.03
G_{250}(100)53	479.3	560	0.86
G_{150}(210)35	167.8	173	0.97
G_{250}(160)37	520.9	477	1.09
Mean			**0.98**
Standard deviation (%)			**8.5**
Coefficient of variation (%)			**8.67**

4.4.3 Experimental load-deflection behaviour validation

All FRP reinforced concrete flat slab specimens were modelled in ABAQUS, and the results of the load-deflection response were used to compare them with experimental results of the current research (Figure 4-10). Most of the comparisons show good agreements in the initial stiffness of the trends except for the specimen G_{250}(100)53. The unexpected experimental behaviour and failure load result of spacemen G_{250}(100)53 were explained in the previous chapter 3. A reduction of the stiffness was recorded after the initial stiffness in all predicted modelling, which coincides with the experimental load-deflection behaviour after cracks were started. In the two specimens G_{150}(210)47 and G_{150}(210)35 more deflections were recorded in the predicted models compared with experimental once. Whereas, the failure load was also having a bit of higher values in the modelled once compared to the two samples of the experimental. In case of specimen G_{250}(160)52, a higher initial stiffness was noticed in the

proposed modelling, but it reduced dramatically compared to the experimental once. Whereas the best modelling was recorded for the specimen G_{250}(160)37, in case of GFRP reinforced concrete flat slab. On the other hand, the predicted modelling for specimen S_{150}(210)37 shows compelling load-deflection behaviour compared with the experimental results. Overall, the proposed modelling can produce a good agreement and acceptable results compared with the experiments.

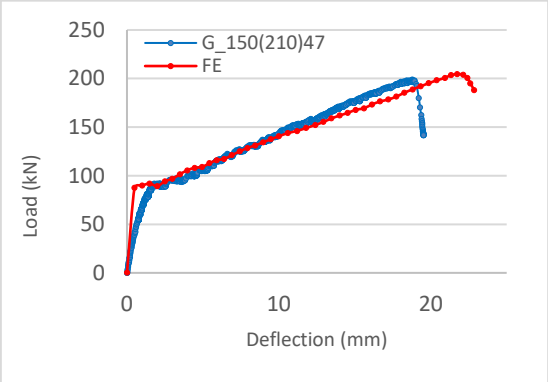

G_{150}(200)47

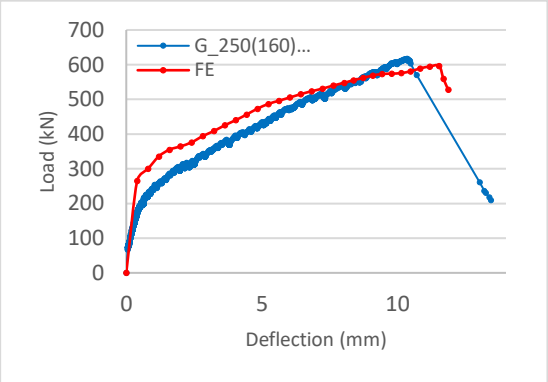

G_{250}(160)52

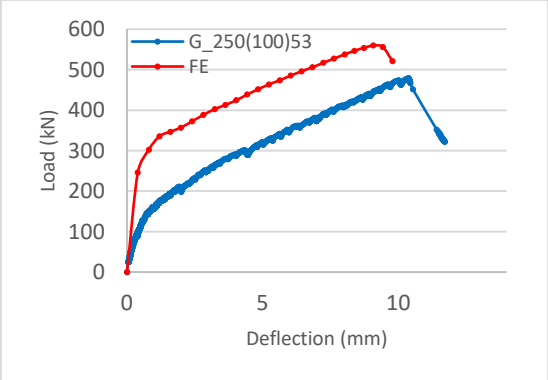

G_{250}(100)53

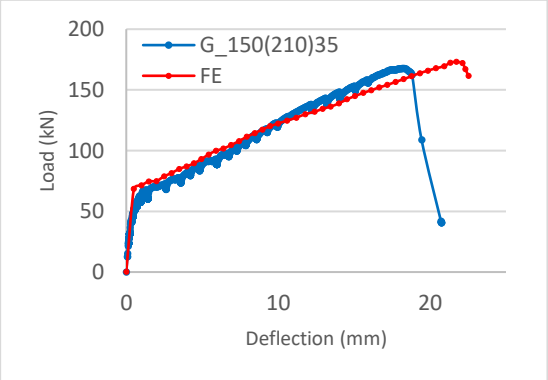

G_{150}(200)35

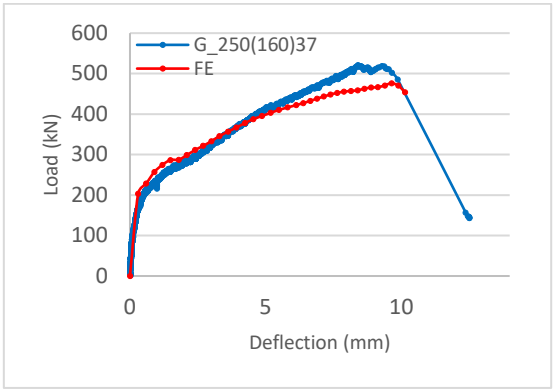

G_{250}(160)37

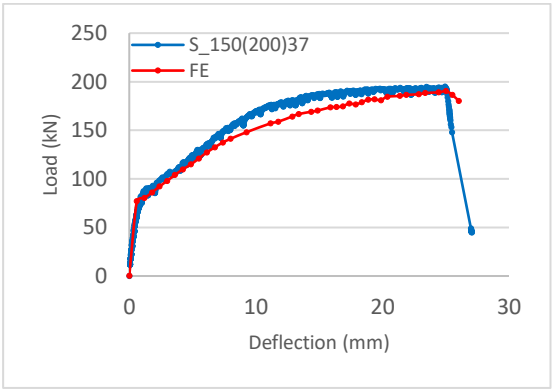

S_{150}(200)37

Figure 4-10. The proposed FE model load-deflection verses the current experimental results

4.4.4 Finite element cracking pattern and maximum tensile stress validation

Load-displacement analysis results for slab G_{250}(160)52 are presented in Figure 4-10. Model simulation gives brittle punching shear failure with softening after failure. Finite element modelling results in Figure 4-11 and Figure 4-12 shows a punching shear failure rather than the local bearing. Figure 4-11 shows the cracking pattern on the tension side of the modelled slab at failure. The cracking spreads inside the slab adjacent to the column. Start with tangential cracks near the column, then extended radially with load increasing. The punching shear cone is visible at ultimate load due to sudden opening of the cracks. Cracks orientation is measured in perpendicular to the maximum principal plastic strain which is the case shown in Figure 4-11. Comparing finite element modelling to the slab G_{250}(160)52 laboratory cracking pattern results at the bottom surface, the cracking initiated at a distance of about 30 mm from the edge of the slab where the simply support is positioned in the real situation of the specimen (Figure 4-11).

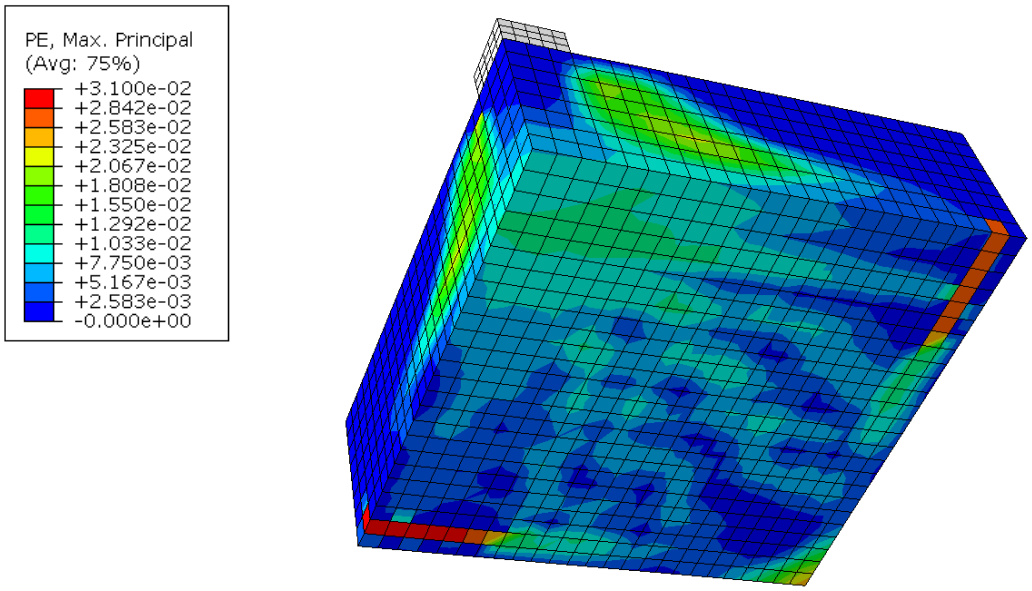

Figure 4-11. Cracking pattern on tension surface at ultimate load for slab $G_{250}(160)52$

The failure of the two surfaces slab at the maximum tensile principal stresses are shown in Figure 4-12. Tension region is around the loaded area in the blue colour whereas, the red colour represents the compression regions which are concentrated in corner regions. This type of tension and compression stress regions are following the same crack pattern that induced by membrane forces in a slab with no in-plane restraint. The cracking patterns can be demonstrated by the principal tensile stresses in the Finite Element Modeling. However, a better representation of the cracks shown by the maximum plastic equivalent principal strains in Figure 4-11.

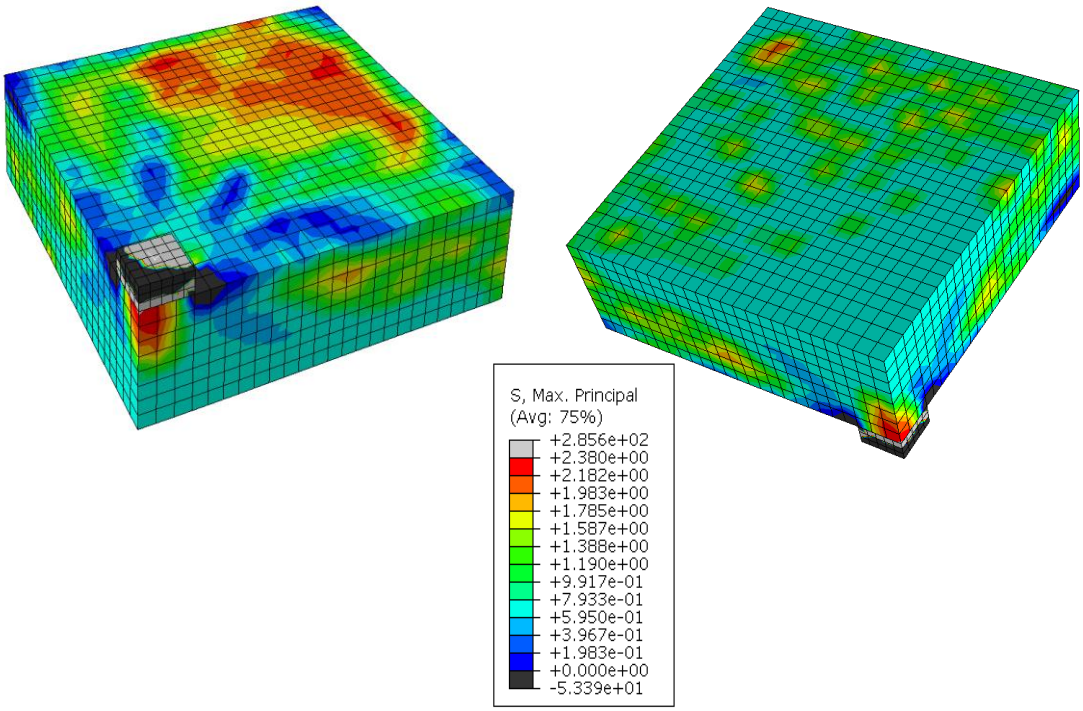

Figure 4-12. Maximum tensile principal stress in concrete at the failure of the slab $G_{250}(160)52$

4.5 Parametric Study

After the proposed ABAQUS model was verified for predicting the behaviour of punching shear of GFRP reinforced concrete flat slab, several parametric studies were carried out to investigate the structural behaviour of GFRP reinforced concrete flat slab with additional variation parameters extended beyond of that current research experimental parameters. The geometrical dimensions of the GFRP reinforced concrete flat slab used in this parametric investigation are similar to those used in the experimental work except columns perimeter (b_o) was altered to gain varied perimeter to depth ratio values. Due to symmetry in the geometry, boundary conditions and loading arrangement, all the slabs specimen were modelled by a quarter size of the real specimen size in ABAQUS (2014). The axis of symmetry was taken in the middle of each side of the slab specimens. The main parameters included in this study were listed in Table 4-4.

Table 4-4. List of the parameters included in the parametric study

f_c' (MPa)		$c\ (mm), \left({}^{b_o}/_{d}\right)$		ρ_f, (spacing of reinforcement)	
H = 150 mm	H = 250 mm	H = 150 mm	H = 250 mm	H = 150 mm	H = 250 mm
30	30	150 (6.4)	150 (3.1)	-	0.85 (200)
50	50	200 (8.5)	200 (4.2)	1 (200)	1.1 (160)
70	70	300 (12.8)	300 (6.3)	1.5 (160)	1.5 (100)
-	-	400 (17)	400 (8.4)	-	2.1 (70)
Where f_c' is the concrete compressive strength in MPa, c is the loaded area one side length, ${}^{b_o}/_{d}$ is the perimeter length of loaded area of loaded area to the depth ratio, ρ_f is flexural reinforcement ratio and H is the depth of slabs.					

Concrete strength is the first parameter included in this study measured in MPa with three values: 30, 50 and 70 MPa. The second parameter is the loading perimeter to the effective depth ratio b_o/d, included four investigated variable values for two depths of the concrete flat slab (150 mm and 250 mm) (Table 4-4) whereas, reinforcement ratio is the third parameter with four variable values included in the investigation for concrete flat slab of depth 250 mm and two variable values for concrete flat slab depth 150 mm. The result of this parametric study led to some conclusions regarding the punching load strength and overall behaviour of GFRP reinforced concrete flat slab.

4.5.1 Concrete strength

One of the main factor considered in the parametric study is the concrete compressive strength. Concrete compressive strength has an important influence that controls the punching shear capacity. Different concrete compressive strengths were used in this study covering a range of normal concrete compressive strength and high concrete compressive strength. The values of concrete compressive strength were limited between 30 MPa and 70 MPa with an increment of 20 MPa to optimise acceptable variation between two increases. Moreover, the selected concrete compressive strength covered the range of

concrete compressive strength implemented in experimental work of the present research. The effect of concrete compressive strength was examined for two different GFRP reinforced concrete flat slab depth: 150 mm and 250 mm.

Figure 4-13 shows the effects of concrete compressive strength on the punching shear load capacity of GFRP reinforced concrete flat slab with the two different slab depths 150 mm and 250 mm. Despite the differences of slab depth, increasing concrete compressive strength will lead to identical general behaviour in all GFRP concrete flat slabs considered in the current study. All specimens exhibited typical bilinear load-deflection behaviour until sudden failure due to punching shear as explained previously in 3.2.2. Regardless the slab thickness values, the prediction of proposed ABAQUS model show an increase in concrete strength will lead to a steady increase in the load carrying capacity. Results show that increasing the concrete strength from 30 MPa to 50 MPa and 50 MPa to 70 MPa in a slab depth of 150mm, will increase punching shear capacity by 20% and 6%, respectively. Whereas, the results of increasing concrete strength (30 MPa to 50 MPa and 50 MPa to 70 MPa) on slab depth of 250 mm, will also increase punching shear capacity by 15% and 8%. It can be apparently noticed that the effect of increasing the concrete compressive strength on punching shear strength is more pronounced in normal concrete strength rather than high concrete compressive strength in both GFRP concrete flat slab depths.

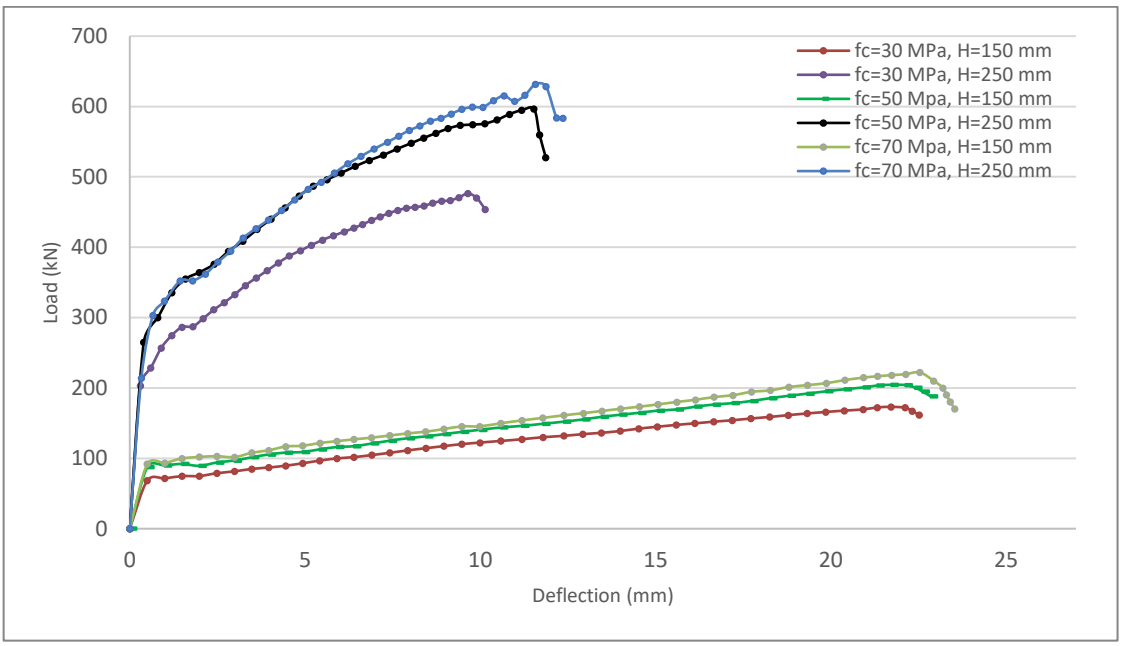

Figure 4-13. Effects of concrete compressive strength on punching shear strength

The relationship between the ultimate punching shear stress and the concrete compressive strength is presented in Figure 4-14. The results show if the concrete compressive strength increase, the maximum punching shear stress will increase accordingly which in turn leads to better resistance. Curve fitting was created for the two depths of 150 mm and 250 mm as shown in Figure 4-14 in order to introduce an equation for a mathematical correlation between the punching shear stress and the concrete compressive strength. According to the relationship, the equations can be described in a linear function. These relationships are also sensitive accordingly to any change in material property, reinforcement ratio and materials, and geometry. Geometry is the only variable parameter in the current study. Each of relationship varied according to the slab depth. The variation is minimal with about 3% between the two relationships corresponding to the two slab depths.

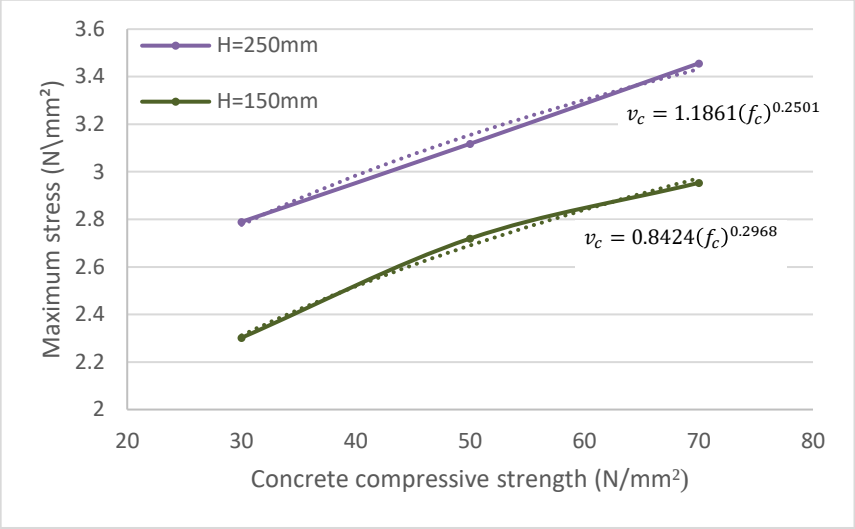

Figure 4-14. Effects of concrete compressive strength on punching shear stress

The study is also should be extended in the future to examine variable reinforcement ratio with the different concrete strength to study the normalised punching shear stress (v_c/f_c) with the effective reinforcement ratio ($\rho\, E_f/E_s$).

4.5.2 Shear load perimeter to effective depth ratio

Since FRP materials are, comparatively, new in structural engineering application field like punching shear in GFRP reinforced concrete flat slab; hence, more researchers are needed to cover all factors affecting the behaviour of a column to slab connection region. One of the vital factor affecting the punching shear strength is column dimension which represented in the current ABAQUS modelling by steel loading cap to simulate the experimental work of the current research. Four square steel loading cap perimeters were chosen to examine the effect of the shear perimeter to effective depth ratio on punching shear capacity. Shear load perimeters to effective depth were examined for 94 mm effective slab depth with the ratio of 6.4, 8.4, 12.8 and 17 corresponding to square steel cap cross-sections of 150, 200, 300, 400 mm; respectively. Whereas the effective depth of 191mm has shear load perimeters to effective depth ratio of 3.1, 4.2, 6.3

and 8.4 corresponding to the same square cap cross-section of that specimen of effective depth 94 mm.

The effect of shear load perimeters on punching shear strength is given in Figure 4-15. Results show that increasing load perimeter from 150 to 200 mm, 200 to 300 mm and 300 to 400 mm in a slab depth of 150 mm, will increase punching shear strength by 7.9%, 15.2% and 9.8%, respectively. There are no significant differences observed regarding deflection when the measurement of the perimeter was changed for each specimen. In case of slabs have an effective depth of 191 mm, the results are also within the range of that slab specimen with a depth of 94. The failures were recorded at an increasing punching shear strength by 10.5%, 9.8% and 12% for the same perimeters included in the previous specimen with the depth 94 mm. In addition, it appears that there is an increase in the degree of nonlinearity of the model at failure as the column cross-section is increased.

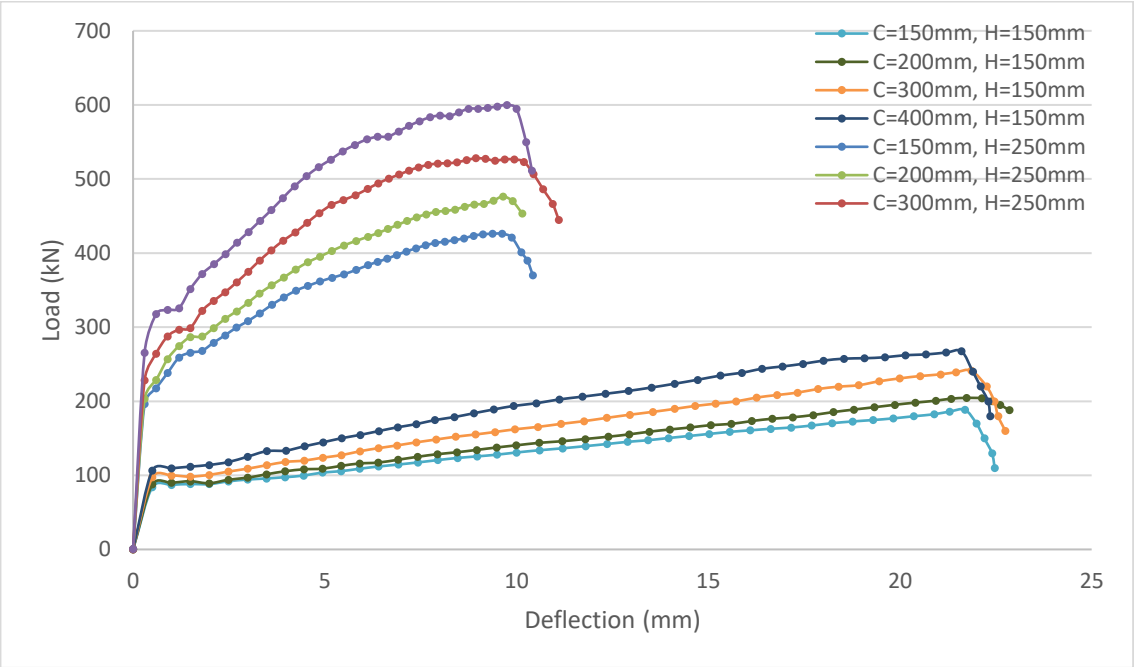

Figure 4-15. Effects of column perimeter on punching shear strength

The relationship between the ultimate punching shear strength and the perimeter to effective depth ratio is presented in Figure 4-16. The results show if the column cross section increase, the punching shear strength will increase accordingly which in turn leads to better resistance according to the fact the shear stress around the column perimeter going to be decreased. Curve fitting was created for the two depths of 150 mm and 250 mm as shown in Figure 4-16 in order to introduce an equation for a mathematical correlation between the punching shear strength and the perimeter to effective depth ratio. According to the relationship, the equations can be described in a linear function. These relationships are also sensitive accordingly to any change in material property, reinforcement ratio and material, and geometry. Geometry is the only variable parameter in the current study. Each of relationship varied according to the slab depth. The variation is about 7% between the two relationships corresponding to the two slab depths.

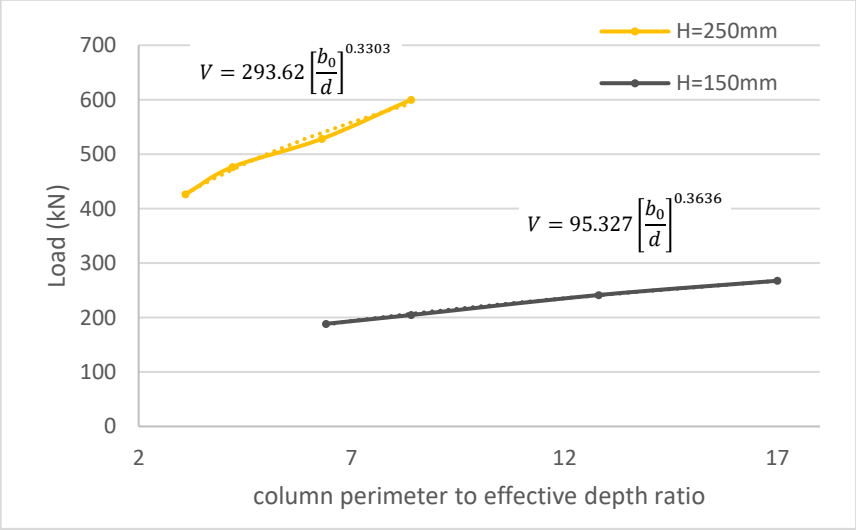

Figure 4-16. Effects of column perimeter to effective depth ratio on punching shear strength

4.5.3 Flexural Reinforcement ratio

Most of the code of practises CSA S806 (Canadian Standards 2012), ACI 440 (ACI Committee 440 2015), and JSCE (JSCE et al. 1997) recommends that FRP reinforced concrete flat slab to be over reinforced in most situation. Also, due to

the fact that the type of GFRP reinforcement and its bond characteristics in addition to GFRP is an elastic material with smaller stiffness compared to that of steel, a larger deflection and cracks widths are expected to be available in the GFRP reinforced concrete flat slab compared to that of SR concrete flat slab. Therefore, the effective compressive area in case of punching shear will be reduced as well as the contribution of aggregate interlock resisting will also be reduced accordingly. A wide range of flexural reinforcement ratio was selected between 0.8, 1, 1.2, 1.5, and 2% (2.2, 2.8, 3.4, 4.2 and 5.6 ρ_b, where ρ_b is the balanced reinforcement ratio) in order to evaluate the effect the flexural reinforcement ratios on the punching shear behaviour GFRP reinforced concrete flat slab under concentric load.

Results of the FE models are similar in the behaviour of that experiments in case of a bi-linear relation with differences in the smoothness of the transition according to the slab's depth (Figure 4-17). In all cases, the deflection increased linearly in the uncracked zone up to the initial first crack. In addition, nonlinearity was observed in the load-deflection curve when the tensile stress is exceeding the tensile strength of the concrete. Generally, the post-cracking stiffness is increased when axial stiffness is increased from about two times the balanced reinforcement ratio to about five times the balanced reinforcement ratio, whereas the deflection is decreased at the same load level.

GFRP bars are unidirectional materials with little strength in the transverse direction which leads to a smaller failure load and almost discounted contribution in case of shear resistance. Figure 4-17 shows the effect of flexural reinforcement ratio on punching shear strength. It can be observed that concrete flat slabs having the same depth exhibited similar behaviour. For a slab having $\mathrm{H} = 150\mathrm{mm}$, increasing reinforcement ratio from 1.0% to 2.0% results in a growth in

load capacity by approximately 23%. In case of slabs having a depth of 250mm, increasing reinforcement from 0.8% to 1.0% improved load capacity by roughly 8.0%, whereas a rise of reinforcement ratio from 1.0% to 1.2% led to a tiny increment in load capacity by about 3.0%. However, the load capacity was improved by approximately 7.0% when reinforcement ratio increased from 1.2% to1.5%.

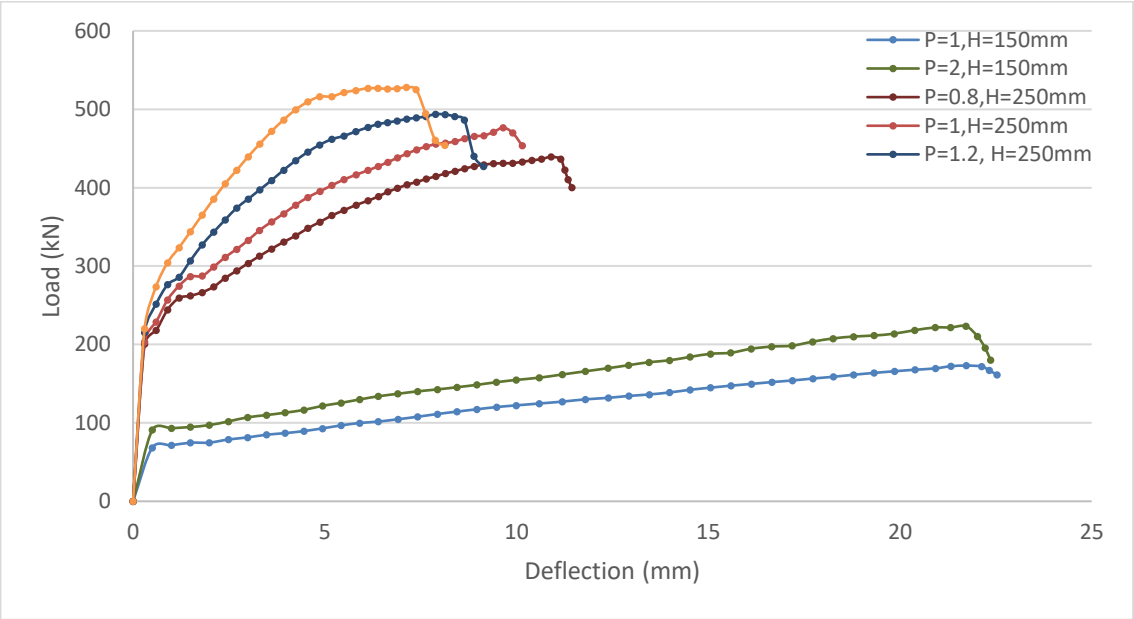

Figure 4-17. Effects of flexural reinforcement ratio on punching shear strength

The relationship between ultimate load strength and reinforcement ratio is presented in Figure 4-18 Though, this relationship can vary according to any change in geometry of the model or material properties.

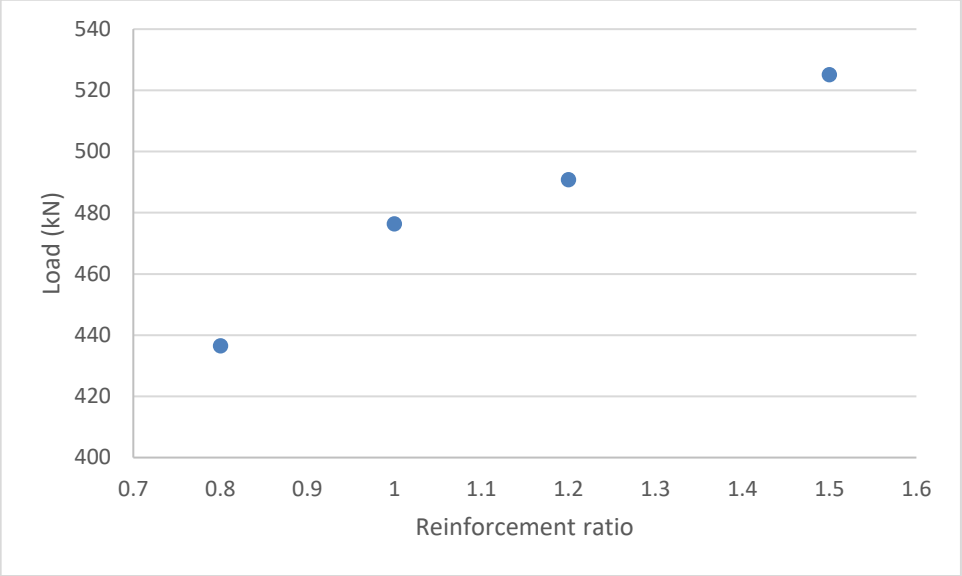

Figure 4-18. Relationships between ultimate load strength and reinforcement ratio

4.6 Conclusions

The finite element analysis was implemented with the concrete damaged plasticity model for predicting punching shear strength of GFRP reinforced concrete flat slab. The proposed FE model can predict the behaviour of GFRP reinforced concrete flat slab under concentric load in terms of ultimate capacity and load deflection curve with reasonable precision. The mean, SD, and COV of experimental to finite element modelling shear strength ratio were approximately 0.98, 8.5% and 8.67%, respectively.

Concrete material modelling is the most challenging part of finite element modelling. The parametric examination was performed in ABAQUS Explicit to calibrate the material model specified in ABAQUS. Many material parameters were included in the study and found to be critical for the accurate definition in the concrete modelling. It was practical that the load-displacement response should be taken into account for implementation of appropriate mesh size. Given the parametric investigation for the material modelling, the analysis of the results gave a precise punching shear prediction. The main conclusions which can be

drawn from the parametric study described previously in this chapter are summarised as follows:

- The mesh size was selected according to the sensitivity of different mesh sizing and on the computational time.
- The shear failure loads predicted from the current computational analysis were very close to those obtained experimentally.
- Overall the load-deflection curves behaviour predicted by ABAQUS showed reasonable agreement with that of experimental results.
- Regardless slabs thickness values, the prediction of the proposed ABAQUS model showed a steady increase in the load carrying capacity by increasing the concrete strength.
- The effect of increasing the concrete compressive strength on punching shear strength is more pronounced in normal concrete strength rather than high concrete compressive strength in both GFRP concrete flat slab depths.
- The effect of the shear perimeter to effective depth ratio is less pronounced on deflection rather than punching shear capacity.
- The effect of tensile reinforcement ratio on deflection is more pronounced in GFRP reinforced flat slab with greater depth.

CHAPTER FIVE

ARTIFICIAL NEURAL NETWORKS (ANN)

5.1 Introduction

The main restriction of previous studies was the uncertainty emphasised by the difference between the predictions and the experimental results of the punching shear strength, as mentioned in section 2.8. The difficult relationship between the parameters considered in the punching shear phenomena, in addition, the lack of knowledge regarding FRP reinforcement and the concrete bond all add up together to complicate the relationship. In addition, the brittle failure of concrete structures, cannot be adequately described by plastic limit analysis. However, using computational techniques delivers an effective and uncomplicated approach for modelling complex and nonlinear functions. Artificial Neural Networks are the biological neuron counterpart in the engineering applications, which are inspired from the ability of the human brain in learning. ANN is used in this research to predict punching shear strength, and the results were shown to match more closely with the experimental results.

Sixty-nine tests results were examined, including all punching shear results of different types of scale specimens. Moreover, from the current parametric study, five parameters were identified which were most effective in the punching shear results. These were used to evaluate the ANN modelling results against the experimental test data and code of practice CSA S806 (2012). It is also evaluated against best modified equation in the prediction of punching shear capacity proposed by Ospina et al (2003).

5.2 Artificial Neural Networks Technique (ANN)

Most of the existing formulas for the estimation of punching shear resistance of FRP reinforced concrete flat slabs are either empirical (Ospina et al. 2003) or based on modified formulas for steel reinforced slabs (Matthys and Taerwe 2000; El-Ghandour et al. 2003; Theodorakopoulos and Swamy 2008; Lee 2009). Nguyen-Minh (2012) applied the first semi-empirical theory which is based on the fracture mechanics approach. When a solution of the problem is very complicated with many different variable parameters, the ANN can be used to overcome the difficulties that arise in science and engineering. ANN is defined as computing systems made up of a number of simple elements operating in parallel (Bashir and Ashour 2012). These elements (called neurons) are inspired by biological nervous systems (Demuth et al. 2008).

5.2.1 Neural network modelling

For the configuration and learning of the Neural Network (NN), 69 experimental tests results were collected and presented in A-1. The database includes slab punching shear strength with FRP bars reinforced concrete. Furthermore, the selected tests present different varieties regarding the geometric slab ratios, reinforcement ratio, material properties and, therefore, failure loads. A neuron with a single input vector is shown in Figure 5-1, in which $p_1, p_2, p_3, \dots p_R$ represents individual element inputs multiplied by weights ($w_{1,1}, w_{1,2}, \dots w_{1,R}$). The weighted values are fed to the summing junction. Their sum is simply $\boldsymbol{W_p}$, the dot product of the (single row) matrix **W** and the vector **p.**

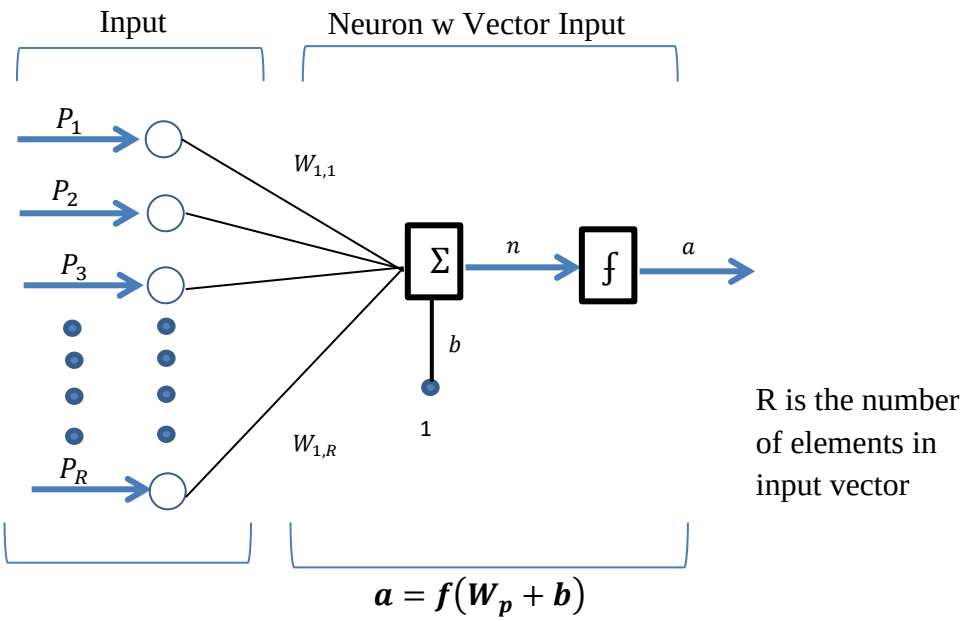

Figure 5-1. A neuron with a single R-element input vector

The neuron has a bias *b*, which is summed up with the weighted inputs to form the net input *n*. This sum, *n*, is the argument of the transfer function *f* (Demuth et al. 2008). This expression can be written in MATLAB® code as:

n = W*p + b 5–1

Two or more of the neurons can be combined into one layer. A layer of a network includes the combination of the weights, the multiplication and summing operation (here presented by product $\boldsymbol{W_p}$), the bias $\boldsymbol{b}$, and the transfer function *f*. The particular network may contain one or more hidden layers. In this study, one hidden layer of neurons was considered as shown in Figure 5-2, where P indicates the input vector, by which each input vector P element is connected to each neuron through the weight matrix **W**. Then, the weight inputs are gathered in each neuron and bias vector b to form its scalar output n. In sequence, n became the net input passed to the transfer function f to obtain the neuron's output, a column vector a. Finally, NN predictions are produced through the

output layer. Each processing element usually has many inputs, but it can send out only one output.

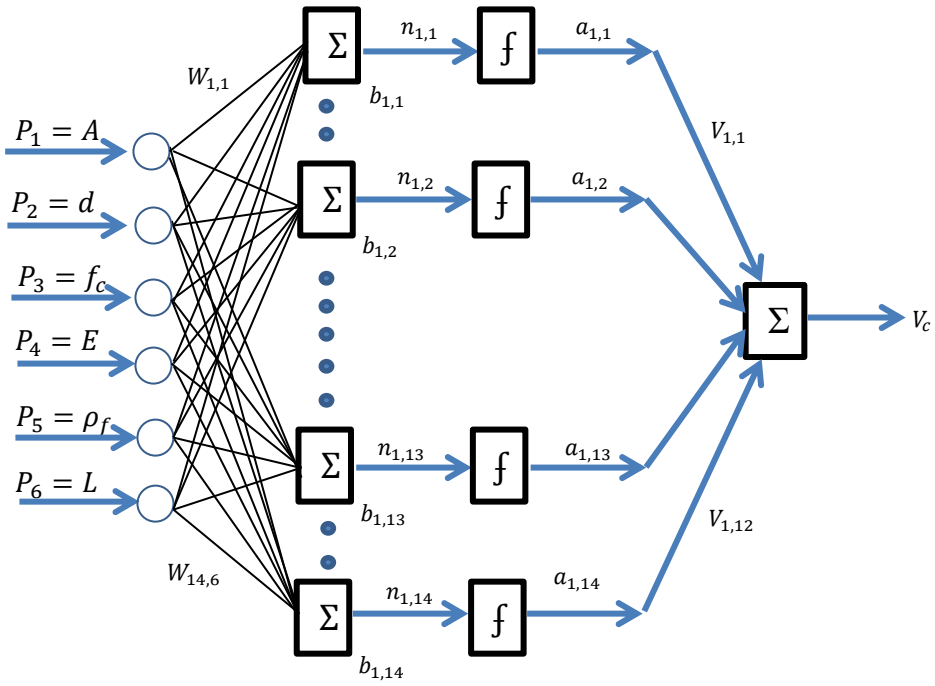

Figure 5-2. Architecture of 6 × 14 × 1 network.

The conventional backpropagation algorithm trains neural network parameters (weights and biases) using gradient descent or conjugate gradient decent methods by calculating the partial derivative of the performance with respect to the weights and biases values (Bashir and El-Hawary 2009). The adjustments of weights are obtained by applying a number of training inputs and the corresponding target values. In addition, updating and correcting the network weights and biases enable an accuracy value to be determined by measuring the error differences between a calculated and an expected target. These are then back propagated from the output layer to the input layer. This process of modifying neuron weights and biases is continued until the network error attains a certain level of accuracy.

5.3 Selected parameters

To be more consistencey in ANN training, all bridge decks were excluded from data analysis of the current research and all two-way concrete flat slabs reinforced with FRP bars were included in the ANN. The number of parameters used in the study with the number of tests performed was found to be the key parameters that enable ANN to give the best prediction. Hence, a nonlinear ANN technique was used in this research to get the best prediction of punching shear capacities, but with larger numbers of data collection options and consistency.

The following range of variables obtained from 69 experimental results of punching shear tests namely; the mean concrete strength, f_c' (from 33 MPa to 121 MPa), effective depth of slabs, d (from 41 mm to 284 mm), tensile reinforcement ratio, ρ_f (from 0.15% to 3.76%), modulus of elasticity of reinforcement, E_f (from 28.4 GPa to 147.0 GPa), and column perimeter, b (320 mm to 1800 mm) were used to generate ANN modelling. Most of the functions used to predict punching shear capacity of flat slabs with FRP reinforcement bars are based on the limited theories and laboratory experiments of each research study. The system which connects a column and a flat slab have interrelated parameters, which effects need to be considered when the main failure is formed by punching shear. The effect of slab depth was included in the study of punching shear in flat slabs reinforced with FRP bars for the first time in 2000 (Matthys and Taerwe 2000). Whereas, between 2003 and 2009, studies focused on two main parameters; FRP reinforcement ratio and concrete strength. Dulude et al (2011) were first to capture the effect of column size in the parametric study. Hence, it can be seen that previous works were complementary and covered the most effective parameters for predicting the punching shear strength in the flat slabs. Selecting the input parameters that adequately represent the features of the

problem studied is one of the vital points to ensure the success of this method. On the other hand, the number of parameters must be large enough to represent the system properly since the number of input parameter should also be chosen according to the number of training data. However, it is not recommended to train ANN with a large number of input neurons since it may reduce the efficiency and accuracy of the training process (Perera et al. 2010). In this case, the choice of the input parameters is guided based on the shear capacity equations of the different design proposals (3.3.3) as summarised previously. Moreover, a parametric study was applied by using ANN to study the most effective parameter affecting the punching shear. Five parameters were chosen based on the literature review in the application of ANN to predict the punching shear strength of two-way flat slabs. These were column perimeter (b), Young's Modulus for the reinforcement (E), compressive strength of the concrete (f_c), reinforcement ratio (ρ_f) and slab effective depth (d).

5.3.1 Experimental database

Experimentally determined punching shear capacities from an initial set of 103 FRP reinforce concrete flat slabs and bridge decks including the specimens in the current research which failed in punching shear were refined to be 58 FRP reinforced concrete flat slabs by excluding the bridge decks and any other failure mode rather than punching shear. The selected 58 specimens were compared with the prediction of the eight punching shear design methods mentioned in chapter three (3.3.3). The filtration of the database is continued for the ANN training purposes to exclude the flat slab specimens having dimensions less than one meter for a reason mentioned in 2.5.1, by which the number of specimens settled on 52. Then, the database was used to train and test ANN to develop the punching shear capacity prediction $V_{pred.}$.

There were four statistical observations included in this study: the mean, SD, COV and MAE. These statistical parameters are provided in Table 5-1. In Figure 5-3 the predictions of punching shear capacity of 52 specimens are consistent with the mean line of the experimentally tested values. It is clear that the trend in punching shear of the two-way slabs (Figure 5-3) is the most likely to be considered in the study where the values of mean, SD, COV and were 1.00, 0.05, 4.87 and 11.52, respectively. The database was then expanded to 58 specimens by including six smaller dimension specimens. Small-scale dimensions with span length not more than 670 mm, of which can be considered a plate rather than flat slab structures. When the six smallest specimens in the training of NN were included, the square error became higher than if they were excluded in that of 52 specimens NN training (Table 5-1). In Figure 5-4, the predictions of punching shear capacity of 58 specimens are less consistent with the mean line of the experimentally tested values compared to that of 52 specimens. Then, the study was continued in the next section to considering three training algorithms in ANN for a function fitting network.

Table 5-1. Two geometry categories of the 52 and 58 test specimens.

Slab span sizes	**NN architecture**	**Slab's quantity**	**Mean**	**SD**	**COV %**	**MAE %**
Slabs span greater than or equal to 1000 mm	5×14×1	52	1.00	0.05	4.87	11.52
All slabs span including less than 1000 mm	5×14×1	58	1.00	0.07	6.88	13.68

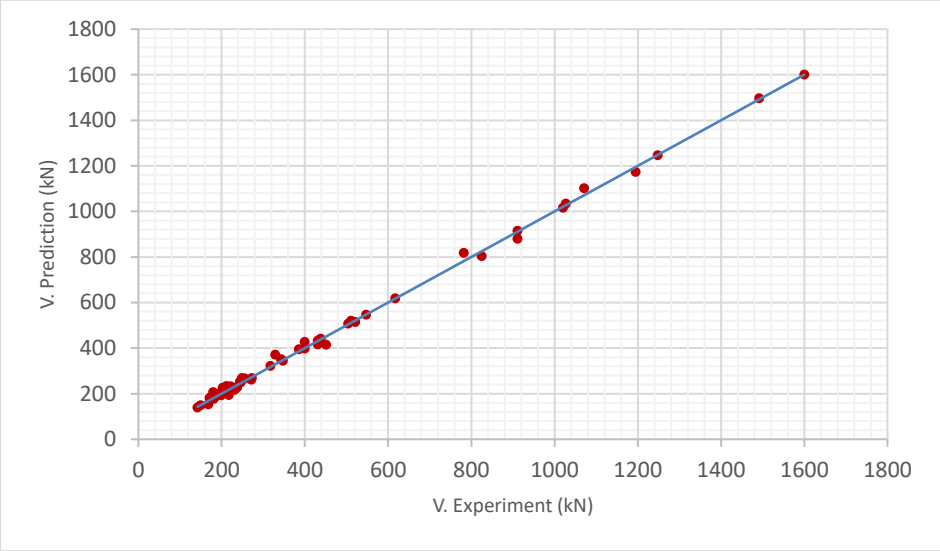

Figure 5-3. NNs prediction of slabs ≥ 1000mm dimension vs experimental punching shear capacities.

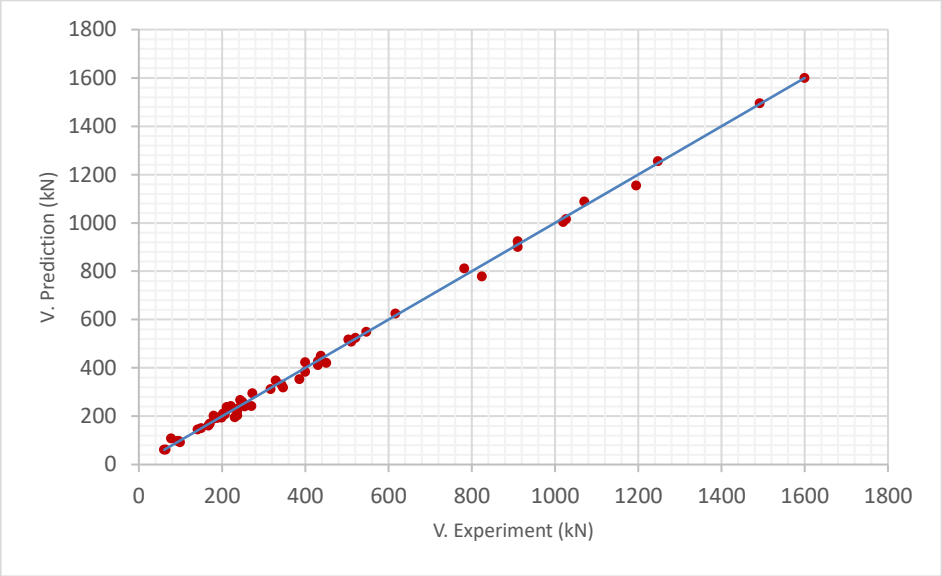

Figure 5-4. NNs prediction of all slabs dimension vs experimental punching shear capacities.

5.3.2 Network training

The network was trained to fit the input parameter data, and the target experimental data results from previous studies. Training was conducted multiple times to generate different results due to different initial conditions and sampling (Hahn and Valentine 2016). The training times stopped when regression (R) value of about one was achieved which means a close relationship. There are three training algorithms in ANN for a function fitting network, namely; Levenberg-

Marquardt, Bayesian Regularization (BR) and Scaled Conjugate Gradient (SCG) (Hahn and Valentine 2016). The R values measure the correlation between outputs and targets. The default training algorithm for a function fitting network is Levenberg-Marquardt. The algorithm Levenberg-Marquardt is requiring more memory than other algorithm but often the fastest backpropagation algorithm in the toolbox. Training automatically stops when generalisation stops improving, which is indicated by an increase in the mean square error of the validation samples. Whereas Conjugate Gradient algorithm requires less memory but the training also automatically stops when generalisation stops improving as same as the Levenberg-Marquardt algorithm and is specified by an increase in the mean square error of the validation samples. On the other hand, BR algorithm typically requires more time but can result in good generalisation for difficult, small or noisy datasets. Training stops according to adaptive weight minimisation. In addition, it minimises a combination of squared errors and weights and then determines the correct combination so as to produce a network that generalises well (Hahn and Valentine 2016).

The first choice of training algorithm in this study was Levenberg-Marquardt algorithm as recommended by Hahn and Valentine (2016) to be a first choice supervised algorithm. The fact that SCG algorithm validation is the same as the Levenberg-Marquardt algorithm, the Conjugate Gradient algorithm was ignored in the training algorithm choices in the toolbox for training the network. Alternatively, BR algorithm is a more convenient choice of training algorithm in the current study compared to the other algorithms in the toolbox. This is due to the fact that the number of input data of the previous experimental investigation considered small datasets as evident in the network results showing in Table 5-2 (Figure 5-5 and Figure 5-6). The two training algorithms in the Table 5-2 were

selected from the best fit of inputs parameter data and the targets experimental data results from previous studies. The training algorithm BR is shown less scattered results in Figure 5-6 compared to that training by the Levenberg-Marquardt algorithm which is shown in Figure 5-5.

Table 5-2. Comparisons between two training algorithms

Parameters	Training algorithm	NN Architecture	Slab's quantity	Mean	SD	COV %	MAE%
b, E_f, f_c, ρ_f, d	Levenberg-Marquardt	5×20×1	52	1.00	0.06	5.81	16.68
	BR	5×14×1		1.00	0.06	5.68	14.90

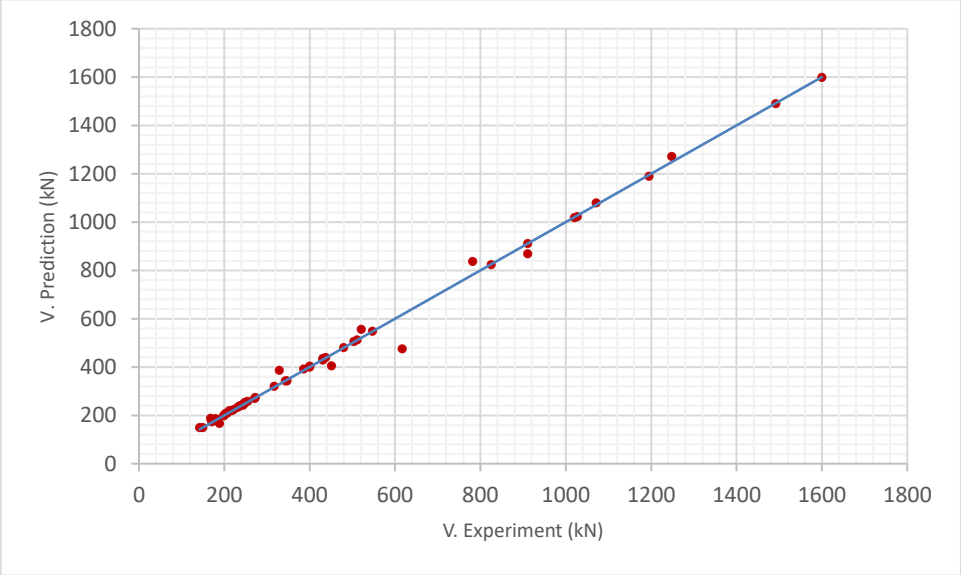

Figure 5-5. NNs prediction of the Levenberg-Marquardt algorithm

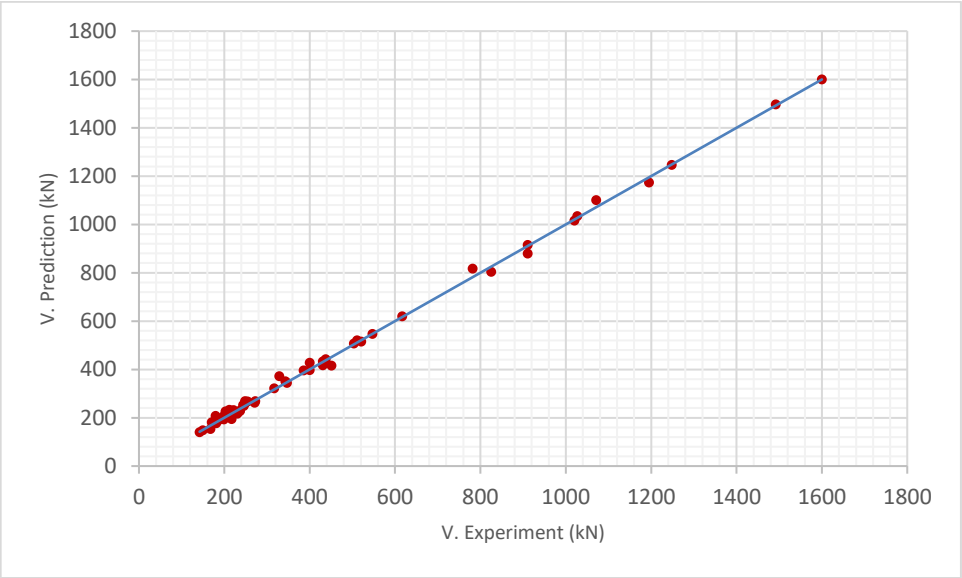

Figure 5-6. NNs prediction of Bayes algorithm

The training of ANN study continued by using two sets of five parameters. The first set was including the column area (A), slab effective depth (d), Young Modulus (E_f), concrete compressive strength (f_c) and reinforcement ratio (ρ_f). Whereas, the other set of parameters included the same parameters as the first one except the column area replaced by a column perimeter (b). The training results of the network for all trails were shown in Table 5-3.

Table 5-3. Train the network to fit the 52 and 58 test specimens

Two-way flat slab categories	Parameters	NN architecture	Mean	SD	COV %	MAE%
Two-way flat slab with five parameters input data including loaded area	A, d, E_f, f_c, ρ_f	**5×2×1**	1.00	0.13	12.95	34.52
		5×4×1	1.01	0.09	8.90	22.7
		5×6×1	1.00	0.06	6.33	16.80
		5×8×1	0.99	0.07	7.22	17.30
		5×10×1	0.99	0.08	8.10	26.91
		5×12×1	0.99	0.07	6.91	20.11
		5×14×1	1.00	0.092	9.21	25.22
		5×16×1	1.00	0.10	9.68	22.89
Two-way flat slab with five parameters input data including loaded parameter (slab span length greater or equal than 1000 mm)	b, E_f, f_c, ρ_f, d	**5×2×1**	1.01	0.15	15.11	33.89
		5×4×1	1.00	0.09	8.75	25.87
		5×6×1	1.00	0.08	8.43	22.69
		5×8×1	1.01	0.10	10.22	23.33
		5×10×1	0.99	0.06	6.31	18.85
		5×12×1	1.03	0.13	12.19	21.90
		5×14×1	0.99	0.05	4.87	11.52
		5×16×1	0.99	0.09	8.96	20.43
Two-way flat slab with five parameters input data including loaded parameter (slab span length less and greater than 1000 mm)	b, E_f, f_c, ρ_f, d	**5×2×1**	0.99	0.13	13.39	28.42
		5×4×1	1.00	0.12	12.10	29.31
		5×6×1	1.01	0.14	14.13	13.65
		5×8×1	1.03	0.13	12.52	10.31
		5×10×1	0.98	0.08	8.51	12.52
		5×12×1	1.03	0.13	13.05	12.93
		5×14×1	1.00	0.07	6.88	13.68
		5×16×1	1.01	0.11	10.64	15.78

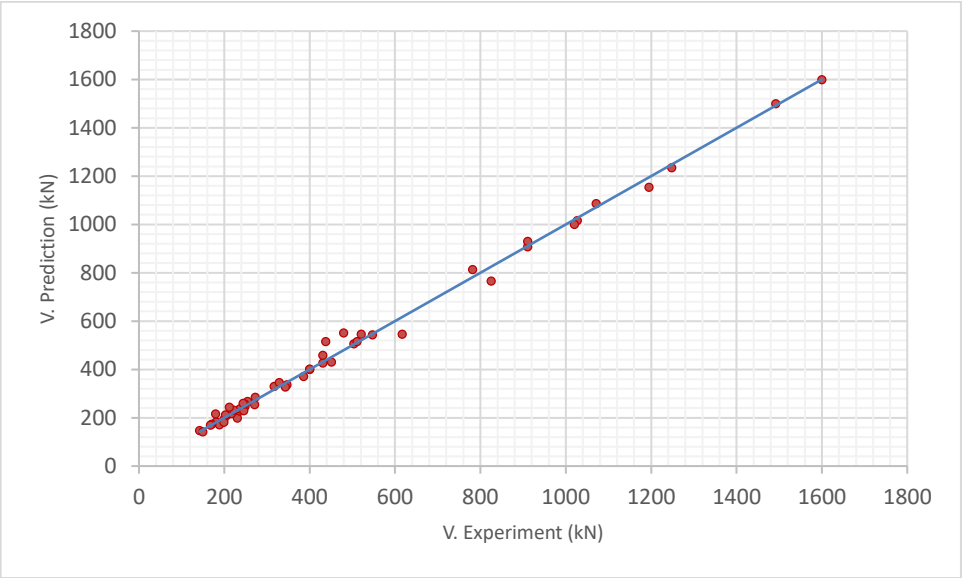

Figure 5-7. NNs (5×6×1) prediction of the Two-way flat slab with five parameters input data (A, d, E_f, f_c, ρ_f) vs experimental punching shear capacities.

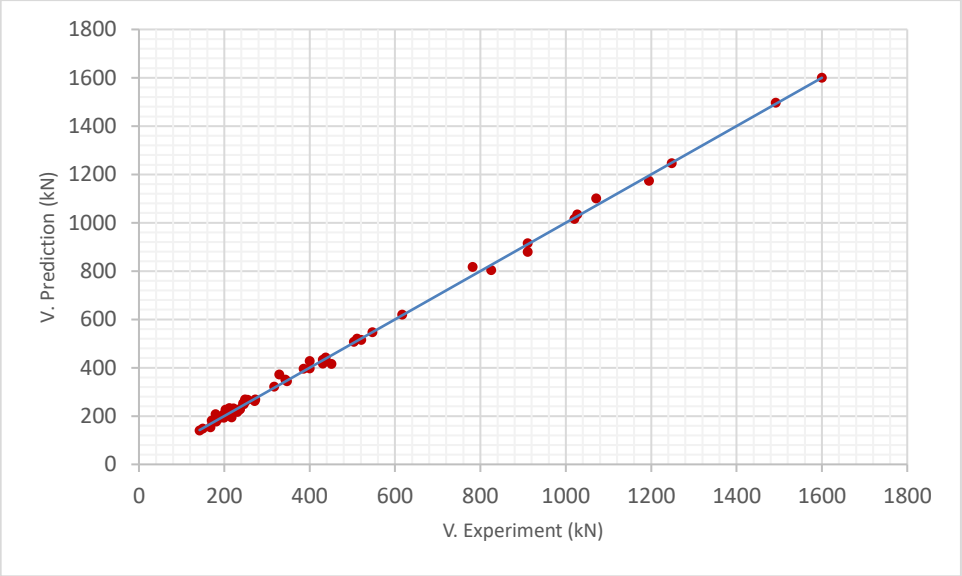

Figure 5-8. NNs (5×14×1) prediction of the Two-way flat slab with five parameters input data b, E_f, f_c, ρ_f, d (slab span ≥ 1000) vs experimental punching shear capacities.

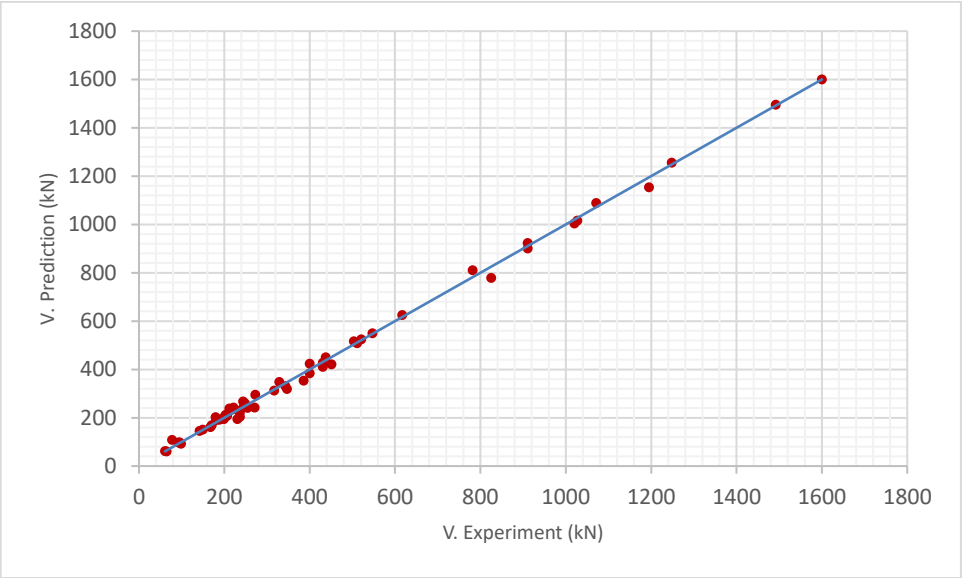

Figure 5-9. NNs (5×14×1) prediction of the Two-way flat slab with five parameters input data b, E_f, f_c, ρ_f, d (all two-way flat slab sizes) vs experimental punching shear capacities.

According to the results in Table 5-3, the study which included the parameter b is shown to give fewer errors and less scattered results compared to that study which included the parameter A (e.g. Figure 5-8 and Figure 5-9 compared to Figure 5-7). The comparison started by comparing the study which included the parameter b and 52 specimens with that study which included the parameter A and the same number of specimens. On the other hand, the study of 58 specimens is mainly used to compare it with that of the same parameters but less number of specimens (52). In fact, the last two studies in Table 5-3 show very close results compared with the first one.

Table 5-4 showing a comparison between the ANN prediction and the current research test specimens. Network with all specimens (58) is showing slightly better statistical results than the other network of 52 specimen.

Table 5-4. Comparison between the NN prediction and the current research test specimens

Two-way flat slab categories	Train network	Mean	SD	COV %	MAE%
Slab span length greater or equal than 1000 mm	52	1.03	0.04	4.10	7.10
slab span length less and greater than 1000 mm	58	1.01	0.03	2.67	5.74

The investigation is carried out on studying the network results by applying a parametric study to examine the workability and preciseness of the network to predict punching shear strength.

5.3.3 Generalization of NN

Over-fitting is one of the problems that can occur during NN training. The network cannot learn to generalise new patterns, whereas, the training feature may be memorised by the network (Bashir and Ashour 2012). On the other hand, NNs are good at fitting functions and recognising patterns in the case of practical functions (Demuth et al. 2008). The research problem was solved by using a graphical user interface; the expression can be written in MATLAB® code as nftool. Bashir and Ashour (2012) illustrated the techniques of early stopping as one effective method to improve generalisation of NNs. 'nftool' has an option to divide data into three subsets for training, validation and testing. The training set is used for calculating the gradient and updating the network weights and biases to reduce the training error. In the case of the validation subset, if the error is increased during a certain number of iterations, the training of weights and biases will stop and be returned to minimum justification error. The test subset is used only to verify the NNs during the training. On the other hand, BR can provide better generalisation performance than the early stopping technique when the dataset is relatively small (Bashir and Ashour 2012). The current problem has a

small dataset, meaning that BR is more practical to solve the problem. The database specimens should be divided into two subsets; training and testing. A validation dataset does not need to be separate from the training dataset. The nftool technique cannot completely ignore the validation set wherever the minimum option number value in the toolbox is given as 5 %. Thus, the training and testing datasets were used to minimise the training error. The testing subset was separated by 15 %, whereas the validation subset was 5 % in order to allocate the remaining 80 % for the training subset. The training algorithm continues until the sum-squared error (SSE) is relatively constant over several iterations which are calculated according to the equation below:

$$SSE = \sum_{i=1}^{m}(V_{i,pred} - V_{i,exp})^2 \qquad 5–2$$

Here m is the total number of training specimens. Overfitting in training and outputs of NNs is usually influenced by the number of hidden layers and the number of neurons in each hidden layer, but since nftool gives no option for choosing the number of hidden layers the only remaining variable is the number of hidden neurons. A trial and error method was used to select an optimum number of neurons in each hidden layer.

5.3.4 Comparisons of NN predictions and experimental shear capacities

A total of 24 different NNs were created with different architectures and were tested with varying numbers of neurons in one layer as listed in Table 5-3. Eight random initialised network weights and biases were created in each of two categories. SSE, which was defined in Equation 5–2, is used to control the network performance. In addition, statistical observations in the results of each network were used to evaluate and compare the outputs as presented in Table 5-3.

According to the statistical results in Table 5-3, the 5×14×1 NN of the second and the third group were selected for the parametric study. Since the network in the second group is the best network result in terms of statistical observations, it set to be a control network for the third group. A comparison is made with the two subsets between 5×14×1 network prediction and experimental results in Figure 5-10. It shows less scattered results around the diagonal line, which in turn reflects the efficiency and uniformity.

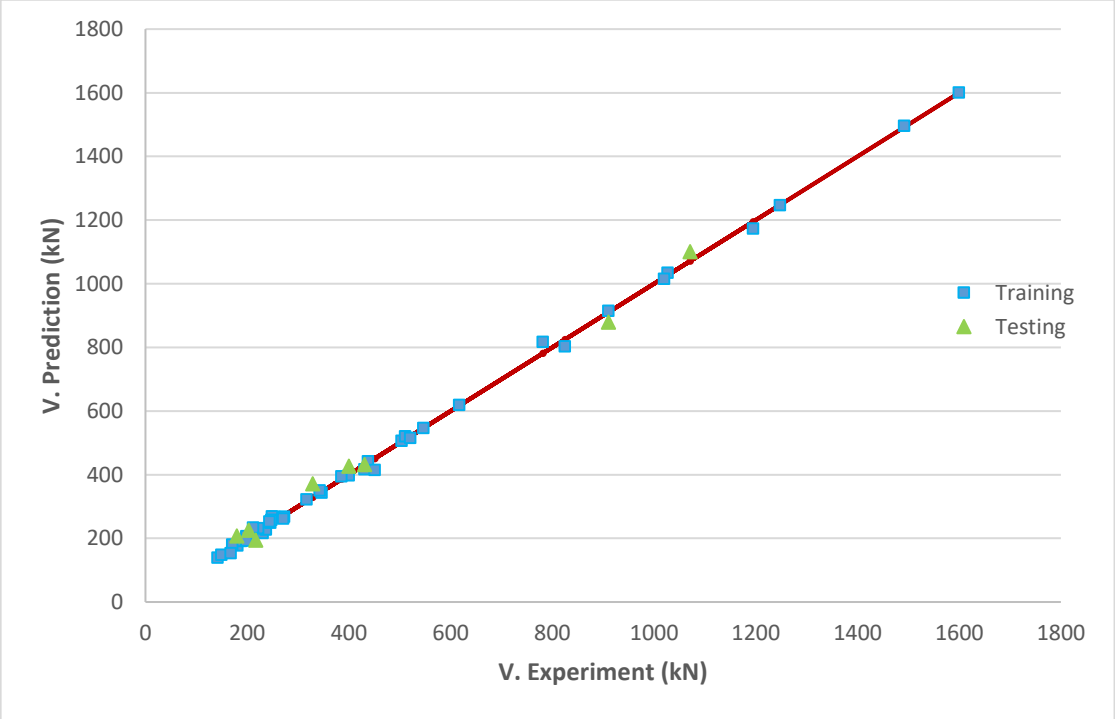

Figure 5-10. NNs (5×14×1) prediction of the Two-way flat slab with five parameters (category three) vs experimental punching shear capacities (Training and Testing sets).

A parametric study was conducted to investigate the accuracy and the effect of each parameter in predicting the punching shear capacity (Figure 5-12 to Figure 5-21). The modelling investigation was carried out to compare the prediction results of the punching shear capacity of the equations 3-6, 3-7, 3-8, and 3-20 (Ospina et al. 2003; Canadian Standards 2012) with the NN prediction and the experimental results, they were found to be very close. Thus, the change in the

trend can be a result of the limited input database of 52 or 58 specimens. To give a better trend and better NN punching shear strength prediction, more experimental data are required to feed into the NN.

5.3.5 Punching shear capacities

Ultimate punching shear capacities and the corresponding normalised punching shear stresses calculated at $0.5d$ and $1.5d$ from the loaded square area are presented in Table 5-5. To interpretation for the variation in the concrete strength the punching shear stresses at failure were normalised to the cubic root of concrete compressive strength. In addition, the difference between the moduli of elasticity of the GFRP and steel bars was measured by considering the effective reinforcement ratio. Figure 5-11 shows the normalized punching shear stress ($V_u/\sqrt[3]{f_c}$) versus the effective reinforcement ratio ($\rho_f E_f/E_s$). This figure combines three relationships of normalised punching shear stresses plotted against the normalised effective reinforcement ratio, and all the three relationships exhibited nonlinear behaviour. The figure also shows that two trends are close to each other which are Hassan et al. (2013b) and the critical perimeter at the distance of $0.5d$, whereas the trend $1.5d$ has considerable lower normalised punching shear stress than the other two. The normalised punching shear stress to the cubic root of the concrete compressive strength is proportional to the effective reinforcement ratio to the power of 0.34 in case of Hassan et al. (2013b), but the ANN in case of $0.5d$ and $1.5d$ is about 0.4. Hassan et al. (2013b) proportional power value is the closest to the punching shear design equations in CSA S806 (Canadian Standards 2012), BS 8110 (British Standard 1997), and JSCE et al. (1997), which considered for FRP axial stiffness to the power of 1/3.

Table 5-5. Normalized punching shear stress

Effective reinforcement ratio $\rho_f E_f / E_s$	NN prediction of punching shear capacity for 58 specimens		Hassan et al. (2013b) $V_u/\sqrt[3]{f`_c}$
	0.5 distance from the column	1.5 distance from the column	
	$V_u/\sqrt[3]{f`_c}$	$V_u/\sqrt[3]{f`_c}$	
0.044089	0.25189	0.21201	0.2962
0.135206	0.384877	0.323941	0.43352
0.226322	0.488657	0.411291	0.51651
0.317439	0.562885	0.473767	0.57947
0.387981	0.601558	0.506316	0.62040
0.479098	0.630533	0.530704	0.66653

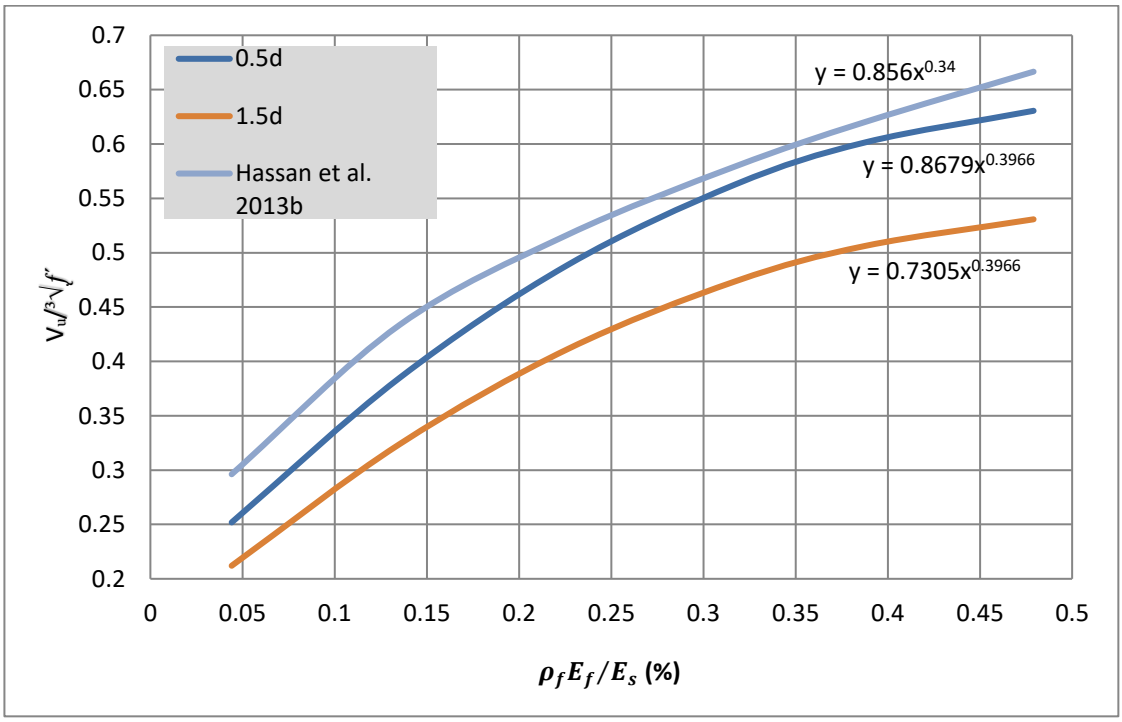

Figure 5-11. Normalized punching shear stress at $0.5d$ and $1.5d$ from the loaded square area.

5.4 Parametric analysis

The two networks ((5×14×1) of 52 and 58 specimens) selected were used to investigate the effect of the five input parameters on the punching shear capacity. The Figure 3-19 to Figure 3-24 have shown that some input parameter values are not covered, especially in the effective slab depth and concrete strength ranges. The other parameter values included in a limited number of tests. Therefore, all parameter values were covered in this study to produce acceptable trends that the NN had generalised for the selected 52 and 58 input data sets. The investigation strategy of the each of the five parameters was implemented by keeping the other parameters constant while the parameter of interest was being changed in the analysis. The values of the constant parameter were given as shown in Table 5-6. These values were selected according to the average of the input data ranges and also occur within the band with high frequency:

Table 5-6. Constant parameters values

d mm	b mm	E_f MPa	f_c MPa	ρ_f (%)
Slabs span greater or equal than 1000 mm (52 specimens)				
156	**1028**	**57976**	**38**	**1.00**
Slabs span less and greater than 1000 mm (58 specimens)				
155	**1028**	**58785**	**39**	**1.00**

Where d is the effective depth of the slab in mm, b is the column perimeter in mm, E_f is GFRP reinforcement Young Modulus in MPa, f_c is the concrete compressive strength in MPa, and ρ_f is the reinforcement ratio.

From Table 5-7, the key parameters included in the parametric study with their corresponding punching shear strength predicted by NN are effective depth, d, column perimeter, b, Young Modulus, E_f, concrete compressive strength, f_c, and the reinforcement ratio, ρ_f. The selected values were based on the input

database ranges between minimum and maximum and also occur within the band with high frequency. The parametric study resulted in some important conclusions relating to the examination variables on the load carrying capacity of GFRP reinforced flat slabs. The parametric study results are presented and discussed in this chapter.

Table 5-7. List of the parameters considered in the parametric study with the corresponding prediction values of ultimate punching shear load

Slabs span greater or equal 1000 mm (52 specimens)									
d **mm**	**NN (V) Prediction KN**	b **mm**	**NN (V) Prediction KN**	E_f **MPa**	**NN (V) Prediction KN**	f_c **MPa**	**NN (V) Prediction KN**	ρ_f (%)	**NN (V) Prediction KN**
90	209	500	294	34000	413	28	451	0.15	301
128	356	760	383	41200	435	38	492	0.46	383
166	515	1020	469	48400	454	46	525	0.77	440
204	695	1280	538	55600	468	54	560	1.08	481
242	906	1540	575	62800	480	62	595	1.32	504
280	1153	1800	605	70000	491	70	625	1.63	527
Slabs span less and greater than 1000 mm (58 specimens)									
d **mm**	**NN (V) Prediction KN**	b **mm**	**NN (V) Prediction KN**	E_f **MPa**	**NN (V) Prediction KN**	f_c **MPa**	**NN (V) Prediction KN**	ρ_f (%)	**NN (V) Prediction KN**
90	222	500	380	34000	409	28	450	0.15	218
128	367	760	415	41200	430	38	471	0.46	333
166	519	1020	472	48400	450	46	497	0.77	423
204	693	1280	526	55600	467	54	534	1.08	488
242	904	1540	566	62800	481	62	577	1.32	521
280	1146	1800	597	70000	492	70	614	1.63	546

5.4.1 Effect of column perimeter

The influence of the column perimeter is presented in Figure 5-12 and Figure 4-15. This parametric study is generalised for the two selected networks result of 52 and 58 specimens. It is clear that as b increases, the shear capacity increases but with different levels of increment in the trend pattern. Consequently, it is proven that the NN has modelled the problem sufficiently in both networks. The increment also coincides with the prediction of equations 3-6 to 3-8 and 3-20 but with different trends of increment in the case of the 52 specimens network,

whereas, the 58 specimens network fits more with the prediction of equation 3-20. In addition, three points were chosen from the database, which have some similarities in the value of their parameters as compared with the parametric study of NN prediction and the other two methods in Figure 5-12 and Figure 5-13. In the case of the 52 specimens network, increasing the column perimeter from 500 to 1800 mm will result in an increase in load carrying capacity, which is more consistent with the prediction of equations 3-6 to 3-8. Whereas, in the case of the 58 specimens network, it results in an increase in load carrying capacity, which is more consistent with the prediction of equation 3-17.

Column perimeter is directly related to slab depth and the concrete material strength. The relationship of column dimension to the slab depth was addressed in equation 3-22. This relationship was given in the form of the c/d ratio. In Figure 5-12, the trend of NN has an intensive rise of punching shear strength from a column perimeter of 500 mm to 1280 mm with a corresponding punching shear strength of 380 kN to 526 kN. After punching shear strength of 526 kN, the trend started to have a steady increment, which indicates that the concrete strength had limited the effects of column area on the increment. In fact, the correlation between rupture and the crushing failure is not fully understood in the case of punching shear of the flat slab. At worst, if the shear stress is calculated below the perimeter of the loaded area of the flat slab specimens, the stress will be found in a very small range between 1.2 N/mm² and 2.5 N/mm² for all of the tested specimens. This is considered lower than the material strength allowable in the British Standard (1997) of which stress shouldn't be taken greater than $0.8\sqrt{f_c}$ or 5 N/mm². On the other hand, the trend of NN in Figure 5-13 has a steady increment compared with the trend in Figure 5-12.

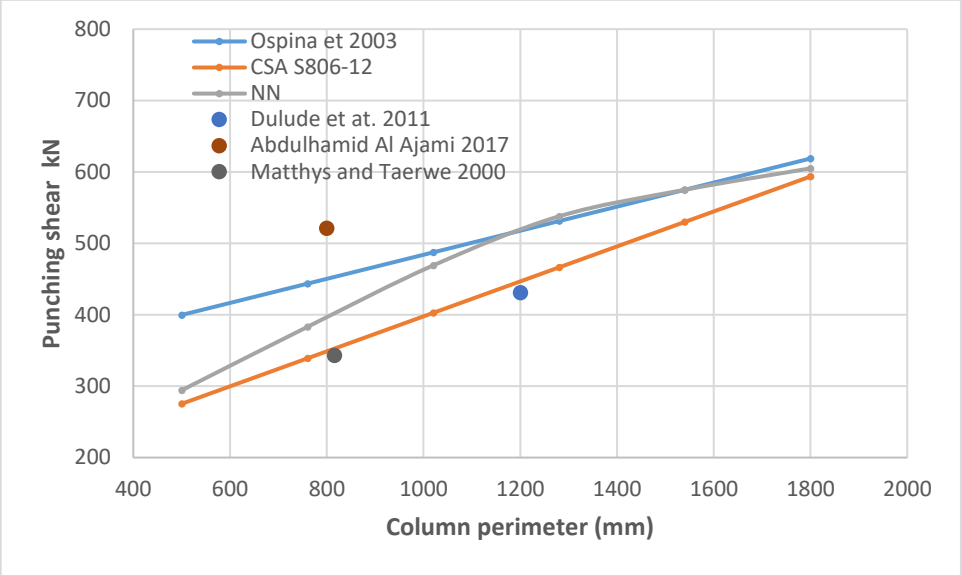

Figure 5-12. Column perimeter (b) effect on shear capacity (52 samples)

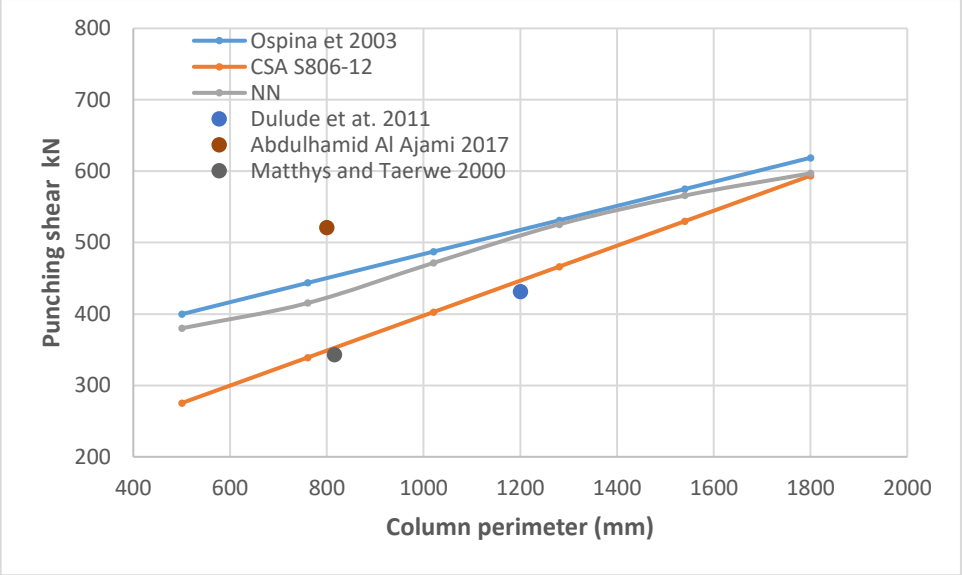

Figure 5-13. Column perimeter (b) effect on shear capacity (58 samples)

5.4.2 Effect of concrete strength

Concrete strength is also a very important parameter influencing the punching shear capacity, and it had been addressed in many studies. Again, equations 3-6 to 3-8 and 3-20 were used herein to improve the NN which has modelled the problem sufficiently in which the increment of the NN trends which also agree with the prediction of the equations. Also, another two points were chosen from the database that had approximately similar values of parameters and close

punching shear results with the parametric study of NN as shown in Figure 5-14 and Figure 5-15. Overall, Figure 5-14 showed that the increase in concrete strength will result in a steady increase in punching shear strength. Concrete strength trend behaviour of NN prediction in Figure 5-14 was parallel to the other two trends resulting from equations 3-6 to 3-8 and 3-20. It is also located above the two trends but closer to the trend of the equation 3-20 rather than the trend of equations 3-6 to 3-8. On the other hand, the trend in Figure 5-15 has a different proportional relationship between the vertical load and the concrete compressive strength. In the current study, concrete compressive strength is varied between 28 MPa to 70 MPa according to the database band with high frequency.

The relationship between nominal concrete compressive strength and load carrying capacity was found to be a linear relationship. The effect of concrete compressive strength was modelled in NN with respect to the other parameters which were included in this study. Increasing compressive strength in Figure 5-14 from 28 MPa to 70 MPa will result in an increase in load carrying capacity by almost the same ratio as that in Figure 5-15. The increment ratio of the punching shear load in both predictions of NN (Figure 5-14 and Figure 5-15) agree with the prediction ratio of equations 3-6 to 3-8 and 3-20.

Increasing compressive strength in both NN predictions from 28 MPa to 54 MPa will result in an increase in load carrying capacity around 18%, which is also validated by the proposed modelling results by ABAQUS (4.5.1).

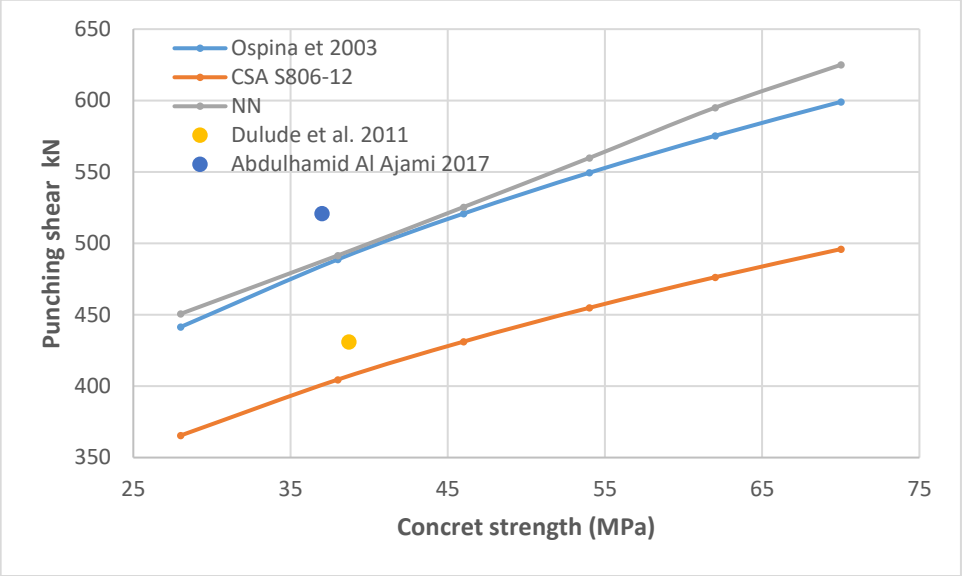

Figure 5-14. Concrete strength (f_c) effect on shear capacity (52 specimens)

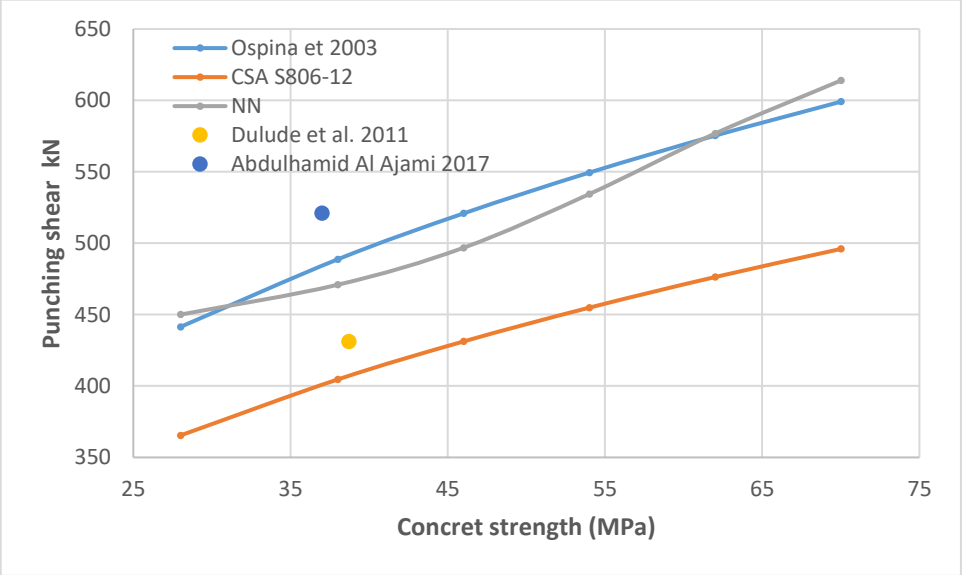

Figure 5-15. Concrete strength (f_c) effect on shear capacity (58 specimens)

It can be concluded that the concrete compressive strength has a relatively high influence on the load carrying capacity especially in the range of concrete compressive strength between 28 MPa and 70 MPa.

5.4.3 Effect of reinforcement ratio

Similar to the previously investigated parameters, the incremental relationship between reinforcement ratio and punching shear strength was also validated by applying equations 3-6 to 3-8 and 3-20 for the same sets of values of the

reinforcement ratio. Moreover, four points were chosen from the database that have similar values of parameters with the parametric study of NN prediction in Figure 5-16 and Figure 5-17. The two Figure 5-16 and Figure 5-17 display the relationship between the load capacity and the flexural reinforcement ratio in GFRP reinforced concrete flat slab. Overall, all punching shear capacity predictions which are included in Figure 5-16 and Figure 5-17 have almost similar behaviour. The trend of NN in Figure 5-16 deviates from the four points, whereas, the trend in Figure 5-17 passes closely through the points. In addition, the trend of NN in Figure 5-16 has a similar proportional relationship between the vertical load and the reinforcement ratio compared with that of the predictions of equations 3-6 to 3-8. On the other hand, the prediction of NN in Figure 5-17 showed a different proportional relationship between the vertical load and the reinforcement ratio with a minimum value overlapping the prediction of equations 3-6 to 3-8. It reaches a maximum result closer to the prediction of equation 3-20. In the case of NN punching shear capacity prediction, increasing reinforcement ratio from 0.15 to 1.63 will result in an increase in load carrying capacity by similar increment ratio of that other two methods used for comparison (equations 3-6 to 3-8 and 3-20).

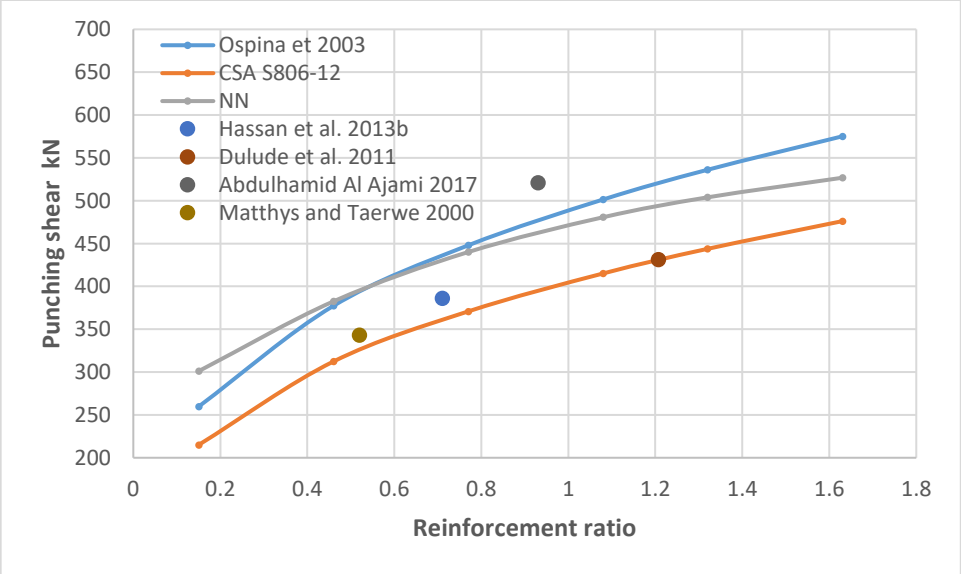

Figure 5-16. Reinforcement ratio (ρ_f) effect on shear capacity (52 specimens)

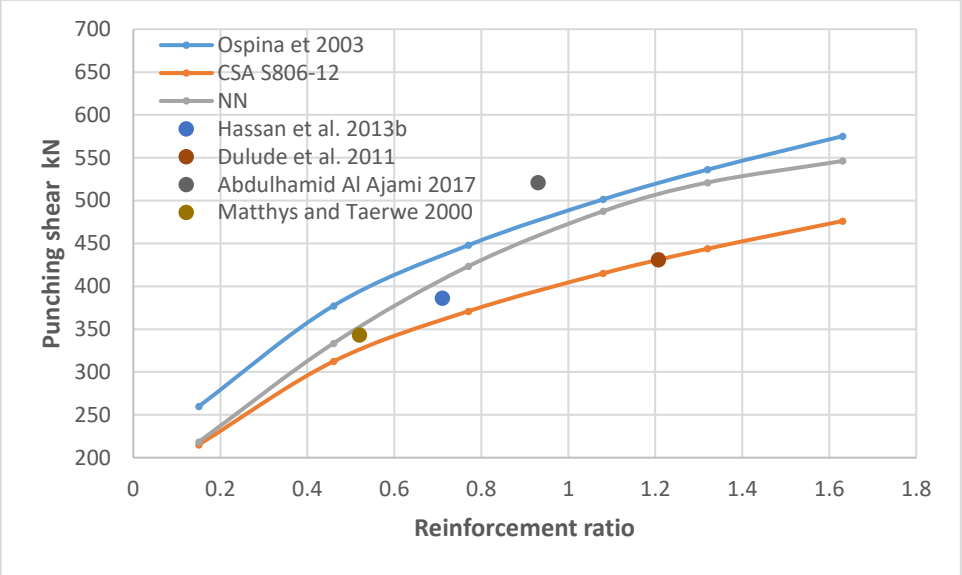

Figure 5-17. Reinforcement ratio (ρ_f) effect on shear capacity (58 specimens)

It can be concluded that the effect of reinforcement ratio has a significant influence on punching shear capacity in GFRP reinforced concrete flat slab compared to the other parameters included in the current study. Prediction of load carrying capacity from NN method has less influence of reinforcement ratio compared to the other methods.

5.4.4 Effect of elastic modulus

The Young Modulus of GFRP is usually one-fourth of that of steel. Most of GFRP Young Modulus values are between 40000 MPa to 50000 MPa, but a wider range is considered in this parametric study especially in a higher limit where most of modern GFRP bars are manufactured to achieve a high young modulus. The effect of young modulus is very vital in punching shear strength especially with high values in which the contraption cannot be ignored in resistance of punching shear strength. Figure 5-18 and Figure 5-19 show the relationship between the load carrying capacity and the young modulus of GFRP reinforcement, which also represents the wide range of values starting from a minimum of 34000 MPa and

spanning up to 70000 MPa. However, this is with a gap of less experimental tests of punching shear of flat slabs in the young modulus ranged between 70000 MPa to 147000 MPa which is excluded from this study. The two chosen points coincide more with the NN and equations 3-6 to 3-8 predictions rather than equation 3-20 (Figure 5-18 and Figure 5-19). Both trends of NN in Figure 5-18 and Figure 5-19 have a similar proportional relationship between the vertical load and the young modulus.

Herein the equations 3-6 to 3-8, 3-20 and NN punching shear predictions have a very steady growth (Figure 5-18 and Figure 5-19). The trend of punching shear capacity predictions by both NN are almost parallel in behaviour to the trend of equations 3-6 to 3-8 predictions, whereas prediction trend by equation 3-20 has more increment behaviour compared to the other two trends. It was expected that increasing E of the reinforcement will directly cause an increase in punching shear strength prediction values.

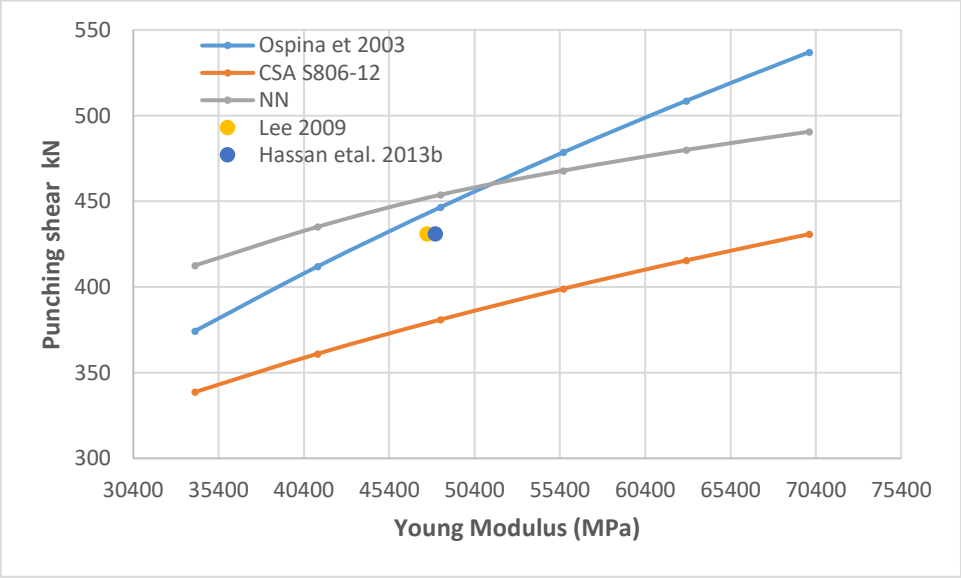

Figure 5-18. Young Modulus (E) effect on shear capacity (52 specimens)

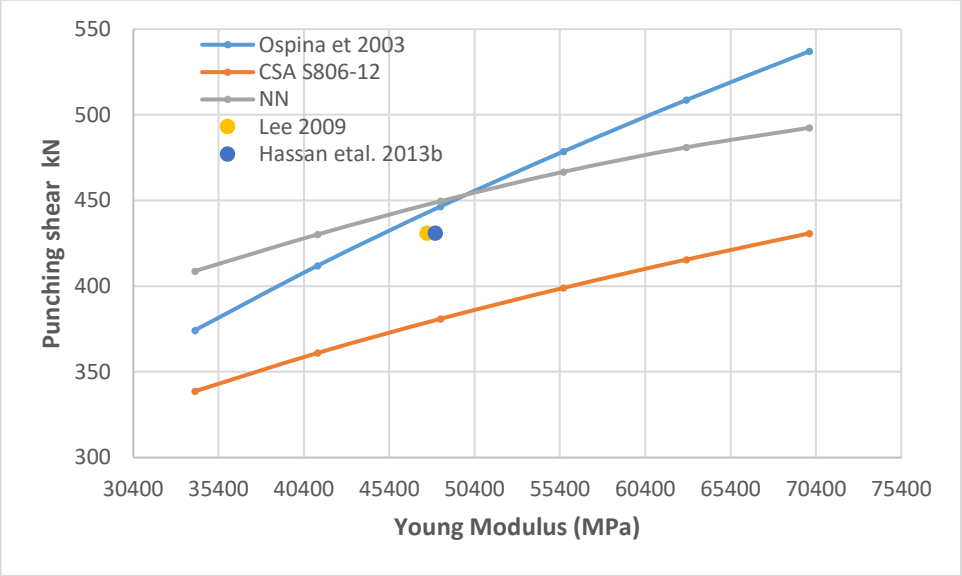

Figure 5-19. Young Modulus (E) effect on shear capacity (58 specimens)

It can be concluded that the elastic modulus of the reinforcement has a minor influence on the load carrying capacity in the range of Young Modulus values between 34000 MPa and 70000 MPa. Due to the fact that most of GFRP reinforced bars have low Young Modulus compared to that of steel bars, and within limited values between 40000 MPa to 50000 MPa, the effect of GFRP Young modulus on punching shear strength is very low and limited.

5.4.5 Effect of the effective depth

The effective depth is the most critical parameter that has a vital influence on the punching shear strength as it is illustrated in this section. Figure 5-20 and Figure 5-21 display the relationship between the load carrying capacity and the effective depth of GFRP reinforced concrete flat slab. The trend in Figure 5-20 and Figure 5-21 showed a very close behaviour with equations 3-6 to 3-8, 3-20 and NN punching shear prediction. The three selected points from the database agree with all trends. A very noticeable effect of effective depth on punching shear strength was recorded in Figure 5-20 and Figure 5-21. The trend of the NN prediction in Figure 5-20 has a very dramatic increase from 267 kN to 1174 kN

with corresponding effective depths of the flat slab 90 to 280 mm respectively. It is expected that if the effective depth of the slap increased, the punching shear strength will increase due the increase of slab depth, which will also cause more resistance material area for the punching shear.

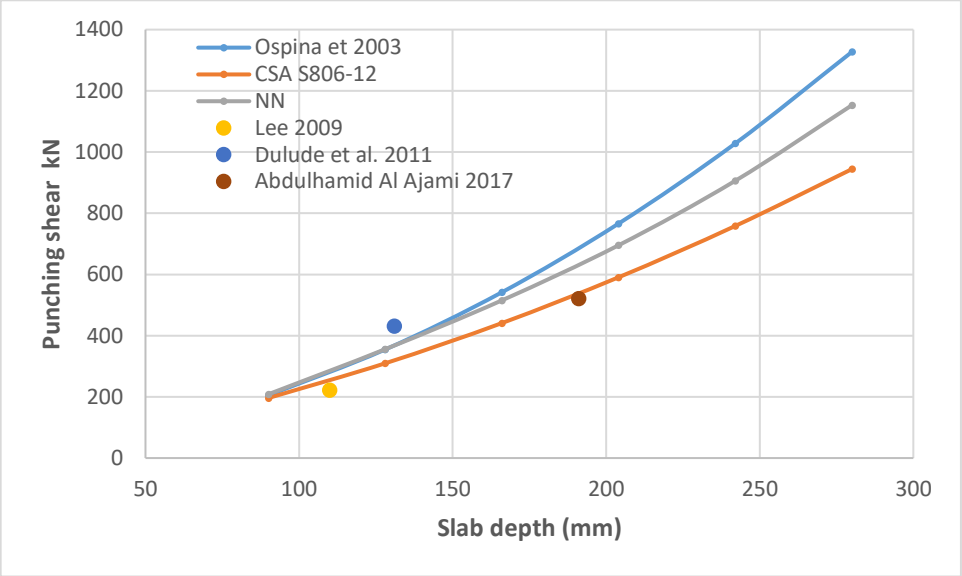

Figure 5-20. Slab effective depth (d) effect on shear capacity (52 specimens)

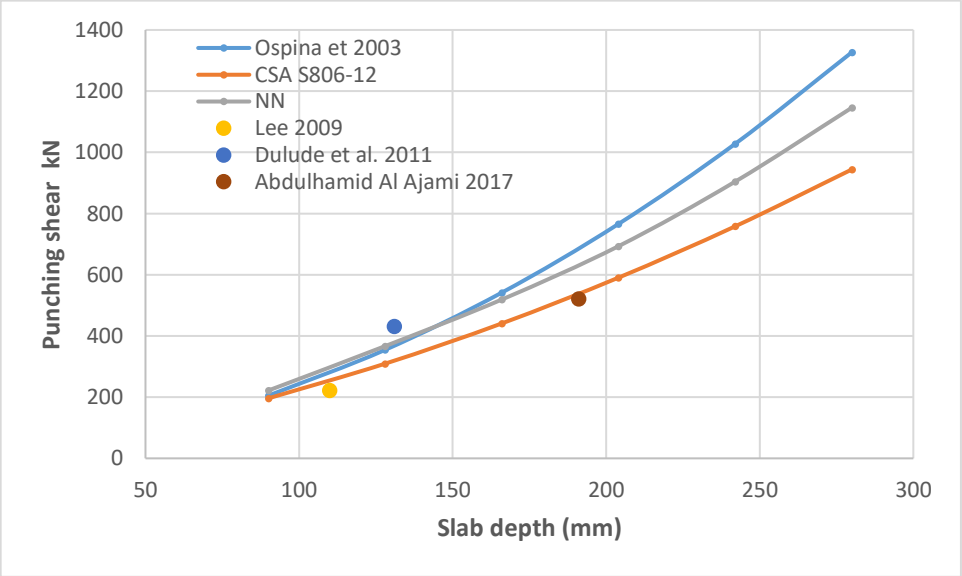

Figure 5-21. Slab effective depth (d) effect on shear capacity (58 specimens)

In conclusion, the effective depth of flat slab has a very high influence on the load carrying capacity in the range of effective depth between 90 mm and 280 mm. This can be attributed to the punching shear stress being reduced by increasing

the area of resistance material which has the major influence on punching shear among all other parameters. The NN succeeded in presenting the modelled problem accurately.

5.5 Conclusions

ANN was used to train two input databases of 52 and 58 flat slabs reinforced with FRP bars. Then, the results were analysed with a parametric study combined five parameters namely, column perimeter, Young's Modulus for the reinforcement, compressive strength of the concrete, reinforcement ratio and slab effective depth. In addition, equations 3-6 to 3-8, 3-20 were also used to examine the results of the parametric study of the NN prediction. Moreover, some experimental results of punching shear capacity chosen from the database have similarities in values of parameters with the parametric study of the NN prediction. Most of these experimental results were identical with the NN prediction of the punching shear capacity. The NN predictions for all parameters were modelled accurately and with expected results of punching shear strength.

The main conclusions which can be drawn from the study described previously in this chapter are summarised as follows:

- The ANN predictions for all parameters were modelled appropriate and with expected relationships of the parametric study results.
- Based on historical data, ANN can be used to predict the punching shear capacity.
- The comparison between the ANN results and the other prediction methods (Ospina et al. 2003; Canadian Standards 2012) showed good agreement in terms of the load carrying capacity of the punching shear.

- Effective depth has the most substantial effect on the load carrying capacity of the punching shear followed by reinforcement ratio, column perimeter and compressive strength of the concrete.
- The elastic modulus of the reinforcement has the lowest impact on the load carrying capacity of punching shear compared to that of the other four parameters.
- A reliable parametric study can be achieved when more data are fed into ANN.

CHAPTER SIX

CONCLUSIONS AND RECOMMENDATION FOR FUTURE WORK

6.1 Summary

The structural behaviour of FRP reinforced concrete flat slabs subjected to concentric load was investigated in this thesis. The research contains two main stages. Firstly, an experimental investigation was conducted in chapter three to study punching shear FRP reinforced concrete flat slabs. Secondly, numerical techniques were developed in order to predict the behaviour of FRP reinforced concrete flat slabs subjected to a concentric load.

The experimental part includes the construction and testing of six concrete flat slabs reinforced with FRP. All the specimens were tested under concentric load until failure. The main parameters investigated were the concrete strength, slab thickness, and reinforcement diameter. The experimental observation focused on the mode of failure, ultimate strength and deflections in the slabs. Besides, this stage is included assessing the recommendations suggested by the current design codes of practice for design of FRP reinforced concrete flat slabs using a database of 69 specimens. Moreover, design methods that have been published were also evaluated and presented in the experimental phase.

The numerical simulation phase consists of two parts of nonlinear technique. A numerical approach is vital to predicting the complete behaviour of punching shear of GFRP reinforced concrete flat slab. In the first part, a three-dimensional FE model was proposed using ABAQUS 6.14 to analyse the behaviour of GFRP reinforced concrete flat slabs. The proposed FE model was verified against experimental results of the current study in addition to some reviews from the open literature. One of the limitations of the proposed model is the definition of

reinforcement as a wire which can't be able to attain stress between concrete and reinforcement. To obtain the stress between the concrete and reinforcement, GFRP bars should be modelled as a 3D element, and a cohesive element or cohesive behaviour should be used. The only way to define the interaction between the concrete and the reinforcement when the definition of wire is used for the GFRP reinforced bars is by using connector or spring and both not able to compute the stress. Besides, the types of constitutive concrete models affect the results. On the other hand, an assumption of symmetry model was used to model the full size of specimens. In the second part, a nonlinear ANN model was developed to predict the punching shear capacity of flat slabs reinforced with FRP. A parametric study was conducted for both techniques to study the effects of main parameters with extended parameter variations on the punching shear strength of GFRP reinforced concrete flat slab.

6.2 Conclusions

A general view of the findings of this research is presented in this section followed by some general recommendations for future work. The following conclusions were drawn based on the research reported in this thesis

- All tested slabs in this research exhibited a brittle punching shear failure. However, the punching shear capacity and maximum deflections were significantly affected by the effective depth of slabs.
- With the lower depth specimens (depth ≤ 150 mm) having the same reinforcement ratio, the value of final deflection will be more likely to be close to failure load despite the difference in concrete strength. While a considerable variance was recorded in case of higher depth specimens (depth ≥ 200 mm).

- Both equations of Matthys and Taerwe (2000) and Ospine et al (2003) gave close predictions of punching shear capacity to the results of the tested slabs than other equations considered in the comparisons section. Whereas, ACI 440. 1R-15 (2015) gave highly conservative prediction of punching shear strength compared with the other two codes of practice CSA S806 (2012) and Japanese Design Recommendations (JSCE 1997).
- Most equations of punching shear strength prediction are highly inaccurate with large-scale flat slab specimens tested under experimental punching shear capacity.
- The proposed model of computational nonlinear finite element (ABAQUS) predicted the behaviour of GFRP reinforced concrete flat slab under concentric load in terms of ultimate capacity and load deflection curve with a reasonable precision.
- Regardless slabs thickness values, the prediction of the proposed ABAQUS model showed a steady increase in the load carrying capacity by increasing the concrete strength, but, the effect of increasing the concrete compressive strength on punching shear strength is more pronounced in normal concrete strength rather than high concrete compressive strength in both GFRP concrete flat slab depths.
- The parametric study of the ABAQUS model showed the effect of shear perimeter to effective depth ratio is less pronounced on deflection rather than punching shear capacity, whereas, the effect of tensile reinforcement ratio on deflection is more pronounced in GFRP reinforced flat slab with greater depth.
- The prediction of the trained ANN was modelled for all parameters accurately and with expected relationships of the parametric study results.

- The comparison between the ANN results and the other prediction methods (Ospina et al. 2003; Canadian Standards 2012) showed good agreement in terms of the load carrying capacity of the punching shear.
- The parametric study of the trained ANN showed that effective depth has the most substantial effect on the load carrying capacity of the punching shear followed by reinforcement ratio, column perimeter and compressive strength of the concrete.
- ANN showed that the elastic modulus of the reinforcement has considerably the lowest impact on the load carrying capacity of punching shear compared to that of the other four parameters.

6.3 Future work

Essential areas in punching shear of FRP reinforced concrete flat slab are still in need of further investigations. Consequently, the following suggestions are recommended for future work:

- It would be advised to investigate the effect of variable FRP reinforced bars diameters on the behaviour of flat slab for punching shear capacity. It is known that as FRP reinforcement diameters increased the bond between the concrete and the reinforcement may be reduced. Bleeding water underneath FRP bars will create voids which reduce the contact area between the bar and concrete. The amount of voids are more in case of larger FRP bars diameter which will adversely affect on concrete and FRP bars bond.
- Since the current research was investigated only one type of FRP reinforcement, then, it is recommended to execute other investigation of

the flat slab reinforced with different types of reinforcement such as CFRP and Basalt Fibre Reinforced Polymers bars.

- Concrete compressive and tensile strength can be improved by adding micro-silica in the concrete mix. It is recommended to study the behaviour of FRP reinforced concrete flat slab containing micro-silica under concentric load.
- Due to small numbers of tested specimens with the different arrangement of FRP flexural reinforcement, it well worth to consider more different reinforcement arrangement to investigate the behaviour of FRP reinforced concrete flat slab under punching shear. Computational nonlinear finite element programs in most cases provide an economical and acceptable solution for the structural elements behaviour. It is recommended to create models by using a computational nonlinear finite element to investigate the effect of different FRP flexural reinforcement arrangement on punching shear capacity and the interaction with other parameters such as effective depth, concrete strength, column dimension and reinforcement ratio.
- It is recommended adding more future experimental data to the ANN for better prediction results. The more input data, the more accurate parametric analysis achieving.

Reference

318-05, A. (2005) Building code requirements for structural concrete (ACI 318-05) and commentary (ACI 318R-05). 2005. American Concrete Institute.

440.3R-4, A. (2004) G*uide Test Methods for Fiber-reinforced Polymers. (FRPs) for Reinforcing Or Strengthening Concrete Structures/reported by ACI Commitee 440*. *American Concrete Institute*.

Abdalla, H. A. (2002) Evaluation of deflection in concrete members reinforced with fibre reinforced polymer (FRP) bars. *Composite Structures* 56 (1), 63-71.

ACI Committee 440, A. C. I. (2015) Guide for the Design and Construction of Structural Concrete Reinforced with Fiber-Reinforced Polymer (FRP) Bars. *American Concrete Institute, Detroit, Michigan*.

Ahmad, S. H. (1993) Punching Shear Tests of Slabs Reinforced with 3-D Carbon Fiber Fabric. *Concrete international* 16 (6).

Ahmad, S. H. (1994) Punching Shear Tests of Slabs Reinforced with 3-D Carbon Fiber Fabric. *Concrete international* 16 (6).

Ahmed, E. A., Benmokrane, B. and Sansfaçon, M. (2017) Case study: Design, construction, and performance of the La Chancelière parking garage's concrete flat slabs reinforced with GFRP bars. *Journal of Composites for Construction* 21 (1), 05016001.

Alexander, S. D. B. and Simmonds, S. H. (1992) Bond model for concentric punching shear. *ACI Structural Journal* 89 (3).

Alih, S. and Khelil, A. (2012) Behavior of inoxydable steel and their performance as reinforcement bars in concrete beam: Experimental and nonlinear finite element analysis. *Construction and Building Materials* 37, 481-492.

Bailey, C. G. (2001) Membrane action of unrestrained lightly reinforced concrete slabs at large displacements. *Engineering Structures* 23 (5), 470-483.

Banthia, N. (1995) Behavior of Concrete Slabs Reinforced with Fiber-Reinforced Plastic Grid. *Materials in Civil Engineering* 7 (4).

Bashir, R. and Ashour, A. (2012) Neural network modelling for shear strength of concrete members reinforced with FRP bars. *Composites Part B: Engineering* 43 (8), 3198-3207.

Bashir, Z. A. and El-Hawary, M. E. (2009) Applying wavelets to short-term load forecasting using PSO-based neural networks. *Power Systems, IEEE Transactions on* 24 (1), 20-27.

Bazant, Z. P. and Cao, Z. (1987) Size effect in punching shear failure of slabs. *ACI Structural Journal* 84 (1).

Bazant, Z. P., Ozbolt, J. and Eligehausen, R. (1994) Fracture size effect: review of evidence for concrete structures. *Journal of structural engineering* 120 (8), 2377-2398.

Bernard Potyrala, P. (2011) Use of fibre reinforced polymeromposites in bridge construction. State of the art in hybrid and all-composite structures.

Bisby, L. A. (2003) ISIS Educational Module 2: An Introduction to FRP Composites for Construction. *ISIS Canada, Intelligent Sensing for Innovative Structures, A Canadian Network of Centres of Excellence, University of Manitoba, Winnipeg* 100.

Bouguerra, K., Ahmed, E. A., El-Gamal, S. and Benmokrane, B. (2011) Testing of full-scale concrete bridge deck slabs reinforced with fiber-reinforced polymer (FRP) bars. *Construction and Building Materials* 25 (10), 3956-3965.

British Standard (1997) 8110-1 (1997). *Structural use of concrete. Part* 1.

Canadian Standards, A. (2012) Design and Construction of Building Structures with Fibre-Reinforced Polymers,(CAN/CSA S806-12). *Canadian Standards Association Mississauga, Ont*.

Chen, W. F. and Han, D. J. (1988) Plasticity for structural engineers. 1988. *Springer, New York.*

Clarke, J. L. and Waldron, P. (1996) The reinforcement of concrete structures with advanced composites. *Structural Engineer* 74 (17).

Code, E. (2004) 2, Design of concrete structures-Part 1-1: General rules and rules for buildings, BS EN 1992-1-1: 2004. *British Standards (BSi)*.

Committee, A. C. I., American Concrete, I. and International Organization for, S. (2008) Building Code Requirements for Structural Concrete (ACI 318-08) and Commentary. 2008. American Concrete Institute.

Demuth, H., Beale, M. and Hagan, M. (2008) Neural network toolbox™ 6. *User's guide*.

Dulude, C., Ahmed, E., El-Gamal, S. and Benmokrane, B. (2011) Testing of large-scale two-way concrete slabs reinforced with GFRP bars. *Advances in FRP Composites in Civil Engineering.* Springer. 287-291.

Dulude, C., Hassan, M., Ahmed, E. A. and Benmokrane, B. (2013) Punching Shear Behavior of Flat Slabs Reinforced with Glass Fiber-Reinforced Polymer Bars. *ACI Structural Journal* 110 (5).

Eder, M. A., Vollum, R. L., Elghazouli, A. Y. and Abdel-Fattah, T. (2010) Modelling and experimental assessment of punching shear in flat slabs with shearheads. *Engineering Structures* 32 (12), 3911-3924.

El-Gamal, S., El-Salakawy, E. and Benmokrane, B. (2005) Behavior of concrete bridge deck slabs reinforced with fiber-reinforced polymer bars under concentrated loads. *ACI Structural Journal* 102 (5).

El-Gamal, S., El-Salakawy, E. and Benmokrane, B. (2007) Influence of reinforcement on the behavior of concrete bridge deck slabs reinforced with FRP bars. *Journal of Composites for Construction* 11 (5), 449-458.

El-Ghandour, A. W., Pilakoutas, K. and Waldron, P. (2003) Punching shear behavior of fiber reinforced polymers reinforced concrete flat slabs: experimental study. *Journal of composites for construction* 7 (3), 258-265.

Genikomsou, A. S. and Polak, M. A. (2015) Finite element analysis of punching shear of concrete slabs using damaged plasticity model in ABAQUS. *Engineering Structures* 98, 38-48.

Grassl, P. and Jirásek, M. (2006) Damage-plastic model for concrete failure. *International journal of solids and structures* 43 (22), 7166-7196.

Guadagnini, M., Pilakoutas, K. and Waldron, P. (2003) Shear performance of FRP reinforced concrete beams. *Journal of Reinforced Plastics and Composites* 22 (15), 1389-1407.

Guandalini, S., Burdet, O. L. and Muttoni, A. (2009) Punching tests of slabs with low reinforcement ratios. *ACI Structural Journal* 106 (1).

Hahn, B. and Valentine, D. T. (2016) *Essential MATLAB for engineers and scientists.* Academic Press.

Hallgren, M. (1996) Punching shear capacity of reinforced high strength concrete slabs.

Hansen, N. R. and Schreyer, H. L. (1994) A thermodynamically consistent framework for theories of elastoplasticity coupled with damage. *International Journal of Solids and Structures* 31 (3), 359-389.

Hassan, M., A. Ahmed, E. and Benmokrane, B. (2013a) Punching shear strength of glass fiber-reinforced polymer reinforced concrete flat slabs. *Canadian journal of civil engineering* 40, 951-960.

Hassan, M., Ahmed, E. and Benmokrane, B. (2013b) Punching-Shear Strength of Normal and High-Strength Two-Way Concrete Slabs Reinforced with GFRP Bars. *Journal of Composites for Construction* 17 (6).

Hassan, M., Ahmed, E. A. and Benmokrane, B. (2014) Punching-shear design equation for two-way concrete slabs reinforced with FRP bars and stirrups. *Construction and Building Materials* 66, 522-532.

Hassan, M., Fam, A., Benmokrane, B. and Ferrier, E. (2017) Effect of Column Size and Reinforcement Ratio on Shear Strength of Glass Fiber-Reinforced Polymer Reinforced Concrete Two-Way Slabs. *ACI Structural Journal* 114 (4), 937.

Hibbitt, D., Karlsson, B. and Sorensen, P. (2014) Abaqus 6.14. 3 Manual.

Hillerborg, A., Modéer, M. and Petersson, P. E. (1976) Analysis of crack formation and crack growth in concrete by means of fracture mechanics and finite elements. *Cement and concrete research* 6 (6), 773-781.

Hollaway, L. C. (2010) A review of the present and future utilisation of FRP composites in the civil infrastructure with reference to their important in-service properties. *Construction and Building Materials* 24 (12), 2419-2445.

Holzapfel, G. A. (2000) *Nonlinear solid mechanics.* Vol. 24. Wiley Chichester.

Hussein, A., Rashid, I. and Benmokrane, B. Two-way concrete slabs reinforced with GFRP bars. 2004.

Hussein, A., Rashid, I. and Benmokrane, B. (2004) Two-way concrete slabs reinforced with GFRP bars. 2004.

JSCE, Machida, A., Uomoto, T., Akimoto, T., Ishibashi, T., Idemitsu, T., Ueda, T., Umehara, H., Ohtsuki, N., Ozawa, K. and Kakauta, Y. (1997) RECOMMENDATION FOR DESIGN AND CONSTRUCTION OF CONCRETE STRUCTURES USING CONTINUOUS FIBER REINFORCING MATERIALS (DESIGN). *Concrete library international* (30), 1-64.

Keyvani, L., Sasani, M. and Mirzaei, Y. (2014) Compressive membrane action in progressive collapse resistance of RC flat plates. *Engineering Structures* 59, 554-564.

Lee, J. and Fenves, G. L. (1998) A plastic-damage concrete model for earthquake analysis of dams. *Earthquake engineering & structural dynamics* 27 (9), 937-956.

Lee, J.-H. (2009) Improving Punching Shear Behavior of Glass Fiber-Reinforced Polymer Reinforced Slabs. *American Concrete Institute* 106 (4), 424-434.

Lemaitre, J. and Chaboche, J.-L. (1994) *Mechanics of solid materials.* Cambridge university press.

Li, R., Cho, Y. S. and Zhang, S. (2007) Punching shear behavior of concrete flat plate slab reinforced with carbon fiber reinforced polymer rods. *Composites Part B: Engineering* 38 (5), 712-719.

Malm, R. (2009) Predicting shear type crack initiation and growth in concrete with non-linear finite element method.

Mamede, N. F. S., Ramos, A. P. and Faria, D. M. V. (2013) Experimental and parametric 3D nonlinear finite element analysis on punching of flat slabs with orthogonal reinforcement. *Engineering Structures* 48, 442-457.

Matthys, S. and Taerwe, L. (2000) Concrete slabs reinforced with FRP grids. II: punching resistance. *Journal of Composites for Construction* 4 (3), 154-161.

Mendis, P. (2003) Design of high-strength concrete members: state-of-the-art. *Progress in Structural Engineering and Materials* 5 (1), 1-15.

Menetrey, P. (1994) Numerical analysis of punching failure in reinforced concrete structures.

Metwally, I. M. (2013) Prediction of punching shear capacities of two-way concrete slabs reinforced with FRP bars. *HBRC Journal* 9 (2), 125-133.

Michaluk, C. R., Rizkalla, S. H., Tadros, G. and Benmokrane, B. (1998) Flexural behavior of one-way concrete slabs reinforced by fiber reinforced plastic reinforcements. *ACI Structural Journal* 95, 353-365.

Mokhtar, A.-S., Ghali, A. and Dilger, W. (1985) Stud shear reinforcement for flat concrete plates. 1985. Vol. 82. ACI.

Murphy, N. (2013) *Feasibility Analysis of a Fiber Reinforced Polymer Bridge*.

Mörsch, E. (1909) *Concrete steel construction (Der Eisenbetonbau). English translation of the 3rd German edition*. McGraw-Hill Book Co., New York.

Nagasaka, T., Fukuyama, H. and Tanigaki, M. (1993) Shear performance of concrete beams reinforced with FRP stirrups. *Special publication* 138, 789-812.

Nanni, A., De Luca, A. and Zadeh, H. J. (2014) *Reinforced Concrete with FRP Bars: Mechanics and Design.* CRC Press.

Nguyen-Minh, L. and Rovňák, M. (2012) Punching Shear Resistance of Interior GFRP Reinforced Slab-Column Connections. *Journal of Composites for Construction* 17 (1), 2-13.

Ospina, C. E., Alexander, S. D. B. and Cheng, J. J. R. (2003) Punching of two-way concrete slabs with fiber-reinforced polymer reinforcing bars or grids. *ACI structural Journal* 100 (5).

Ozbolt, J., Vocke, H. and Eligehausen, R. (2000) Three-dimensional numerical analysis of punching failure. *Trita-BKN. Bulletin* 57, 65-74.

Perera, R., Barchín, M., Arteaga, A. and De Diego, A. (2010) Prediction of the ultimate strength of reinforced concrete beams FRP-strengthened in shear using neural networks. *Composites Part B: Engineering* 41 (4), 287-298.

Pilakoutas, K., Guadagnini, M., Neocleous, K. and Matthys, S. (2011) Design guidelines for FRP reinforced concrete structures. *Proceedings of the Institution of Civil Engineers-Structures and Buildings* 164 (4), 255-263.

Pirayeh Gar, S., Mander, J. B., Head, M. and Hurlebaus, S. (2014) FRP Slab Capacity Using Yield Line Theory. *Journal of Composites for Construction*.

Pultrall, V. (2013) *Technical Specifications*. Pultrall, Inc. http://www. pultrall. com/products/construction/TechMech2. html (accessed June 19, 2006).

Pérez Caldentey, A., Padilla Lavaselli, P., Corres Peiretti, H. and Ariñez Fernández, F. (2013) Influence of stirrup detailing on punching shear strength of flat slabs. *Engineering Structures* 49, 855-865.

Rahman, A. H., Kingsley, C. Y. and Kobayashi, K. (2000) Service and ultimate load behavior of bridge deck reinforced with carbon FRP grid. *Journal of composites for construction* 4 (1), 16-23.

Rizk, E. and Marzouk, H. (2013) Minimum shear reinforcement for thick plates and two-way slabs. *Engineering Structures* 46, 1-13.

Sayed, A. (2015) Punching shear behaviour of FRP-reinforced concrete interior slab-column connections.

Shi, X., Xie, N., Fortune, K. and Gong, J. (2012) Durability of steel reinforced concrete in chloride environments: An overview. *Construction and Building Materials* 30, 125-138.

Simo, J. C. and Ju, J. W. (1989) Strain-and stress-based continuum damage models—I. Formulation. *Mathematical and Computer Modelling* 12 (3), 378.

Theodorakopoulos, D. D. and Swamy, N. (2007) Analytical model to predict punching shear strength of FRP-reinforced concrete flat slabs. *ACI structural journal* 104 (3), 257.

Theodorakopoulos, D. D. and Swamy, R. N. (2008) A design model for punching shear of FRP-reinforced slab-column connections. *Cement and Concrete Composites* 30 (6), 544-555.

Thorhallsson, E., Erlendsson, J. Ó. and Erlendsson, Ö. (2013) Basalt fiber introduction.

Tureyen, A. K. and Frosch, R. J. (2002) Shear tests of FRP-reinforced concrete beams without stirrups. *Structural Journal* 99 (4), 427-434.

Voyiadjis, G. Z. and Taqieddin, Z. N. (2009) Elastic plastic and damage model for concrete materials: Part I-theoretical formulation. *The International Journal of Structural Changes in Solids* 1 (1), 31-59.

Wosatko, A., Pamin, J. and Polak, M. A. (2015) Application of damage–plasticity models in finite element analysis of punching shear. *Computers & Structures* 151, 73-85.

Wu, J. Y., Li, J. and Faria, R. (2006) An energy release rate-based plastic-damage model for concrete. *International Journal of Solids and Structures* 43 (3), 583-612.

Yamada, T., Nanni, A. and Endo, K. (1992) PunchingShear Resistance of Flat Slabs: Influence of Reinforcement Type and Ratio. *ACI Structural journal* 89 (5).

Yitzhaki, D. (1966) Punching strength of reinforced concrete slabs. 1966. Vol. 63. ACI.

Yu, H., Burgess, I. W., Davison, J. B. and Plank, R. J. (2008) Numerical simulation of bolted steel connections in fire using explicit dynamic analysis. *Journal of Constructional Steel Research* 64 (5), 515-525.

Zaghloul, A. E. (2003a) Punching shear behavior of CFRP reinforced concrete flat plates. *Composites in Constructions.* Vol. 2.

Zaghloul, A. E. R. (2003b) Behaviour and strength of CFRP-reinforced flat plate interior column connections subjected to shear and unbalanced moments.

Zhang, Q. I. (2003) The punching strength of high strength flat slabs—experimental study. *Research Study, Memorial University of Newfoundland*.

Zhao, W., Maruyama, K. and Suzuki, H. (1995) Shear behavior of concrete beams reinforced by FRP rods as longitudinal and shear reinforcement. 1995. CHAPMAN & HALL.
Zheng, Y., Yu, G. and Pan, Y. (2012) Investigation of ultimate strengths of concrete bridge deck slabs reinforced with GFRP bars. *Construction and Building Materials* 28 (1), 482-492.

APPENDIX A. DATABASE OF FRP REINFORCED CONCRETE FLAT SLABS AND BRIDGE DECK

Table A-1 shows the details of the database of FRP reinforced concrete flat slabs and bridge decks. The database was used in chapter three to identify the most critical parameters that affect the behaviour of FRP reinforced flat slabs and bridge decks. The database in Table A-1 is also used in chapter three, four, and five to validate different design approaches that suggested by the code of practices for FRP reinforced concrete flat slabs subjected to a concentric load. The validation was continued to include different design approach that proposed by various researchers.

Table A-1: Database details of two-way and bridge deck slabs specimens

Design Description	Slab Dimensions			Column Dimensions			Slab effective depth d mm	FRP Mechanical Property		Compressive strength of concrete, fc (N/mm²)	Reinforcement ratio ρ_f %
	Length mm	Width mm	Depth mm	Length mm	Width mm	Diameter mm		E N/mm²	f_y N/mm²		
(Ahmad 1994) Two-way slab	550	550	80	80	80		50	113000	3431.7	41	0.0095
	550	550	80	80	80		50	113000	3431.7	45	0.0095
	550	550	80	100	100		50	113000	3431.7	39	0.0095
	550	550	80	100	100		50	113000	3431.7	37	0.0095
(Banthia 1995) Two-way slab	600	600	75			100	55	100000	1200	41	0.0031
	600	600	75			100	55	100000	1200	53	0.0031
	600	600	75			100	55	100000	1200	42	0.0031
(Matthys and Taerwe 2000) Two-way slab	1000	1000	120			150	96	91800	1690	30	0.0027
	1000	1000	120			230	96	91800	1690	30	0.0027
	1000	1000	120			150	95	92000	1350	30	0.0105
	1000	1000	120			230	95	92000	1350	30	0.0105

Design Description	Slab Dimensions			Column Dimensions			Slab effective depth d mm	FRP Mechanical Property		Compressive strength of concrete, fc (N/mm²)	Reinforcement ratio ρ_f %
	Length mm	Width mm	Depth mm	Length mm	Width mm	Diameter mm		E N/mm²	f_y N/mm²		
	1000	1000	150			150	126	95000	1340	28	0.0052
	1000	1000	150			230	126	95000	1340	28	0.0052
	1000	1000	120			150	95	147000	2300	27	0.0019
	1000	1000	120			230	95	147000	2300	27	0.0019
	1000	1000	120			150	95	37300	665	97	0.0062
	1000	1000	120			150	89	44800	640	29	0.0376
	1000	1000	120			80	89	44800	640	29	0.0376
	1000	1000	150			150	122	40700	555	26	0.0122
	1000	1000	150			80	122	40700	555	26	0.0122
(El-Ghandour et al. 2003) Two-way slab	2000	2000	175	200	200		142	45000	800	32	0.0018
	2000	2000	175	200	200		142	110000	1400	33	0.0015
	2000	2000	175	200	200		142	45000	800	35	0.0018
	2000	2000	175	200	200		142	110000	1400	27	0.0015
	2000	2000	175	200	200		142	45000	800	46	0.0038
	2000	2000	175	200	200		142	45000	800	30	0.0038
	2000	2000	175	200	200		142	110000	1400	30	0.0035
	2000	2000	175	200	200		142	45000	800	34	0.0038
(Ospina et al. 2003) Two-way slab	2150	2150	155	250	250		120	34000	663	30	0.0073
	2150	2150	155	250	250		120	34000	663	29	0.0146
	2150	2150	155	250	250		120	28400	566	38	0.0087
(Zaghloul 2003a) Two-way slab	1760	1760	100	250	250		75	100000	1700	46	0.01
	1760	1760	100	250	250		75	100000	1700	47	0.0065
	1760	1760	100	250	250		75	100000	1700	46	0.01
	1760	1760	125	250	250		100	100000	1700	46	0.01184
	1760	1760	100	250	250		75	100000	1700	45	0.01

Design Description	Slab Dimensions			Column Dimensions			Slab effective depth d mm	FRP Mechanical Property		Compressive strength of concrete, fc (N/mm²)	Reinforcement ratio ρ_f %
	Length mm	Width mm	Depth mm	Length mm	Width mm	Diameter mm		E N/mm²	f_y N/mm²		
	1760	1760	125	250	350		100	100000	1700	47	0.01184
(Hussein et al. 2004) Two-way slab	1900	1900	150	250	250		100	42000	630	40	0.0118
	1900	1900	150	250	250		100	42000	630	35	0.0105
	1900	1900	150	250	250		100	42000	630	29	0.0167
	1900	1900	150	250	250		100	42000	630	26	0.0095
(El-Gamal et al. 2005) Bridge deck slabs	3000	2500	200	600	250		159.1	39000	636	50	0.01
	3000	2500	200	600	250		159.1	44600	727	44	0.02
	3000	2500	200	600	250		156	44000	637	49	0.012
	3000	2500	200	600	250		162.3	122000	1444	50	0.0034
	3000	2500	200	600	250		162.3	122000	1444	44	0.0068
(El-Gamal et al. 2007) Bridge deck slabs	3000	2500	200	600	250		157.55	44500	637	49	0.01221
	3000	2500	200	600	250		157.55	44500	637	44	0.01221
	3000	2500	200	600	250		159.15	44500	637	44	0.01209
(Lee 2009) Two-way slab	2500	2500	150	225	225		110	48200	761	36	0.0118
	2500	2500	150	225	225		110	48200	761	36	0.0215
	2500	2500	150	225	225		110	48200	761	36	0.03
	2500	2500	150	225	225		110	48200	761	36	0.03
(Dulude et al. 2011) Two-way slab	2000	2000	350	450	450		284	48200	751	49	0.00297
	2000	2000	200	450	450		134	48200	751	45	0.00559
	2000	2000	200	450	450		131	47600	728	39	0.01207
	2000	2000	200	300	300		131	47600	728	39	0.01207
(Bouguerra et al. 2011) Bridge deck slabs	3000	2500	200	600	250		156	44500	637	39	0.012
	3000	2500	175	600	250		134	41600	778	28	0.012

Design Description	Slab Dimensions			Column Dimensions			Slab effective depth d mm	FRP Mechanical Property		Compressive strength of concrete, fc (N/mm²)	Reinforcement ratio ρ_f %
	Length mm	Width mm	Depth mm	Length mm	Width mm	Diameter mm		E N/mm²	f_y N/mm²		
	3000	2500	150	600	250		109	41600	778	28	0.012
	3000	2500	175	600	250		134	41600	778	52	0.012
	3000	2500	175	600	250		134	41600	778	42	0.007
	3000	2500	175	600	250		137	41000	769	42	0.0035
	3000	2500	175	600	250		141	122000	1444	32	0.004
(Nguyen-Minh and Rovňák 2012) Two-way slab	2200	2200	150	200	200		129	48000	582	39	0.004
	2200	2200	150	200	200		129	48000	582	39	0.006
	2200	2200	150	200	200		129	48000	582	39	0.008
(Hassan et al. 2013b) Two-way slab	2500	2500	200	300	300		132	57400	1109	76	0.0121
	2500	2500	200	300	300		132	64900	1065	38	0.0166
	2500	2500	350	300	300		275	56700	1065	38	0.0161
	2500	2500	350	300	300		275	56700	1065	76	0.0161
(Hassan et al. 2013a) Two-way slab	2500	2500	200	300	300		134.0	48200	769	34	0.0071
	2500	2500	200	300	300		134.0	48200	769	39	0.0071
	2500	2500	200	300	300		131.0	48100	765	39	0.0156
	2500	2500	200	300	300		131.0	48100	765	32	0.0156
	2500	2500	200	450	450		134.0	48200	769	45	0.0071
	2500	2500	200	450	450		131.0	48100	765	32	0.0156
	2500	2500	200	450	450		131.0	48100	765	39	0.0156
	2500	2500	350	300	300		284.0	48200	769	34	0.0034
	2500	2500	350	300	300		284.0	48200	769	39	0.0034
	2500	2500	350	300	300		281.0	48100	765	39	0.0073
	2500	2500	350	300	300		281.0	48100	765	30	0.0073
	2500	2500	350	300	300		281.0	48100	765	47	0.0073

Design Description	Slab Dimensions			Column Dimensions			Slab effective depth d mm	FRP Mechanical Property		Compressive strength of concrete, fc (N/mm²)	Reinforcement ratio ρ_f %
	Length	Width	Depth	Length	Width	Diameter		E N/mm²	f_y N/mm²		
	mm	mm	mm	mm	mm	mm					
	2500	2500	350	450	450		284.0	48200	769	49	0.0034
	2500	2500	350	450	450		284.0	48200	769	32	0.0034
	2500	2500	350	450	450		281.0	48100	765	30	0.0073
Abdulhamid Al Ajami 2016 Two-way slab	1700	1700	150	200	200		94	52500	1130	47	0.0096
	1700	1700	250	200	200		191	52500	1110	52	0.0093
	1700	1700	150	200	200		94	52500	1130	35	0.0096
	1700	1700	250	200	200		191	52500	1110	37	0.0093

Table A-2 shows the details of the databases of FRP reinforced concrete flat slabs for 52 and 58 specimens. The databases were used in chapter five for the training of ANN.

Table A-2: Database details of 52 and 58 two-way specimens

	Reference	Slab Dimensions			Column Dimensions			Slab effective depth d mm	FRP Mechanical Property		Compressive strength of concrete, fc (N/mm²)	Reinforcement ratio ρ_f %
		Length mm	Width mm	Depth mm	Length mm	Width mm	Diameter mm		E N/mm²	f_y N/mm²		
1	(Ahmad 1994) Slabs < 1000 mm	550	550	80	80	80		50	113000	3432	41	0.0095
2		550	550	80	80	80		50	113000	3432	45	0.0095
3		550	550	80	100	100		50	113000	3432	39	0.0095
4		550	550	80	100	100		50	113000	3432	37	0.0095
5	(Banthia 1995) Slabs < 1000 mm	600	600	75			100	55	100000	1200	41	0.0031
6		600	600	75			100	55	100000	1200	53	0.0031
7	(Matthys and Taerwe 2000) Slabs ≥ 1000 mm	1000	1000	120			150	96	91800	1690	30	0.0027
8		1000	1000	120			230	96	91800	1690	30	0.0027
9		1000	1000	120			150	95	92000	1350	30	0.0105
10		1000	1000	120			230	95	92000	1350	30	0.0105
11		1000	1000	150			150	126	95000	1340	28	0.0052
12		1000	1000	150			230	126	95000	1340	28	0.0052
13		1000	1000	120			150	95	147000	2300	27	0.0019
14		1000	1000	120			230	95	147000	2300	27	0.0019
15		1000	1000	120			150	95	37300	665	97	0.0062
16		1000	1000	120			150	89	44800	640	29	0.0376
17		1000	1000	120			80	89	44800	640	29	0.0376
18		1000	1000	150			150	122	40700	555	26	0.0122

	Reference	Slab Dimensions			Column Dimensions			Slab effective depth d mm	FRP Mechanical Property		Compressive strength of concrete, fc (N/mm²)	Reinforcement ratio ρ_f %
		Length mm	Width mm	Depth mm	Length mm	Width mm	Diameter mm		E N/mm²	f_y N/mm²		
19		1000	1000	150			80	122	40700	555	26	0.0122
20	(El-Ghandour et al. 2003) Slabs ≥ 1000 mm	2000	2000	175	200	200		142	45000	800	46	0.0038
21		2000	2000	175	200	200		142	45000	800	30	0.0038
22		2000	2000	175	200	200		142	110000	1400	30	0.0035
23	(Ospina et al. 2003) Slabs ≥ 1000 mm	2150	2150	155	250	250		120	34000	663	30	0.0073
24		2150	2150	155	250	250		120	34000	663	29	0.0146
25		2150	2150	155	250	250		120	28400	566	38	0.0087
26	(Zaghloul 2003a) Slabs ≥ 1000 mm	2500	2500	100	250	250		75	100000	1700	45	0.01
27	(Lee 2009) Slabs ≥ 1000 mm	2500	2500	150	225	225		110	48200	761	36	0.0118
28		2500	2500	150	225	225		110	48200	761	36	0.0215
29		2500	2500	150	225	225		110	48200	761	36	0.03
30	(Dulude et al. 2011) Slabs ≥ 1000 mm	2000	2000	350	450	450		284	48200	751	49	0.003
31		2000	2000	200	450	450		134	48200	751	45	0.0056
32		2000	2000	200	300	300		131	47600	728	39	0.0121
33	(Nguyen-Minh and Rovňák 2012) Slabs ≥ 1000 mm	2200	2200	150	200	200		129	48000	582	39	0.004
34		2200	2200	150	200	200		129	48000	582	39	0.006
35		2200	2200	150	200	200		129	48000	582	39	0.008
36	(Hassan et al. 2013b) Slabs ≥ 1000 mm	2500	2500	200	300	300		132	57400	1109	76	0.0121
37		2500	2500	200	300	300		132	64900	1065	38	0.0166
38		2500	2500	350	300	300		275	56700	1065	38	0.0161

	Reference	Slab Dimensions			Column Dimensions			Slab effective depth d mm	FRP Mechanical Property		Compressive strength of concrete, fc (N/mm²)	Reinforcement ratio ρ_f %
		Length mm	Width mm	Depth mm	Length mm	Width mm	Diameter mm		E N/mm²	f_y N/mm²		
39		2500	2500	350	300	300		275	56700	1065	76	0.0161
40	(Hassan et al. 2013a) Slabs ≥ 1000 mm	2500	2500	200	300	300		134	48200	769	34	0.0071
41		2500	2500	200	300	300		134	48200	769	39	0.0071
42		2500	2500	200	300	300		131	48100	765	39	0.0156
43		2500	2500	200	300	300		131	48100	765	32	0.0156
44		2500	2500	200	450	450		134	48200	769	45	0.0071
45		2500	2500	200	450	450		131	48100	765	32	0.0156
46		2500	2500	200	450	450		131	48100	765	39	0.0156
47		2500	2500	350	300	300		284	48200	769	34	0.0034
48		2500	2500	350	300	300		284	48200	769	39	0.0034
49		2500	2500	350	300	300		281	48100	765	39	0.0073
50		2500	2500	350	300	300		281	48100	765	30	0.0073
51		2500	2500	350	300	300		281	48100	765	47	0.0073
52		2500	2500	350	450	450		284	48200	769	49	0.0034
53		2500	2500	350	450	450		284	48200	769	32	0.0034
54		2500	2500	350	450	450		281	48100	765	30	0.0073
55	Abdulhamid Al Ajami 2016 Slabs ≥ 1000 mm	1700	1700	150	200	200		94	52500	1130	47	0.0096
56		1700	1700	250	200	200		191	52500	1110	52	0.0093
57		1700	1700	150	200	200		94	52500	1130	35	0.0096
58		1700	1700	250	200	200		191	52500	1110	37	0.0093

Table A-3 shows the validation of different design approaches that suggested by the code of practices as well as a various design approach that proposed by different researchers for FRP reinforced concrete flat slabs subjected to a centric load.

Table A-3: Evaluation of the Proposed and Existing Formula

		V(tested)/V(predicted)							
	Experimental	CSA	ACI	JSCE	Matthys	El-Ghandour at al	Ospina	El- Gamal et al	Nguyen
	Results	S806	440		And				
	$V_{u,Exp.}$	2012	1R-15	1997	Taerwe				
	kN				2000	2003	2003	2005	2012
(Ahmad 1994)	93	1.41	2.19	1.38	1.40	2.03	1.32	1.49	1.47
	78	1.16	1.80	1.16	1.15	1.65	1.08	1.21	1.22
	96	1.28	1.99	1.28	1.36	1.87	1.28	1.46	1.33
	99	1.35	2.10	1.32	1.43	1.99	1.35	1.56	1.40
(Banthia 1995)	65	1.57	3.01	1.53	1.26	1.22	1.18	1.31	1.02
	61	1.36	2.66	1.45	1.09	1.02	1.02	1.09	0.89
(Matthys and Taerwe 2000)	181	1.88	3.63	1.76	1.54	1.47	1.37	1.58	1.60
	189	1.50	2.90	1.51	1.37	1.17	1.23	1.41	1.25
	255	1.72	2.83	1.62	1.41	2.12	1.26	1.46	1.47
	273	1.40	2.31	1.42	1.29	1.73	1.15	1.34	1.18
	347	1.98	3.50	1.80	1.62	1.95	1.34	1.57	1.45
	343	1.53	2.71	1.50	1.40	1.51	1.16	1.37	1.10
	142	1.49	2.82	1.43	1.22	1.06	1.01	1.28	1.26
	150	1.20	2.27	1.23	1.10	0.85	0.91	1.16	1.00
	207	1.51	3.21	1.92	1.24	1.29	1.29	1.06	1.34
	231	1.42	2.23	1.36	1.17	2.69	1.20	1.23	1.18
	171	1.46	2.29	1.26	1.02	2.77	1.05	1.08	1.15
	237	1.44	2.54	1.33	1.18	1.91	1.14	1.17	1.08
	217	1.75	3.08	1.46	1.24	2.32	1.19	1.22	1.28
(El-Ghandour et al. 2003)	170	1.14	2.59	1.06	1.03	0.77	0.87	0.85	1.12
	229	1.20	2.47	1.11	1.09	0.76	0.79	0.90	1.18

		V(tested)/V(predicted)							
	Experimental	CSA	ACI	JSCE	Matthys	El-Ghandour at al	Ospina	El- Gamal et al	Nguyen
	Results	S806	440		And				
	$V_{u,Exp.}$	2012	1R-15	1997	Taerwe				
	kN				2000	2003	2003	2005	2012
	271	1.25	2.62	1.24	1.13	1.02	0.96	0.88	1.25
	237	1.26	2.56	1.18	1.14	1.10	0.97	0.95	1.24
	317	1.29	2.37	1.22	1.18	1.11	0.86	0.98	1.28
(Ospina et al. 2003)	199	1.03	1.99	1.04	1.00	1.01	0.99	0.87	1.13
	249	1.03	1.82	1.04	1.00	1.28	0.99	0.87	1.13
	203	0.97	1.91	0.96	0.94	0.97	0.96	0.79	1.07
(Zaghloul 2003a)	171	0.87	1.47	1.00	0.91	0.99	0.79	0.86	1.21
	144	0.84	1.49	0.97	0.88	0.82	0.77	0.83	1.17
	134	0.68	1.15	0.78	0.72	0.77	0.62	0.68	0.95
	250	0.84	1.39	0.92	0.88	1.01	0.71	0.77	0.91
	234	1.20	2.02	1.36	1.26	1.37	1.09	1.20	1.67
	235	0.69	1.14	0.76	0.75	0.82	0.61	0.66	0.85
(Hussein et al. 2004)	249	1.16	2.09	1.21	1.21	1.42	1.13	1.09	1.46
	218	1.10	2.00	1.11	1.15	1.32	1.07	1.06	1.43
	240	1.11	1.89	1.15	1.16	1.60	1.08	1.10	1.47
	210	1.21	2.19	1.29	1.27	1.48	1.18	1.22	1.65
(Lee 2009)	222	0.98	1.73	0.96	0.92	1.09	0.82	0.80	1.36
	246	0.89	1.47	0.87	0.84	1.21	0.75	0.72	1.23
	248	0.80	1.29	0.78	0.76	1.22	0.67	0.65	1.11
(Dulude et al. 2011)	911	1.02	2.21	1.15	1.14	0.68	0.80	0.74	0.96
	400	0.99	1.95	1.13	1.12	0.83	0.95	0.88	1.10
	431	1.21	1.59	1.23	1.11	1.00	0.95	0.82	0.99
(Nguyen-Minh and Rovňák 2012)	180	0.97	1.97	0.92	0.88	0.74	0.75	0.72	0.97
	212	1.00	1.92	0.95	0.91	0.87	0.78	0.74	1.00
	244	1.04	1.94	0.99	0.95	1.00	0.81	0.78	1.05

		V(tested)/V(predicted)							
	Experimental	CSA	ACI	JSCE	Matthys	El-Ghandour at al	Ospina	El- Gamal et al	Nguyen
	Results	S806	440		And				
	$V_{u,Exp.}$	2012	1R-15	1997	Taerwe				
	kN				2000	2003	2003	2005	2012
(Hassan et al. 2013b)	547	1.15	2.07	1.46	1.16	1.14	0.96	0.85	1.50
	438	1.00	1.66	1.01	1.02	1.24	0.83	0.83	1.28
	1492	1.29	2.17	1.25	1.30	1.58	0.90	0.88	1.68
	1600	1.10	1.92	1.34	1.11	1.20	0.76	0.67	1.46
(Hassan et al. 2013a)	329	1.11	2.09	1.11	1.13	1.06	0.96	0.94	1.39
	386	1.25	2.36	1.27	1.27	1.16	1.07	1.03	1.57
	431	1.11	1.90	1.13	1.12	1.33	0.96	0.91	1.42
	451	1.24	2.10	1.25	1.25	1.54	1.07	1.06	1.57
	400	0.92	1.75	1.04	1.03	0.83	0.87	0.82	1.25
	504	1.02	1.74	1.10	1.15	1.28	0.98	0.97	1.41
	511	0.97	1.67	1.06	1.09	1.17	0.93	0.89	1.35
	825	1.25	2.59	1.21	1.26	0.93	0.88	0.86	1.57
	782	1.13	2.37	1.11	1.14	0.82	0.80	0.76	1.43
	1071	1.22	2.30	1.20	1.23	1.14	0.87	0.83	1.56
	1027	1.28	2.37	1.26	1.28	1.25	0.91	0.90	1.62
	1195	1.28	2.44	1.34	1.29	1.16	0.91	0.84	1.65
	911	0.97	2.07	1.10	1.09	0.68	0.76	0.70	1.23
	1020	1.26	2.59	1.31	1.40	0.94	0.99	0.97	1.57
	1248	1.24	2.29	1.30	1.38	1.21	0.97	0.97	1.55
Abdulhamid Al Ajami 2016	199	1.12	2.04	1.20	1.10	0.76	1.01	0.71	1.27
	617.2	1.26	2.31	1.23	1.22	0.69	0.94	0.60	1.49
	167.8	1.04	1.86	1.03	1.03	0.74	0.94	0.69	1.17
	520.9	1.19	2.14	1.04	1.16	0.69	0.89	0.60	1.39

APPENDIX B. DEFLECTION PROFILES

Figures B-1 to B-4 shows the deflection-profile of specimens $G_{150}(200)47$, $G_{250}(100)53$, $G_{250}(160)52$, and $G_{250}(160)37$. Figures were used in chapter three as apart of results discussion.

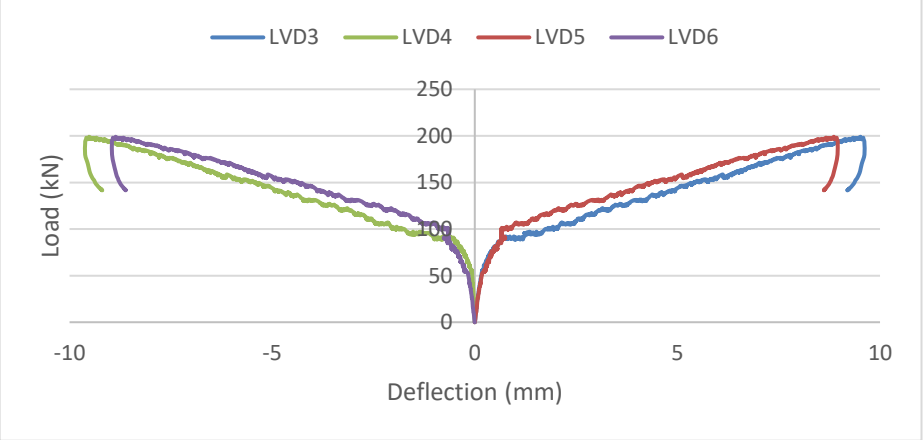

(a) Balanced deflection in the two-opposite direction LVDTs

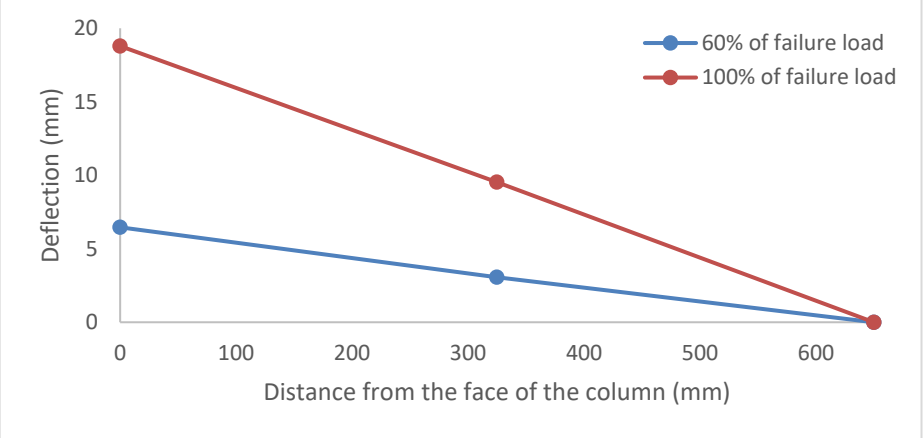

(b) average values of all direction LVDTs

Figure B-1. Deflection-profile for specimen $G_{150}(200)47$

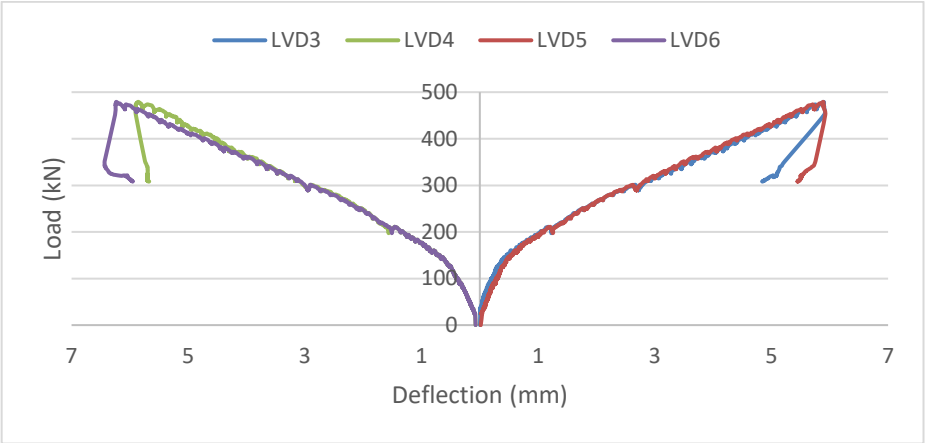

(a) Balanced deflection in the two-opposite direction LVDTs

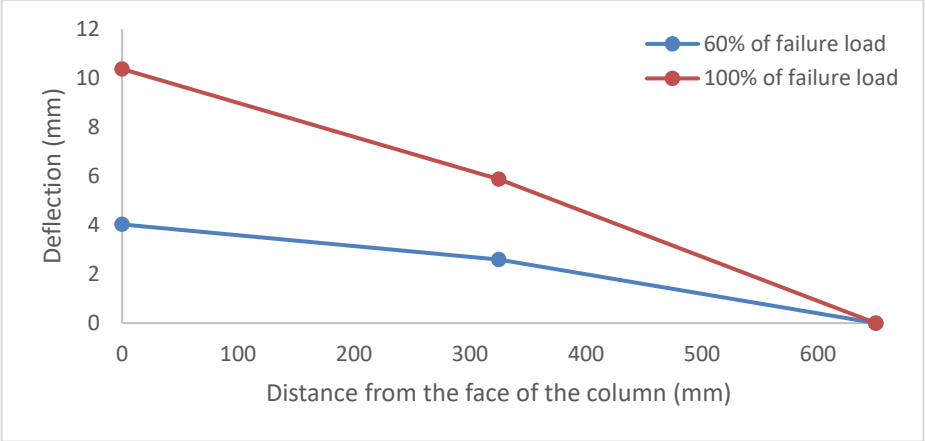

(b) average values of all direction LVDTs

Figure B-2. Deflection-profile for specimen G_{250}(100)53

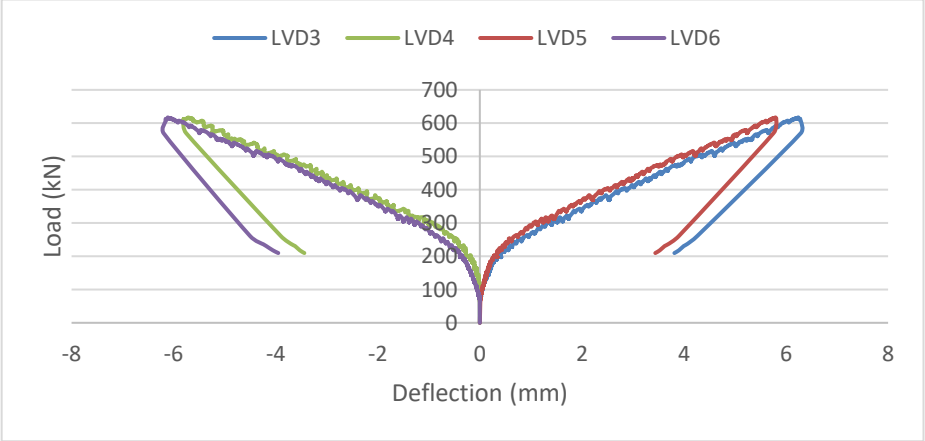

(a) Balanced deflection in the two-opposite direction LVDTs

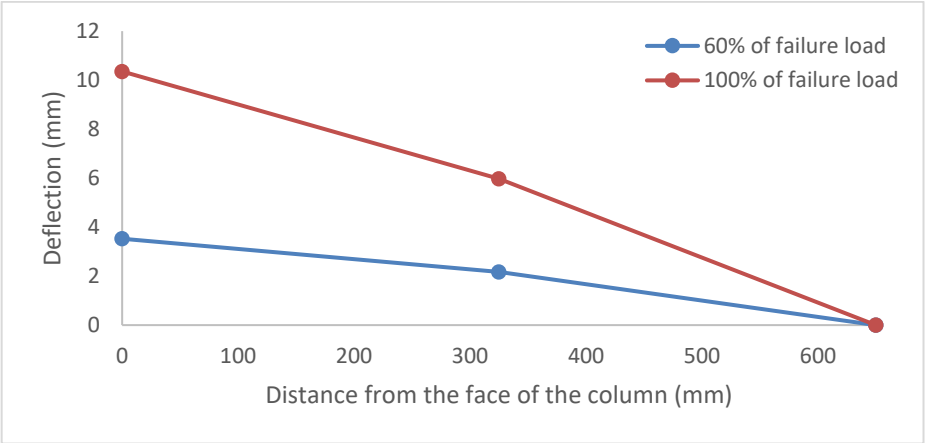

(b) average values of all direction LVDTs

Figure B-3. Deflection-profile for specimen $G_{250}(160)52$

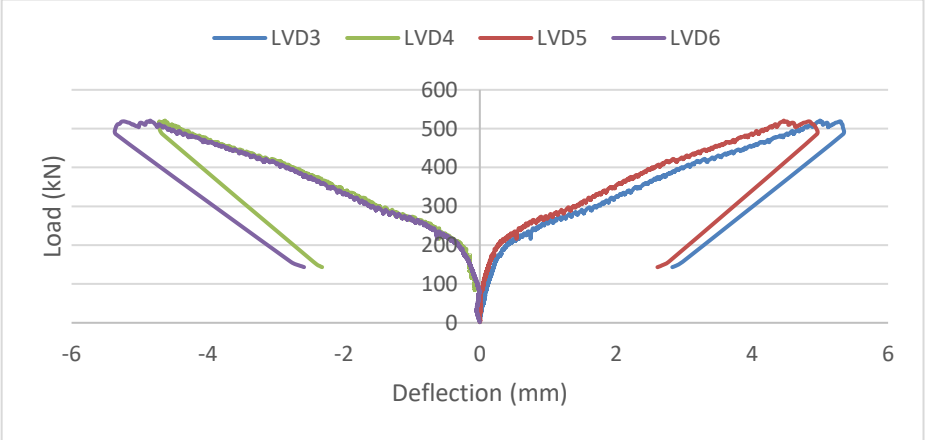

(a) Balanced deflection in the two-opposite direction LVDTs

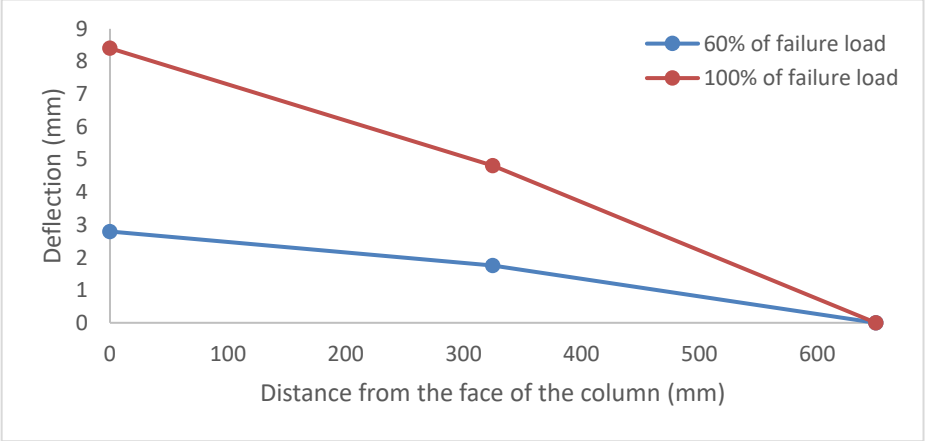

(b) average values of all direction LVDTs

Figure B-4. Deflection-profile for specimen $G_{250}(160)37$